

Improving cancer therapy through unconventional strategies

João Manuel Fernandes Neto

Improving cancer therapy through unconventional strategies

Het verbeteren van kankertherapie door onconventionele strategieën

(met een samenvatting in het Nederlands)

Proefschrift

ter verkrijging van de graad van doctor aan de
Universiteit Utrecht
op gezag van de
rector magnificus, prof.dr. H.R.B.M. Kummeling,
ingevolge het besluit van het college voor promoties
in het openbaar te verdedigen op

dinsdag 11 januari 2022 des middags te 4.15 uur

door

João Manuel Fernandes Neto

geboren op 12 januari 1993
te Porto, Portugal

The research described in this thesis was performed at the Division of Molecular Carcinogenesis of the Netherlands Cancer Institute (Amsterdam, The Netherlands) and was financially supported by the Oncode Institute and the Dutch Cancer Society.

ISBN: 978-94-6419-355-8

Cover concept: João Neto

Cover: Ilse Modder, www.ilsemodder.nl

Lay-out: Ilse Modder, www.ilsemodder.nl

Printed by: Gildeprint Enschede, www.gildeprint.nl



Copyright © 2022 João Manuel Fernandes Neto

Promotor:

Prof. dr. R. Bernards

Table of contents

Chapter 1	General introduction and thesis rationale <i>Adapted from “Thinking differently about cancer treatment regimens” Cancer Discovery (2021)</i>	9
Chapter 2	Multiple low dose therapy as an effective strategy to treat EGFR inhibitor-resistant NSCLC tumours <i>Nature Communications (2020)</i>	23
Chapter 3	Identifying selective multi-drug combinations using Comparative Network Reconstruction <i>Submitted</i>	51
Chapter 4	Using a fluorescent-based sensor to identify microsatellite instability regulators in colon cancer <i>In preparation</i>	73
Chapter 5	Optimized Cas9 expression improves performance of large-scale CRISPR screening <i>Submitted</i>	89
Chapter 6	General discussion	107
Appendix	References	115
	Nederlandse samenvatting	128
	Curriculum vitae	131
	Publication list	133
	Acknowledgements	134

1

General introduction and thesis rationale

Adapted from
Thinking differently about cancer treatment regimens
Jeff Settleman, João M. Fernandes Neto and René Bernards
Cancer Discovery (2021)

The adage “*If you do what you did, you get what you got*” is often used to remind us that meaningful change sometimes requires a fundamentally different approach. This certainly appears to apply to cancer drug development. The vast majority of novel cancer drugs are developed as single agent therapies and are delivered to patients at a maximum tolerated dose. For a variety of reasons, both economic and regulatory, this drug development model has remained virtually unchanged for several decades, resulting in the attrition of more than 30% of early stage investigational agents due to lack of single agent efficacy (1), contributing to the high cost of the few that are granted regulatory approval. Moreover, approved drugs often deliver only modest clinical benefit to patients with advanced disease due to the development of resistance. However, a drug without single agent activity is not necessarily a bad drug. As one example, small molecule inhibitors of the BRAFV600E oncoprotein do not elicit clinical responses in most patients with BRAF mutant colorectal cancer (a case of intrinsic resistance (2)), but do provide benefit to most patients with BRAF mutant melanoma (3). It is fortunate in retrospect that Tsai et al (4) developed their BRAF inhibitor PLX4720 in melanoma, even though Davies et al (5) had initially found that a significant fraction of colon cancers similarly harbour activating mutations in the BRAF gene. Otherwise, the drug known as vemurafenib, which has become a major clinical and commercial success, would most likely also have ended up on the graveyard of compounds lacking single agent activity, together with many other potentially useful candidate drugs (4). We discuss here a number of rational drug combination strategies that we feel have the potential to decrease attrition rates during clinical development and deliver additional benefit for patients with cancer, while highlighting some of the current challenges in the field.

Synthetic lethal drug combinations

Based on drug approval history, it has been argued that drugs that lack single agent activity are not worth pursuing in combination, due to low success rate and marginal combination benefit in the face of considerable combination toxicity (6). However, the 18 or so combination therapies these investigators evaluated largely consisted of combinations of targeted agents that lacked single agent activity with chemotherapies or hormonal therapies, combinations for which there was no rational mechanistic basis. In many trial and error combination studies, each compound has demonstrated some single agent activity and the expectation is that the combination would be superior. One salient example that highlights the risk of this approach is the combination of cetuximab (EGFR inhibitor) and bevacizumab (VEGF inhibitor), two blockbuster drugs approved for the treatment of colon cancer. A large study in colon cancer found that addition of cetuximab to a regimen of chemotherapy and bevacizumab resulted in worse outcome for some patients (7).

These findings highlight the potential harm to patients of combination treatments without rational basis. The substantial number of trials testing combinations with PD1 or PDL1 antibodies also highlights the lack of mechanistic basis for many such trials.

In the case of BRAF mutant colon cancer, genetic screens to identify synthetic lethal interactions, together with biochemical analyses, have revealed that BRAF inhibition results in feedback reactivation of EGFR. Moreover, a combination of BRAF and EGFR inhibitors was shown to be effective in pre-clinical models of BRAF mutant colon cancer (8,9). Based on a positive phase III study, this drug combination was recently approved for this indication (10). This example highlights how fundamental insights into crosstalk and feedback mechanisms that operate in cancer cells can help inform rational and effective combination therapies (Figure 1A). This type of approach may therefore be useful to resuscitate compounds that were unsuccessful as single agents in oncology such as, for example, inhibitors of the unfolded protein response kinase ERN1. Such drugs were shown to be potent inhibitors of the ERN1 kinase, but did not have significant effects on a large panel of cancer cell lines (11). Moreover, emerging evidence indicates that the highly selective KRASG12C inhibitors produce only modest clinical efficacy as single agents due to adaptive resistance and could benefit from treatment combinations to extend response duration (12–16). Indeed, CRISPRi modifier screens have identified “collateral dependencies” of cancer cells treated with KRASG12C inhibitors that inform potentially effective combinations with this drug (17). Collectively, these data point towards the utility of unbiased genetic approaches to identify rational combination therapies that may provide superior benefit as compared to the corresponding monotherapies.

Sequential drug treatment

A potential challenge associated with drug combinations identified through synthetic lethality genetic screens is the issue of combination toxicity in the clinic. This begs the question as to whether it is possible to avoid combination toxicity by developing treatment regimens that show synergy without concomitant drug administration. Theoretically, this could be achieved if the first of two drugs induces a major vulnerability in the cancer cell that is targeted by a second drug to kill the cell (Figure 1B). Indeed, Fang et al (18) demonstrated that while a combination of PARP and WEE1 inhibitors was highly toxic in animal models of ovarian cancer, the sequential therapy with these two drugs caused minimal toxicity and showed significant efficacy. That this sequential therapy showed synergy is explained by the finding that monotherapy-induced DNA damage or G2 cell cycle arrest was maintained after drug removal, allowing the acquired vulnerability to be maintained during the second drug treatment cycle (18). Similarly, it has been

shown that sequential, but not simultaneous, treatment of triple negative breast cancer cells with EGFR inhibitors and DNA damaging drugs leads to efficient cell killing (19). Finally, pre-clinical data also support the use of sequential drug regimens for combination immunotherapies (reviewed in (20)).

Successful sequential drug treatment strategies require that a metastable state is induced by the first therapy that persists beyond cessation of the first therapy and is associated with a significant new vulnerability. We and others have argued that induction of senescence in cancer cells might be an effective first step in a sequential drug treatment strategy, as senescence is a stable proliferation arrest characterized by major changes in metabolism, gene expression and cytokine production (21,22). Such senescence-induced cellular changes might cause vulnerabilities that enable selective killing of senescent cells with drugs that specifically target them--so-called "senolytic" drugs (Figure 1B). Therapy-induced senescence has been described as a side effect of several cancer therapeutics, including many chemotherapies (23). Thus, cancer cells are still able to become senescent, even though they have successfully bypassed the classical telomere-shortening senescence checkpoint (24). Indeed, both chemical and genetic screens have identified targets and compounds to induce senescence in cancer or kill senescent cancer cells (25–27). Moreover, pre-clinical evidence indicates that a combination of a pro-senescence drug and a senolytic compound may be effective therapeutically (28,29).

Senescent cells also secrete a number of cytokines, due to the activation of the cGAS-STING pathway as a result of the accumulation of cytoplasmic nucleic acids in senescent cells (30). This attracts a broad spectrum of inflammatory cells, including T cells, NK cells and macrophages to the senescent cancer cell mass, which provides additional opportunities to eliminate senescent cancer cells. For instance, it was shown that pancreatic cancer cells rendered senescent by a combination of a CDK4/6 inhibitor and a MEK kinase inhibitor are efficiently cleared by treatment with PD1 checkpoint immunotherapy (31).

The notion that pre-treatment with a drug can sensitize to PD1 therapy has also been observed clinically. Induction therapy of metastatic breast cancer patients with some, but not all, forms of chemotherapy resulted in enhanced responses to nivolumab (anti-PD1). Pre-treatment with cisplatin and doxorubicin in particular was associated with inflammatory gene signatures and response to PD1 therapy (32). The stimulatory effect of certain chemotherapies on the PD1 response may be caused by immunogenic cell death or by induction of senescence, leading to changes in the tumor microenvironment due to cytokine production (33,34). These examples highlight the considerable promise of sequential treatments for future clinical application.

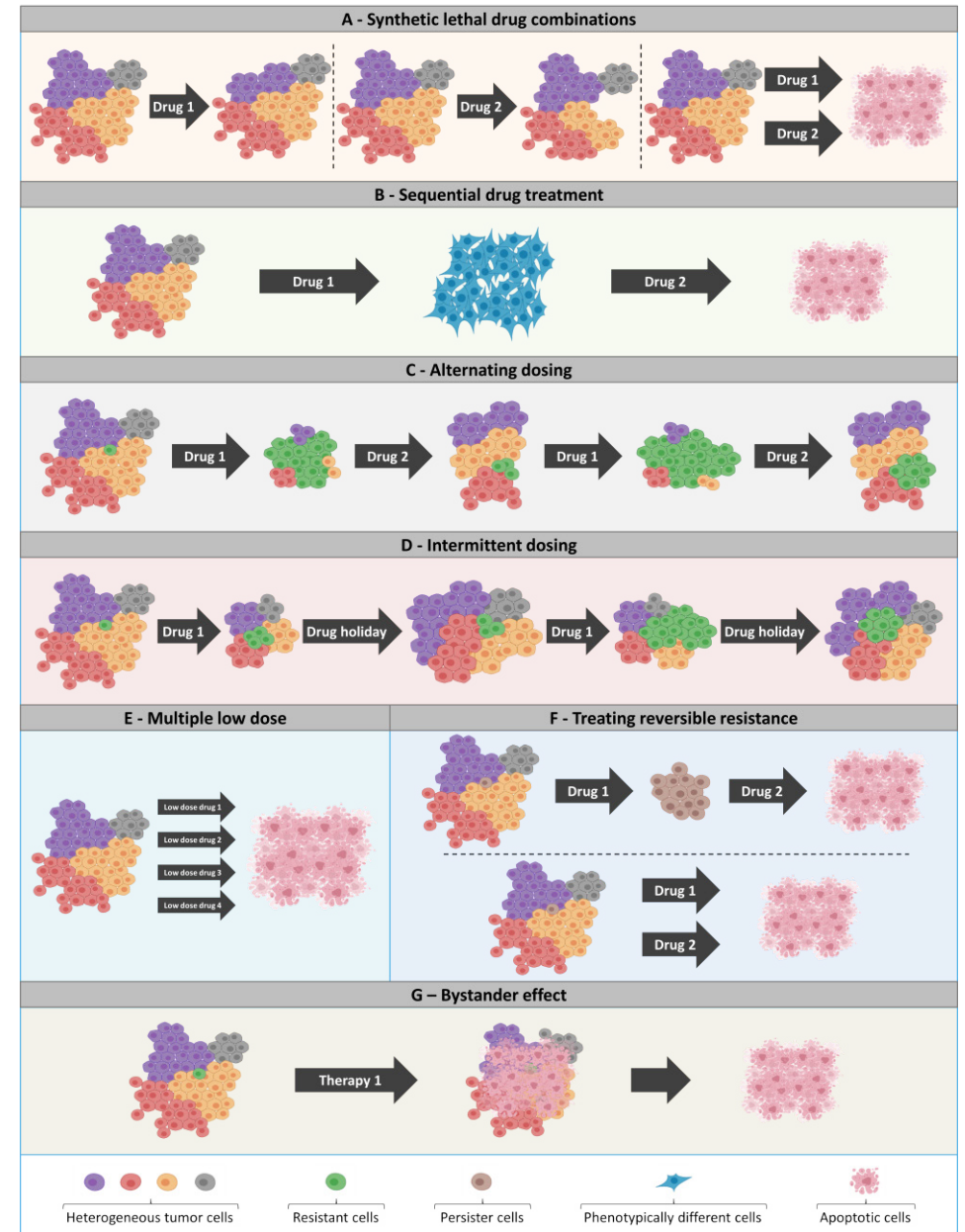


Figure 1: Schematic representation of the drug treatment regimens discussed.

A – Synthetic lethal drug combinations. Synthetic lethality refers to a situation in which two agents are individually non-lethal, but become lethal when used in combination. B – Sequential drug treatment. The first drug is used to bring the cancer cells in a metastable state having an acquired vulnerability (e.g. senescence), the second drug acts on the acquired vulnerability (e.g. a senolytic agent). C – Alternating dosing. Drug resistance comes with an associated fitness cost. Resistance to drug 1 is associated with an acquired vulnerability to drug 2. Alternating treatment of the drug-sensitive and drug-resistant populations can keep the tumor in control over longer periods of time. D – Intermittent dosing. Termination of drug

administration following development of resistance can result in tumor regression due to a disadvantage of the drug-resistant population in the absence of drug. After a drug-holiday, the drug-resistant population is depleted and the drug-sensitive population tumors respond again to the original drug. E – Multiple low dose. Targeting the same oncogenic signaling pathway with multiple drugs, each at low dose, can add up to complete pathway inhibition, while at the same time reducing the pressure on each of the nodes to develop resistance mutations. F – Treating reversible resistance. A minor fraction of a cancer may be epigenetically distinct, such that these cells enter a state of dormancy during treatment, which would allow re-population of the tumor following termination of therapy. Targeting these “drug tolerant persisters” with selective drugs can eliminate this population, preventing tumor re-growth. G – Bystander effect. A therapy that kills the majority of the cancer cells can lead to killing of drug-insensitive cells, for example by the release of signals (e.g. cytokines) by the dying cancer cells.

Alternating dosing

It is observed generally in the clinic that second-line therapies are less effective than first-line therapies, with third line being even less effective than second line treatments. However, it has been appreciated for nearly sixty years that resistance to one cancer drug might come at a “fitness cost”, which can yield a vulnerability to another drug, a phenomenon referred to as “collateral sensitivity” (35). Identification of collateral sensitivities of drug-resistant cancer cells represents a large untapped opportunity for the discovery of potentially important drug targets for selectively killing drug-resistant cancer cells. We have collectively been remarkably unsuccessful in finding collateral sensitivities of chemotherapy-resistant cancer cells, most likely due to the heterogeneity in chemotherapy resistance mechanisms. The recent identification of sensitization to checkpoint immunotherapy by some chemotherapies discussed above, is a notable exception. However, there is reason to be more optimistic that collateral sensitivities associated with resistance to targeted cancer drugs may be more homogeneous. This optimism is based on the limited options cancer cells have to develop resistance to targeted cancer drugs. Most often, such drug-resistant cancer cells will reactivate the inhibited pathway through upstream, downstream or parallel pathway activation, which makes the acquired vulnerabilities more predictable. As one example, biochemical studies have demonstrated that resistance of melanoma to BRAF inhibitors is associated with a marked increase in sensitivity to histone deacetylase (HDAC) inhibitors. A pilot study in patients demonstrated that a brief treatment of BRAF-inhibitor resistant melanoma patients with HDAC inhibitors eliminated the drug-resistant cell population (36). This model suggests a treatment strategy in which the drug-sensitive and drug-resistant subpopulation is targeted in an alternating fashion (Figure 1C). This alternating treatment concept is currently being tested in a phase 1 trial (NCT02836548). Along the same lines, it has been observed that resistance of EGFR mutant lung cancer cells to selective EGFR inhibitors is associated with a greatly increased sensitivity to AURORA kinase inhibitors, making AURORA kinase inhibition a collateral sensitivity of EGFR inhibitor-resistant lung cancers (37,38).

The use of AURORA kinase inhibitors in patients having EGFR inhibitor-resistant NSCLC is also undergoing clinical testing (NCT04085315).

Intermittent dosing

A relatively rare clinical phenomenon is the observation that termination of drug administration following development of resistance can lead to tumor regression. Moreover, after such a “drug-holiday”, tumors often have re-gained sensitivity to the original drug—the so-called “retreatment response” (39) (Figure 1D). This phenomenon is most readily explained by an addiction of the drug resistant cell to the drug, leading to a selective disadvantage of the drug-resistant population in the absence of drug. Indeed, in pre-clinical models of melanoma, intermittent dosing with BRAF inhibitors provides longer-lasting tumor control as compared to continuous dosing (40). However, recent clinical data appear to indicate that intermittent BRAF inhibitor dosing is inferior to continuous drug administration, highlighting the challenge of translating dosing and treatment schedules from mice to humans (41).

Multiple low dose treatment

In advanced cancers, development of resistance is almost unavoidable due to secondary mutations. When targeted drugs are used as single agents, resistance mutations often emerge that involve mutations in the drug target itself. For instance, secondary mutations in the genes encoding the BCR-ABL, EGFR and ALK kinases have been described upon inhibition of these kinases, but mutations in genes that act either upstream, downstream or in parallel to the oncogenic pathway that is being targeted have been observed as well (42). To avoid this type of resistance, “vertical targeting” of two components in the same oncogenic signaling pathway has been shown to lead to longer-lasting therapeutic responses. Thus, in BRAF mutant melanoma and lung cancer, combined inhibition of the BRAF and MEK kinases was more effective than treatment with the single agents (43,44). In pre-clinical models of BRAF mutant melanoma it was possible to forestall resistance through a triple combination of BRAF, MEK and ERK inhibitors (each at high concentration) to prevent resistance, but drugs had to be administered intermittently to limit toxicity (45).

It is generally believed that for a drug combination to be efficient, each drug must have considerable single agent activity to suppress clonal diversity. This is seen for example in the treatment of HIV, where combinations of drugs that target the viral reverse transcriptase, protease and integrase proteins are used to prevent resistance (46). However, recent evidence indicates that vertical targeting of EGFR mutant lung cancers with three or four drugs that act in the EGFR signaling pathway can be an effective treatment strategy, even when the four drugs are used

at only 20% of the effective single agent concentration (47). In a related study, low dose inhibition of RAF and ERK proved effective in KRAS mutant cancers (48). A key difference between the viral and cancer therapies is that in the latter, all drugs target the same signaling pathway, thereby allowing synergistic inhibition at low drug concentrations. At the same time, partial inhibition of multiple nodes of a pathway reduces the selective pressure on these nodes to gain a resistance mutation. These observations of synergy between low drug doses in the MAP kinase pathway are clearly at odds with the generally held view that this pathway serves to amplify signals. As such, these data highlight that much remains to be learned about crosstalk and feedback mechanisms that operate in this signaling context. Collectively, these findings emphasize that we may have to consider combinations of more than two targeted agents, preferably in the same signaling cascade, to forestall resistance (Figure 1E). That such combinations are not necessarily overly toxic was demonstrated in a recent study, in which BRAF, MEK and EGFR inhibitors were successfully combined in the clinic (10).

Treating reversible resistance

Much of our current understanding of cancer drug resistance mechanisms has been informed by the identification of specific mutational events that underlie stable, propagatable states of resistance (49). The development of such resistance-conferring mutations is certainly consistent with fundamental principles of Darwinian evolution, and likely reflects the stochastic emergence of such mutations at low frequency in tumor cell populations prior to drug exposure—resulting in the outgrowth of stably drug-resistant cancer cell clones through natural selection. However, non-mutational, and therefore potentially reversible mechanisms of drug resistance are becoming increasingly recognized. For example, the drug-induced senescence described above may be reversible, such that, upon drug withdrawal, such “senescent” cancer cells could lose their senescence features and resume proliferation. Similarly, cancer cell “dormancy” is another relatively poorly understood cell state associated with transient quiescence and treatment resistance (50).

The differentiation and de-differentiation of cancer cells has also been linked to fluctuation between states of differing drug sensitivity and resistance. For example, the epithelial-mesenchymal transformation (51), a slowly reversible state change, has been associated with the acquisition of drug resistance in many epithelial cancers (52). Moreover, the molecular features exhibited by the generally more treatment-refractory mesenchymal cell state are often shared by cancer stem cells, a subpopulation of phenotypically “plastic” tumor cells that have also been associated with drug resistance (53).

Another form of reversible drug resistance has been described as the “drug-

tolerant persister” (DTP) state (54). When propagated in the laboratory, clonal cancer cell lines have been found to exhibit phenotypic heterogeneity that typically includes the presence of small subpopulations of cells that do not share the same vulnerabilities to drug treatment as are seen with the bulk population of cells (54). Consequently, these DTPs survive an otherwise lethal drug exposure and maintain viability for long periods of time in the presence of continuous drug exposure. Significantly, upon drug withdrawal, DTPs can resume proliferation, giving rise to a largely drug-sensitive cell population. Collectively, reversibly senescent cells, dormant cells, mesenchymal cells, cancer stem cells, and DTPs share features that suggest that they are highly related and may in fact reflect common underlying mechanisms. Consequently, they may exhibit overlapping vulnerabilities that could provide opportunities to target such tumor cell populations with therapeutics aimed specifically at overcoming drug resistance as part of a combination treatment regimen that also targets the bulk cell population (Figure 1F).

The reversible nature of these various states of drug resistance implicates epigenetic regulation. Indeed, the role of epigenetic control in the EMT process in cancer cells is now well established (55). Similarly, epigenetic changes appear to be the critical determinants of “decisions” to enter and exit stem cell states—including those exhibited by cancer stem cells (56). Senescent cells are characterized by a distinct organizational structure of heterochromatin, suggesting that epigenetic regulation is likely to play a role in the transition into and out of senescence (57). DTPs have also been found to harbor distinct chromatin features, including a repressed chromatin state associated with specific alterations in histone methylation (54,58). Importantly, despite their resistance to “conventional” therapeutics, these distinct chromatin features associated with reversibly drug-tolerant states appear to yield specific therapeutic vulnerabilities. For example, the DTP state can be disrupted by targeting the KDM5 family histone demethylases, the SETDB1, G9a, and EZH2 methyltransferases, and the class I histone deacetylases (54,58,59).

In addition to chromatin regulators, various other vulnerabilities have been associated with reversible states of drug resistance. These include, for example, the senolytic agents described above, cancer stem cell-targeted agents such as BMI1 inhibitors (60) and the antibiotic salinomycin (61), as well as agents that have been reported to selectively kill mesenchymal cells, such as the multi-kinase inhibitor dasatinib (62). In addition to epigenetic modulators, other potential target-associated vulnerabilities have been described for DTPs, including the cancer stem cell-enriched protein ALDH1A1 (aldehyde dehydrogenase) (63) and the selenocysteine family protein GPX4 (glutathione peroxidase 4) (64). Recently, it was reported that targeting YAP-TEAD pathway signaling disrupts a senescence-like state of cancer cell dormancy associated with resistance to EGFR kinase inhibition, with the potential to prolong treatment effects (65).

Considering that these non-mutational mechanisms of drug resistance reflect a form of dynamic phenotypic heterogeneity that appears to be broadly present within tumor cell populations, the potential benefit resulting from disruption of such states could be substantial. Thus, combination treatments could be deployed in which an agent that targets the bulk population of cancer cells could be combined with an agent that selectively targets the “pre-existing” phenotypically distinct, and more treatment-refractory subpopulation of cells, with the goal of forestalling resistance (Figure 1F). An alternative approach would be to target mechanisms that enable the transition of cancer cells into the transiently-maintained states of drug tolerance—for example, with agents that block the EMT process. Similarly, it may be possible to drive the drug-resistant subpopulation of cells into a state that “matches” the drug sensitivity of the bulk population—effectively “leveling the playing field” by promoting a greater degree of homogeneity among tumor cell subpopulations. In any of these treatment schemes, the “up-front” administration of the combination therapy is expected to delay or prevent the emergence of drug resistance. However, it is also possible that such treatments could be sequenced, especially if the transition between plastic states of sensitivity and resistance require significant time, thereby yielding a window during which treatments could be spaced (Figure 1F). If effective, this approach provides an opportunity to reduce the potential for dosing limitations imposed by overlapping toxicities between the combination agents.

Overcoming heterogeneity

The presence of intra-tumor heterogeneity represents a formidable obstacle to successful therapy, independent of the treatment strategy and cancer type. Changes in selective pressures during the lifetime of a cancer can yield a diversity of subclones having different genotypes. Nevertheless, there are reasons to be hopeful that heterogeneity can ultimately be overcome. First, cancer subclones share “truncal” mutations that can be targeted for therapy (66). For instance, the anti HER2 antibody trastuzumab is very effective both in HER2-positive metastatic breast cancer and as an adjuvant therapy for early breast cancer (67). Second, sequencing of tumor subclones provides clear evidence for convergent evolution, indicating that subclones have limited options to evolve (66). Third, even patients with advanced disease (and consequently likely have more heterogeneous tumors), can still have long-lasting responses, indicating that in these patients, drug-resistant subclones were unable to dominate the tumor cell population. In the treatment of advanced melanoma, secondary resistance mutations to BRAF inhibitor therapy occur so frequently that survival benefit is limited (3). In contrast, treatment of such patients with immunotherapy leads to a subgroup of patients experiencing very long survival (68). This is not because mutations that confer resistance

to immunotherapy cannot occur, as sequencing of resistant tumors has shown (69). Hence, it seems plausible that the superior responses of immunotherapies compared to MAP kinase inhibitors in melanoma can be explained by killing of resistant cancer cells through a bystander effect. Such bystander effects can be caused by signals (e.g., cytokines) that are secreted by the dying cancer cells. While the precise mechanism of action of bystander effects are understood only poorly, this clearly represents an opportunity to overcome intra-tumor heterogeneity (Figure 1G).

Conclusions

First, the paradigm that new oncology drugs should first show single agent activity before combinations are considered needs to be revisited. Rather than waiting for a phase 2 (single agent) trial to report results, drug developers could invest earlier in finding the best combinations and consider developing the drugs further in combination after phase 1 (Figure 2). A good example of this is the clinical development of SHP2 inhibitors. While they may have single agent activity in tyrosine kinase-driven cancers (70), ample pre-clinical evidence indicates that these drugs are more effective when combined with MEK inhibitors (71–73). While the dose escalation of one of these agents (RMC4630) as a single agent is still ongoing, studies are also underway to test this inhibitor in combination with MEK inhibitors (NCT03989115). Fortunately, the Food and Drug Administration appreciates the need for co-development of such drug combinations and has recently released a guidance document to assist in the development of “two or more new drugs that have not been previously developed for any indication to be used in combination to treat a disease or condition” (<https://www.fda.gov/media/80100/download>). Second, more efforts could be directed to identifying the vulnerabilities of drug-resistant cancer cells. Identification of such vulnerabilities may result in development of second line therapies that are potentially more effective than the first line therapy—rather than less effective, as is currently often the case. The study of such vulnerabilities can also uncover new classes of drug targets that are distinct from the oncogenic drivers that are currently a main focus of drug development. Alternating dosing schedules that target the drug-sensitive and drug-resistant populations in a periodic fashion may then be used to control the tumor over prolonged periods of time. Finally, greater effort could be made to study the synergistic effects of multiple targeted agents used in combination. The notion that such drugs can still be combined efficiently when used at low dose may provide ample opportunity to combine such agents with limited toxicity.

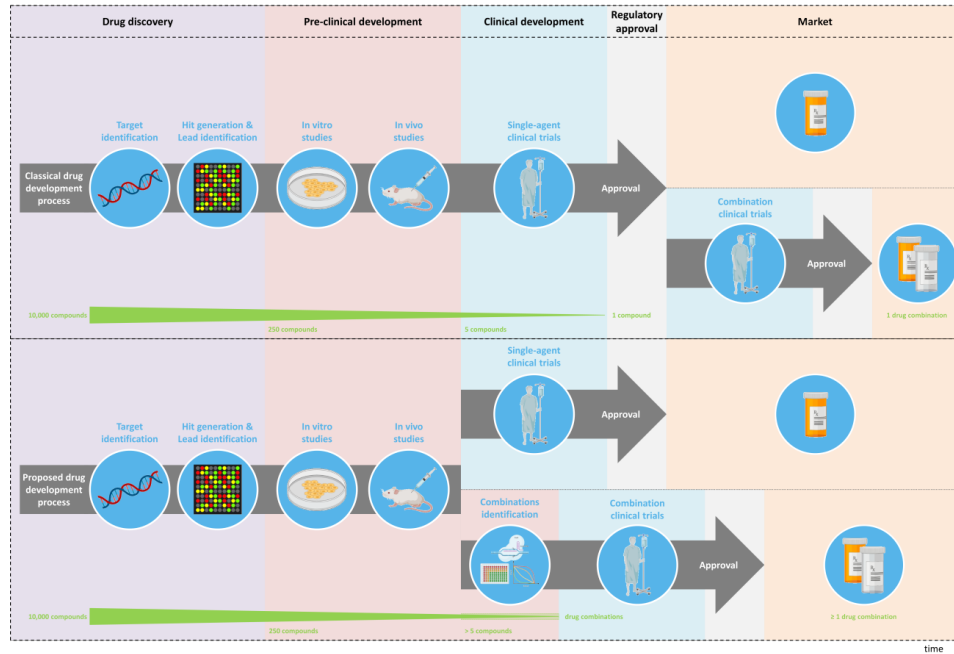


Figure 2: Schematic representation of the drug development process.

Top: In conventional drug development, new chemical entities are first tested as single agents in clinical studies. Only after single-agent approval, combination studies are considered. Bottom: Proposed drug development model. During the pre-clinical phase of drug development, genetic and biochemical studies are performed to identify rational and effective combination therapies. These combination regimens are developed in parallel to (or even instead of) the development of the novel chemical entity as a single agent. This model could lead to less attrition of new chemical entities and longer lasting therapeutic benefits for patients.

Thesis rationale and outline

As mentioned in this introduction, development of new cancer drug treatment regimens based on insights into signalling pathway interactions and cancer cell vulnerabilities can increase the success of cancer therapies. The work described in this thesis aimed to address opportunities we consider promising to overcome drug resistance associated with interactions between signalling pathways and the presence of multiple co-existing cell states within tumors with distinct vulnerabilities.

In **chapter 2** we identify a novel treatment regimen for resistant NSCLC tumors, which we named Multiple Low Dose (MLD). We show that partial inhibition of multiple components of cancer-activated signalling pathways is difficult to circumvent and we argue that single-agent MTD type of regimens should be revisited. The promising pre-clinical data in mice suggest that MLD therapy could deliver clinical benefit and its potential goes beyond NSCLC.

The increasing number of cancer compounds together with the notion that drug combinations deliver more benefit has created a big challenge in cancer therapy: with so many drugs, testing all combinations is becoming an impossible task. In **chapter 3** we show that by combining perturbation experiments with mathematical models of signal transduction it is possible to predict which multi-drug combinations will selectively kill certain cells.

In **chapter 4** we developed a fluorescent-based MSI sensor to identify cells with an increased rate of frameshift mutations and, using CRISPR screens, we identified MED12 as a new potential regulator of microsatellite instability (MSI).

CRISPR is an invaluable technology nowadays, which we used throughout this thesis. With the increased experience with this tool we noticed that some aspects could be optimised. In **chapter 5** we show that by optimizing Cas9 expression levels, the time necessary for gene editing can be reduced, contributing to improved performance of CRISPR based screening.

In **chapter 6**, I provide a general discussion that places my own findings in the context of the work of others. I also provide a future perspective of the field in general.

2

Multiple low dose therapy as an effective strategy to treat EGFR inhibitor-resistant NSCLC tumours

João M. Fernandes Neto¹, Ernest Nadal², Evert Bosdriesz^{1,10}, Salo N Ooft³,
Lourdes Farre^{2,4}, Chelsea McLean³, Sjoerd Klarenbeek⁵, Anouk Jurgens¹,
Hannes Hagen¹, Liqin Wang¹, Enriqueta Felip^{6,7}, Alex Martinez-Marti^{6,7},
August Vidal², Emile Voest³, Lodewyk F.A. Wessels¹, Olaf van Tellinghen⁸,
Alberto Villanueva^{2,9} and René Bernards¹

¹Division of Molecular Carcinogenesis & Oncode Institute. The Netherlands Cancer Institute, Plesmanlaan 121, 1066 CX Amsterdam, The Netherlands.

²Group of Chemoresistance and Predictive Factors, Subprogram Against Cancer Therapeutic Resistance (ProCURE), ICO, Oncobell Program, IDIBELL, L'Hospitalet del Llobregat, Barcelona, Spain.

³Division of Molecular Oncology and Immunology, The Netherlands Cancer Institute, 1066 CX Amsterdam, The Netherlands.

⁴Instituto Gonçalo Moniz. Fundação Oswaldo Cruz (FIOCRUZ), Brasil.

⁵Experimental Animal Pathology, The Netherlands Cancer Institute, 1066 CX Amsterdam, The Netherlands.

⁶Department of Medical Oncology, Vall d'Hebron University Hospital and Vall d'Hebron Institute of Oncology (VHIO), Barcelona, Spain.

⁷Autonomous University of Barcelona (UAB), Barcelona, Spain.

⁸Division of Clinical Pharmacology, The Netherlands Cancer Institute, 1066 CX Amsterdam, The Netherlands.

⁹Xenopat S.L., Business Biocubator, Bellvitge Health Science Campus, Barcelona, Spain.

¹⁰Department of Computer Science, Faculty of Science, Vrije Universiteit, Amsterdam, The Netherlands

Abstract

Resistance to targeted cancer drugs is thought to result from selective pressure exerted by a high drug dose. Partial inhibition of multiple components in the same oncogenic signalling pathway may add up to complete pathway inhibition, while decreasing the selective pressure on each component to acquire a resistance mutation. We report here testing of this Multiple Low Dose (MLD) therapy model in EGFR mutant NSCLC. We show that as little as 20% of the individual effective drug doses is sufficient to completely block MAPK signalling and proliferation when used in 3D (RAF+MEK+ERK) or 4D (EGFR+RAF+MEK+ERK) inhibitor combinations. Importantly, EGFR mutant NSCLC cells treated with MLD therapy do not develop resistance. Using several animal models, we find durable responses to MLD therapy without associated toxicity. Our data support the notion that MLD therapy could deliver clinical benefit, even for those having acquired resistance to third generation EGFR inhibitor therapy.

Introduction

Inhibition of signalling pathways that are activated by oncogenic mutations elicit therapeutic responses due to “addiction” of the cancer to the activated pathway (74). However, in advanced cancers, development of resistance is practically inevitable due to secondary mutations that restore signalling through the drug-inhibited pathway. Such acquired resistance mutations affect either the drug target itself or components that act upstream, downstream or parallel to the activated signalling component (42,75). In BRAF mutant melanoma and NSCLC, inhibition of two components of the same oncogenic pathway (BRAF+MEK, referred to as “vertical targeting”) has been shown to provide more lasting clinical benefit compared to inhibition of only BRAF (44,76). More recently, both clinical (10,77) and pre-clinical (78) studies have shown that inhibition of three components of the same oncogenic pathway further increases therapeutic benefit. In these scenarios the drugs are usually administered at maximum tolerated dose (MTD). The increase in the number of drugs being used in combination is often accompanied by an increase in toxicity and to this date virtually no studies have been done to assess the efficacy of using drugs below-MTD. In a preclinical model, multiple drugs used at low dose also demonstrated promising activity in ovarian clear cell carcinoma (79). In this study we explore the use of a Multiple Low Dose (MLD) strategy in EGFR mutant NSCLC. In this approach, multiple drugs that act in the same oncogenic signalling pathway are combined at low concentration. We hypothesized that this might add up to complete pathway inhibition without causing prohibitive toxicity. Further, by using low drug concentrations, the pressure exerted on each node of the pathway should greatly diminish, reducing the selective pressure on each node and therefore diminishing the chances of acquiring resistance.

Results

The mechanisms of resistance to EGFR inhibition (standard-of-care) in EGFR mutant NSCLC are well understood. We therefore compared the efficacy of MLD therapy to standard-of-care MTD therapies in this indication. We used PC9 NSCLC cells, which harbour an activating mutation in the gene encoding EGFR (54). We used four drugs, each inhibiting a different node in the MAPK pathway: gefitinib (EGFR inhibitor), LY3009120 (pan-RAF inhibitor (80)), trametinib (MEK inhibitor) and SCH772984 (ERK inhibitor (81)), as shown schematically in Fig. 1a. We established dose-response curves for each of the four drugs using 5-day culture assays (Fig. 1b). From these data, we inferred for all 4 inhibitors the IC20 dose, i.e. a drug concentration that inhibits cell viability by 20% - henceforth referred

as Low Dose (LD). To assess the efficacy of the MLD strategy we then tested the impact of all possible drug combinations of the 4 drugs at LD on cell viability (assessed by CellTiter-Blue® assay), on cell proliferation (assessed by long-term colony formation assay) and on pathway activity (measured by p-RSK levels (82) using Western Blotting) (Figs. 1c-e). The expected viability and the synergy scores were calculated using the Bliss independence model (83). We found that PC9 cells treated with the single drugs at low dose were only minimally affected, as expected. However, some of the drug combinations showed a striking combination effect, much higher than expected based on drug additivity. In particular, the combination of RAF+MEK+ERK inhibitors at low dose (henceforth called 3D combination) and the combination of EGFR+RAF+MEK+ERK inhibitors at low dose (henceforth called 4D combination) showed an almost complete inhibition of cell viability and proliferation, along with a complete blockade of MAPK pathway signalling. Due to these notable findings we pursued the MLD study focusing on the 3D and 4D combinations.

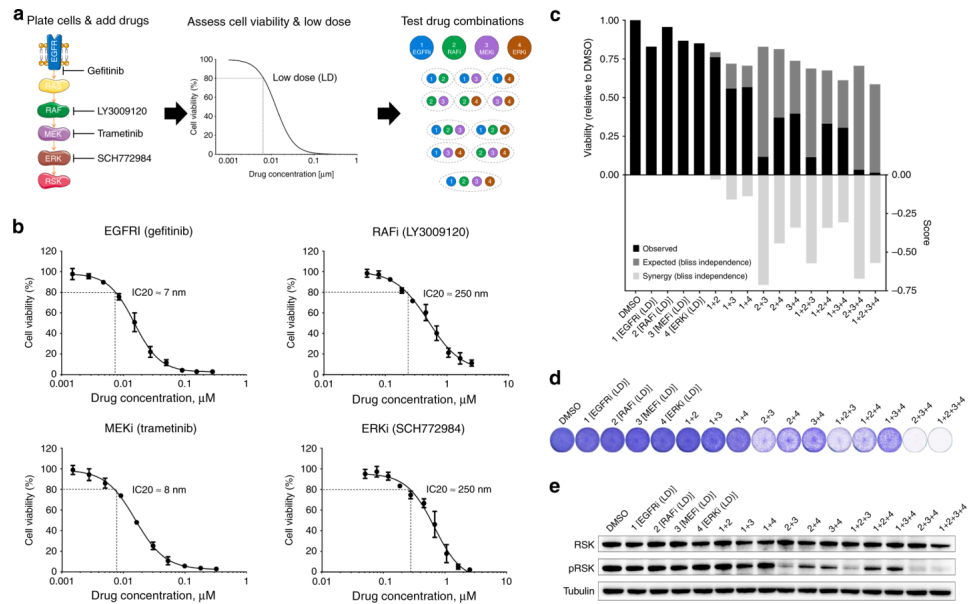


Figure 1: Multiple Low Dose therapy blocks MAPK pathway and proliferation in PC9 cells. a, Schematic of the Multiple Low Dose (MLD) efficacy determination. After plating, cells are treated with increasing drug concentrations. Four days later cell viability is measured and the low dose (LD) is assessed. At last, the efficacy of all the possible combinations at LD is determined. b, Dose-response curves of EGFR, RAF, MEK and ERK inhibitors in PC9 cells. PC9 cells were cultured with increasing concentrations of EGFRi Gefitinib, RAFi LY3009120, MEKi Trametinib or ERKi SCH772984 for 4 days, after which cell viability was measured using CellTiter-Blue®. Standard deviation (SD) from 3 biologically independent replicates (each with 3 technical replicates) is plotted. Low doses (IC20s) were then determined: gefitinib=7nM, LY3009120=250 nM, 292 trametinib=8nM and SCH772984=250nM. c-e, Determination of the efficacy of all

the possible combinations of EGFR, RAF, MEK and ERK inhibitors at LD in PC9 cells. PC9 cells were cultured with all possible drug combinations of EGFR, RAF, MEK and ERK inhibitors at the low doses determined in (b). In (c) cell viability from 3 biologically independent replicates (each with 3 technical replicates) was measured by CellTiter-Blue® assay after 4 days of treatment; In black the observed experimental viability; In dark-grey the expected viability and in light-grey the synergy scores, calculated using the Bliss independence model, are plotted. In (d) cells were treated for 10 days, after which plates were stained and scanned; A representative image from the 3 biologically independent replicates performed is displayed. In (e) protein for western blotting was harvested after 24 hours of treatment; The level of pathway inhibition was determined by examining pRSK protein levels in the western blot. Tubulin was used as loading control. A representative image from the 3 biologically independent replicates performed is displayed.

To address if we could further reduce the drug concentrations, we diluted the 4D combination. When the drugs were reduced to half of the IC20 concentrations, the 4D combination was no longer able to achieve complete inhibition of proliferation and was similarly unable to mediate complete MAPK pathway inhibition, indicating that there is a threshold that limits efficacy (Supplemental Figs. 1a, b). Based on this, we continued our MLD studies using the IC20 concentrations as “Low Dose”. To make sure our findings were not drug-specific, we tested the MLD approach using different inhibitors for each of the nodes in the MAPK pathway (erlotinib as EGFRi, BGB-283 as RAFi, selumetinib as MEKi and LY-3214996 as ERKi). Supplemental Figs. 1c, d show that we obtained essentially the same effect with these drugs in 3D and 4D combinations. This, together with the notion that each drug is used at low dose, makes it very unlikely that off target effects of the four drugs are responsible for the observed effects.

Next, we tested how MLD therapy compares to standard-of-care high dose therapy in terms of resistance development. To mimic high dose therapy, we treated PC9 cells with a concentration of EGFR inhibitor gefitinib that inhibited cell viability by ~99% in a 5-day culture assay – henceforth referred as High Dose (HD). We found that 3D and 4D combinations inhibit cell proliferation and induce apoptosis at comparable levels to cells treated with HD of gefitinib (Fig. 2a and Supplemental Fig. 2a, b). The level of pathway inhibition is also similar between cells treated with 3D and 4D combinations and HD of gefitinib (Fig. 2d). Additionally, we performed RNA-Seq transcriptome analyses in cells treated with 4D combination (Supplemental Fig. 2c, d). These data showed that 4D combo treated cells displayed a significant downregulation of MYC and E2F target genes as well as cell cycle genes. Moreover, MAPK activity markers (84) were significantly downregulated and several pro-apoptotic genes were found to be upregulated, while anti-apoptotic genes were downregulated. To study how MLD therapy compares to HD therapy regarding resistance, we treated PC9 cells with 3D or 4D combinations and with HD of gefitinib or osimertinib for one month (Fig. 2b). As seen by others previously(85,86), cells treated with HD of gefitinib or osimertinib quickly developed resistance, but the cells treated with 3D or 4D combinations did not. Additionally, we treated PC9 cells

for 16 days with high dose of gefitinib or with 3D or with 4D MLD combinations; we then either removed the drugs, continued to treat with the original drug, or treated with 4D MLD combination for another 16 days (Supplemental Fig. 2e). We observed resistant colonies after 32 days of gefitinib treatment, but not in the cells treated with 3D or 4D combinations. Apparently, 16 day-treatment with 3D or 4D combinations had killed all cells, as continued culturing for another 16 days in media without drugs did not yield any colonies. Importantly, PC9 cells that had developed resistance to high dose EGFR inhibitor, were still responsive to 4D MLD combination. This striking result indicates that EGFR inhibitor-resistant cells remain sensitive to 3D and 4D combinations. This suggests that MLD therapy might be an option for patients having developed resistance to standard-of-care EGFR inhibitor therapy.

To study further if EGFRi-resistant cells are indeed sensitive to 3D and 4D combinations, we generated PC9 cells resistant to clinically-used EGFR inhibitors. We cultured PC9 cells in the presence of gefitinib (PC9-GR) or osimertinib (PC9-OR) until cells were no longer responsive to the inhibitors (see methods). We performed exome sequencing of the two resistant cell populations to gain insight into the mechanisms of acquired resistance. These data showed acquisition of the well-known T790M mutation in the PC9-GR cells and a number of mutations in the PC9-OR cells, none of which has been previously associated with resistance to osimertinib (Supplemental Table 2). We then tested the sensitivity of the resistant lines to 3D and 4D combinations. In both resistant cell populations, we saw an almost complete inhibition of cell viability after only 4 days of MLD therapy treatment and a complete MAPK pathway signalling blockade (Fig. 2c, d).

We then tested if the MLD strategy would also be effective in additional in vitro tumour models. After low dose determination (Supplemental Figs. 3a-c and Supplemental Table 1) we tested the MLD strategy in patient-derived (colorectal and NSCLC) organoids. Treatment with 3D and 4D combinations resulted in a major reduction in cell viability (Fig. 3a). In addition, we tested 6 different MAPK pathway addicted cell lines: HCC827 and H3255 (EGFR mutant lung cancer), H2228 and H3122 (EML4-ALK translocated lung cancer, in which EGFRi was replaced with ALK inhibitor crizotinib in the 4D combination), DiFi and Lim1215 (EGFR dependent colorectal cancer) and in 2 different PI3K pathway addicted cell lines: SKBR3 and HCC1954 (HER2 amplified breast cancer, in which 4D combination consisted of HER2, PI3K, AKT and mTOR inhibitors). When treated with 4D combination, proliferation of all cell lines was inhibited, regardless of the tumour type/driver/genotype, pointing towards a broad applicability of the MLD treatment strategy (Supplemental Fig. 3d).

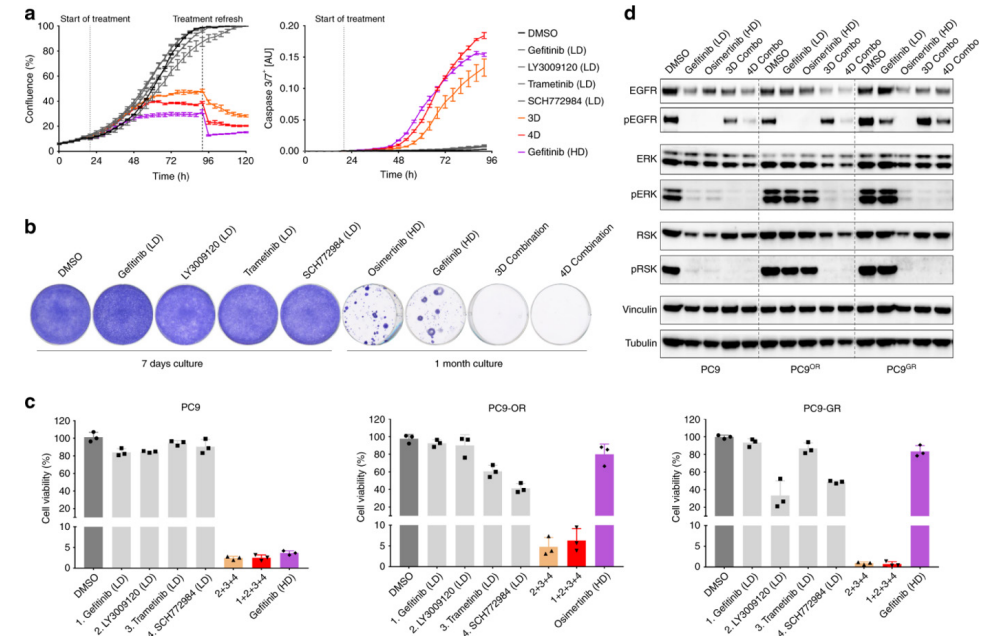


Figure 2: MLD therapy minimizes therapeutic resistance and is effective in EGFRi-resistant PC9 cells. a, MLD therapy abrogates cell proliferation and induces apoptosis in PC9 cells. PC9 cells were plated and incubated overnight to allow attachment to the plate. Cells were then treated with DMSO, with EGFR, RAF, MEK, ERK inhibitors at low dose, with 3D Combo (RAF+MEK+ERK inhibitors at LD) or with 4D Combo (EGFR+RAF+MEK+ERK inhibitors at LD) and placed in the IncuCyte®. Confluence (left) and caspase 3/7 activation (right) over time was measured by the IncuCyte®. Standard error of the mean (SEM) from 2 biologically independent replicates (each with 3 technical replicates) is plotted. b, MLD therapy prevents the acquisition of drug resistance in PC9 cells. PC9 cells were cultured with DMSO, with EGFR, RAF, MEK and ERK inhibitors at low dose (for 7 days) and with high dose (HD) of Osimertinib (200 nM), HD of Gefitinib (280 nM) and with 3D and 4D Combinations (for 1 month), after which plates were stained and scanned; A representative image from 3 biologically independent replicates is displayed. c, EGFRi-resistant PC9 cells remain sensitive to MLD therapy. PC9, PC9-OR (Osimertinib-resistant) and PC9-GR (Gefitinib-resistant) cells (see methods) were cultured with DMSO, with low doses of EGFR, RAF, MEK or ERK inhibitors, with 3D or 4D combinations or with HD of Gefitinib or Osimertinib for 4 days, after which cell viability was measured using CellTiter-Blue®. Standard deviation (SD) from 3 biologically independent replicates (each with 3 technical replicates) is plotted. d, MLD therapy blocks MAPK pathway in EGFRi-resistant PC9 cells. PC9, PC9-OR and PC9-GR cells were cultured with DMSO, HD of Osimertinib, HD of Gefitinib or with 3D or 4D combinations. Protein for western blotting was harvested after 24 hours of treatment; The level of pathway inhibition was measured by examining pERK and pRSK protein levels and the level of EGFR inhibition was measured by examining pEGFR protein levels in the western blot. Tubulin and Vinculin were used as loading control. A representative image from 2 biological replicates is displayed.

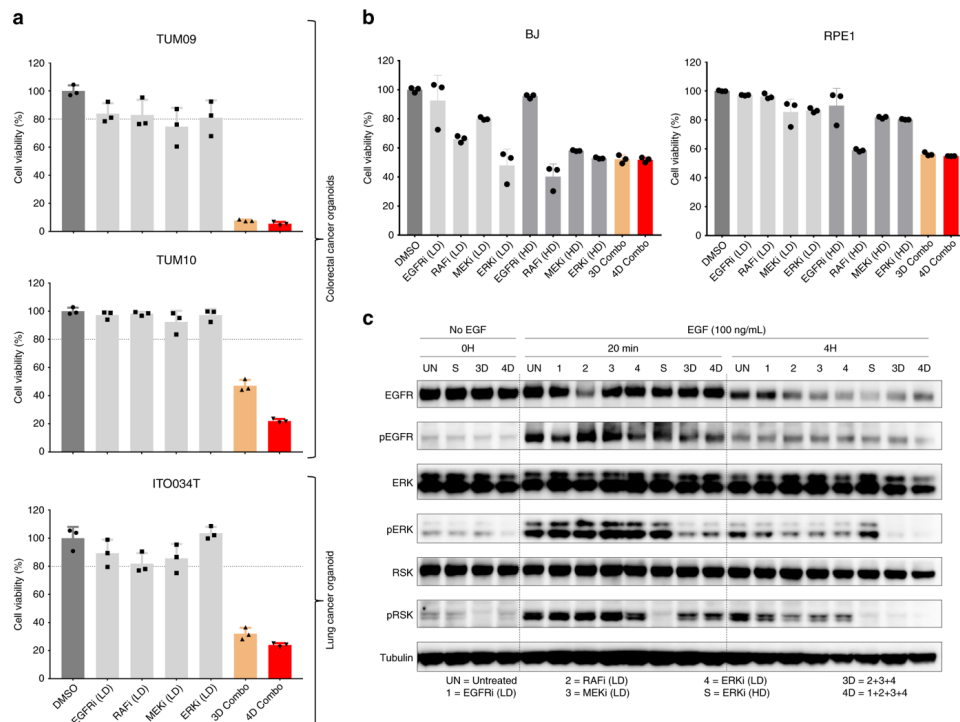


Figure 3: MLD therapy is effective in patient-derived organoids and is tolerated by normal cell lines. a, MLD therapy is effective in several colorectal and lung cancer patient-derived organoids. Organoids were cultured with DMSO, with EGFR, RAF, MEK and ERK inhibitors at LD and with 3D and 4D combos. After 5 days of drug treatment cell viability was measured using CellTiter-Glo®. SEM from 3 biologically independent replicates (each with 3 technical replicates) is plotted. b, Cell viability of normal cells is much less affected by MLD therapy than tumour cells. BJ and RPE1 cells were treated with DMSO, with EGFR, RAF, MEK and ERK inhibitors at low and high doses and with 3D and 4D Combos (using the LD and HD concentrations determined for PC9 cells). After 4 days of drug treatment cell viability was measured. SD from 3 replicates is plotted. c, MLD therapy allows pulsed signaling in normal cells. BJ cells, after overnight starvation, were treated with the indicated inhibitors/concentrations for 2 hours, after which EGF (100 ng/mL) was added. Cells were harvested before, 20 minutes and 4 hours after EGF stimulation. The level of pathway inhibition was measured by examining pERK and pRSK protein levels. The level of EGFR inhibition was measured by examining pEGFR protein levels in the western blot. Tubulin was used as loading control. A representative image from 2 biological replicates is displayed.

One of the major concerns when using multiple drugs in combination is the possible toxicity to normal tissues (87). To test the effect of the MLD strategy on “normal” (non-tumorigenic) cell lines we used primary human BJ (fibroblast) and RPE1 (retinal pigment epithelium) cells. Upon 3D and 4D MLD drug combination treatment, cell viability was reduced, but to a much lesser extent than in cancer cells. This indicates that the MLD strategy might be tolerated by normal tissues (Fig. 3b). Since the MAPK pathway is rich in cross-talk and feedback control circuits (88,89), we also tested how a pulse of signalling through the EGFR pathway would

be affected by 3D or 4D MLD treatment. We serum-starved BJ cells overnight and then incubated with 3D or 4D MLD drug combinations for two hours. After this, cells were stimulated with 100 ng/ml of EGF in the presence of 3D or 4D drug combinations. Twenty minutes after EGF stimulation, a significant amount of p-RSK was detected, which was no longer detected at 4 hours post EGF stimulation (Fig. 4c). These data suggest that the efficient inhibition of MAPK signalling exerted by 3D and 4D MLD treatment is the result of an effect of these drugs on homeostatic feedback/cross-talk signalling (88,90), as pulsatile signalling through the MAPK pathway seems to be much less affected than persistent signalling through an oncogene-activated MAPK pathway.

To address if the MLD strategy is effective in vivo, we used patient derived xenograft (PDX) tumours from four different patients who had developed resistance to first- or second-line therapy with EGFR inhibitors erlotinib or osimertinib (91) in the clinic by acquiring EGFR T790M mutation, KRAS mutation or MET amplification (Supplemental Table 3). For the in vivo studies we defined LD as 20% (for gefitinib and trametinib) and 30% (for LY3009120 and SCH772984 – due to the shorter half-lives) of the published maximum tolerated dose (MTD) in mice for each of the individual drugs (80,81,92,93). Osimertinib-resistant PDX-1 was implanted subcutaneously and orthotopically in the lungs. In both models, treatment with 3D or 4D combination resulted in a reduction in tumour volume, without associated toxicity (Fig. 4a-d). Interestingly however, treatment with 4D combo was slightly more effective than 3D combo. Due to this finding we focused the in vivo studies that followed on the 4D combination. In all PDX models tested we observed similar results to PDX-1, i.e., a reduction in tumour volume, without significant toxicity (Figs. 4e, f and Supplemental Fig. 4e). Additionally, in gefitinib-resistant models PDX-2 and PDX-3 we tested if it would be possible to acquire resistance to the 4D MLD combination therapy during a drug holiday. In both PDX models, re-starting of 4D MLD therapy after a drug holiday resulted in a second response to the drug combination, indicating that overt resistance had not developed in vivo (Figs. 4e, f).

We also implanted PC9 cells in nude mice and treated them with vehicle, with EGFR, RAF, MEK and ERK inhibitors individually at low dose and with 4D combination. The use of low dose regimens was inadequate to suppress PC9 tumour growth when used as single agents, but when used in combination we observed a sustained reduction in the tumour volume of PC9 xenografts over a period of 70 days, which was associated with an extended survival (Supplemental Fig. 4a, b). These observations are also supported by immunohistochemical staining of the tumours, which show decreased Ki67 (a proliferation marker) and pERK (MAPK activation) levels in the tumours treated with 4D combination (Fig. 4g). Significantly, mice treated with 4D combination did not show any significant signs of toxicity, assessed by the weight of the mice over time and by the morphology of the GI tract and bone marrow (Supplemental Figs. 4c,

f). In the clinic, the T790M mutation is already present (at very low percentages) in the majority of the tumours before undergoing anti-EGFR treatment (94,95). To mimic this scenario, we implanted in nude mice a mix of PC9 cells and PC9-GR cells (which are T790M positive) in a 9:1 ratio, respectively. Mice were treated with vehicle, with MTD of gefitinib and with 4D combination. Treatment with MTD of gefitinib resulted in a quick reduction of tumour volume which was followed by outgrowth of resistant cells, unlike the mice treated with 4D combination, where a sustained tumour control was observed (Supplemental Fig. 4d).

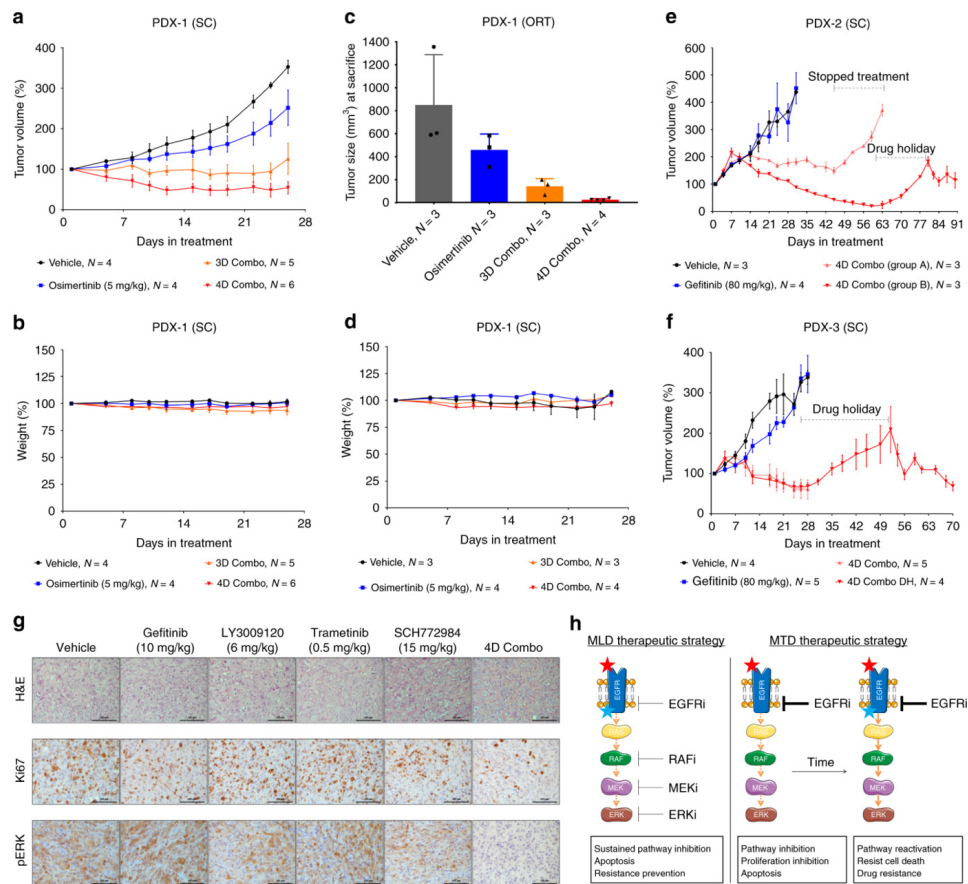


Figure 4: MLD therapy induces tumour regression without toxicity in vivo. a-f, Patient derived xenografts (PDX) are sensitive to MLD therapy. PDX tumours (see Supplemental Table 3) were implanted subcutaneously (a, e, f) or orthotopically in the lungs (c) of CrI:NU-Foxn1nu mice. PDX-1 was derived from a biopsy of a patient who became resistant to 3rd generation EGFR inhibitor osimertinib. PDX-2 and PDX-3 were derived from biopsies of patients who became resistant to 1st generation EGFR inhibitor erlotinib. PDX1 was implanted both subcutaneously (a) and orthotopically in the lungs (c). We defined the in vivo LD as 20-30% of the MTD for each of the individual drugs - gefitinib (10 mg/kg), LY3009120 (6 mg/kg), trametinib (0.5 mg/kg) and SCH72984 (15 mg/kg). After tumour establishment, mice were treated 5 days/week with vehicle, with osimertinib (5 mg/kg) and with 3D

or with 4D Combos for 26 days, after which mice were sacrificed. In (a) tumour volume percentages \pm SEM is shown, in (c) tumour size (mm³) at sacrifice \pm SEM is shown and in (b) and (c) the mice weight percentages \pm SEM is shown. (e) After tumour establishment, mice were treated 5 days/week with Vehicle (N=3), with gefitinib (80 mg/kg) (N=4) or with 4D Combo for 6 weeks (group A, N=3) or with 4D Combo for 8 weeks (group B, N=3). Mice treated with vehicle and gefitinib were sacrificed when tumours reached \sim 2000mm³. After 6 weeks, Group A was taken off treatment and mice were sacrificed when tumours reached \sim 2000mm³. After 8 weeks Group B was taken off treatment and was given 3 weeks of drug holiday. Mice were then treated for another 2 weeks with 4D combo, after which they were sacrificed. Tumour volume percentages \pm SEM is shown. (e) After tumour establishment, mice were treated 5 days/week with vehicle (N=4), with gefitinib (80 mg/kg) (N=5) or with 4D Combo (N=9) for 4 weeks, after which mice were sacrificed, except for 4 animals from the 4D Combo group. These 4 mice were spared and were given 3 weeks drug holiday (4D Combo DH group), followed by another 3 weeks of treatment, after which they were sacrificed. Tumour volume percentages \pm SEM is shown. g, Representative H&E, Ki67 and pERK stainings from tumour sections of PC9 xenografts are displayed. h, Schematic representation of the MLD therapy for the treatment of EGFR mutant NSCLC. While MTD therapy often results in secondary mutations which ultimately lead to resistance, MLD therapy is able to minimize therapeutic resistance even in EGFRi-resistant tumours without toxicity, both in vitro and in vivo.

Despite the significant tumour regressions observed in the in vivo experiments none of the mice were fully cured, unlike in the in vitro data where all the cells were killed by the 3D or 4D combinations. To study why this is the case we studied the pharmacokinetics and pharmacodynamics of the four drugs in vivo over time. We found that drug plasma concentrations of gefitinib and trametinib dropped relatively slowly (T_{1/2} 8 hours), but the pan-RAF and ERK inhibitors were less stable in plasma (T_{1/2} of 5 and 4 hours, respectively). A similar difference was seen for intra-tumoural drug concentrations (Supplemental Figs. 5a, b). Consistent with this, we observed a complete inhibition of pRSK in tumour biopsies two hours after 4D combination drug administration, which progressively decreased after 8 and 24 hours (Supplemental Fig. 5c). These data indicate that, unlike in the in vitro experiments, two of the four drugs were not present at a significant concentration during at least 12 hours of the 24-hour treatment cycle. As a result of this, a sustained MAPK pathway inhibition was not achieved in vivo, possibly explaining why we didn't achieve full tumour regressions. We tested this hypothesis in vitro, by removing RAF and ERK inhibitors from the treatment for approximately 8 hours every day. We found that, as hypothesized, when the drugs in the 3D or 4D combination were not present continuously the MLD therapy became less effective (Supplemental Fig. 5d). Finally, we tested whether there was any drug-drug interaction by measuring the half-lives of the drugs when given alone or in combination (Supplemental Fig. 5e). Overall, there is not any apparent drug-drug interaction, except for LY3009120, for which the half-life increases when given in the 4D Combo.

Discussion

We report here that treatment of EGFR mutant NSCLCs with MLD therapy effectively suppresses development of drug resistance, without associated toxicity. As such, our data challenge the common paradigm that patients should be treated with the MTD of a targeted agent. Our data are consistent with a model in which diffuse inhibition of an oncogenic pathway at multiple nodes reduces selective pressure on each of the nodes to mutate and thereby increase response time (Fig 4h). Our findings also challenge the current model for MAPK pathway signalling, which postulates that the MAPK kinase cascade functions to amplify signals. Such amplification cascade model is clearly at odds with the data obtained here in which a very partial inhibition of each of 4 nodes in this cascade adds up to complete pathway inhibition. Further mechanistic studies are required to better understand the efficacy of the MLD strategy.

Importantly, we show that tumours having the most common mechanisms of clinically-observed resistance to high dose standard of care EGFR inhibitors still respond to MLD therapy. Therefore, MLD treatment strategy appears especially promising for patients that have already developed resistance to all clinically used EGFR inhibitors, including osimertinib. In such resistant tumours, multiple metastases may be present having different resistance mutations. In this study we have shown that MLD therapy is effective in PDX models having diverse EGFR inhibitor resistance mechanisms, including EGFR T790M mutation, KRAS mutation, MET amplification and even SCLC transformation, highlighting that MLD therapy could apply to a diverse range of EGFR TKI resistant tumours. However, not all the resistance mechanisms have been tested and it is possible that some might not respond to MLD therapy. Indeed, in clinical practice, an MLD treatment strategy can only be tested in patients having developed resistance to standard-of-care EGFR inhibitors. We find in PDX models that 4D MLD is consistently somewhat better than 3D MLD, which may relate to the notion that not all EGFR alleles in the tumour may have acquired resistance mutations to the EGFR inhibitor therapy. Furthermore, it will be important to maintain osimertinib in an experimental MLD therapy trial, as this drug crosses the blood-brain barrier, and such late-stage patients may have (latent) brain metastases. We therefore suggest that clinical testing of the MLD strategy should include osimertinib.

While we never observed development of resistance to MLD therapy *in vivo*, even after long drug exposure, we did not achieve complete tumour regressions. This is most likely due to the short half-lives of the RAF and ERK inhibitors used in this study, which resulted in a situation in which we did not achieve a continuous pathway blockade. This may be improved by using continuous release formulations of these drugs, or by using drugs with longer half-lives.

The MLD therapy described here is fundamentally different from metronomic chemotherapy (96,97). In this latter scenario, low doses of chemotherapy are given at high frequency with the aim to suppress division of endothelial cells of the tumour vasculature. In the present MLD schedule, we target the MAPK pathway of the tumour itself, as growth inhibition in all cases parallels inhibition of the MAPK pathway (as judged by pRSK). Three-drug combinations given at MTD have been used before in pre-clinical (78) and clinical studies (10,77) for BRAFV600E mutant tumours, showing clear therapeutic benefits, but such regimen have an associated cost of toxicity.

The lack of significant toxicity of the MLD therapy in mice may be explained by the fundamentally different nature of MAPK pathway signalling between normal and EGFR mutant cancer cells. In the former, signalling is transiently activated when growth factors are present. In the latter, oncogenic mutations result in persistent activation of the pathway. Importantly, we show here that transient signalling in normal cells is, at least initially, not interrupted by MLD treatment (Fig. 3c). This may explain why long-term exposure of mice to MLD treatment is without major toxicity, as judged by lack of weight loss and lack of toxicity to gut epithelium and bone marrow. However, mice and humans are fundamentally different with respect to drug toxicity and only a phase I clinical trial will be able to fully assess the toxicity of this strategy in humans.

Extrapolation of dose from animals to humans based only on mg/kg conversion is difficult, since body surface area and differences in pharmacokinetics should also be taken into consideration. To convert the animal dose in mg/kg to human equivalent doses (HED) in mg/kg, it is recommended to divide by 12.3 (98). If we estimate the HED based on the low-doses used in our *in vivo* experiments for Gefitinib and Trametinib (where dosing in humans is known) using this approach then Gefitinib (10mg/kg in mice) corresponds to 57mg once daily in patients, which is approximately one quarter of the dose used in patients (250mg qd). And Trametinib (0.5mg/kg in mice) corresponds to 2,8mg once daily in patients, which is a bit higher than the dose used in patients (2mg qd). However, we also performed an *in vivo* experiment using lower concentrations of Gefitinib (1mg/kg) and Trametinib (0.1mg/kg) (Supplemental Figure 4d). These drug concentrations correspond to 2,5% of the human daily dose for gefitinib and 28% of the daily human dose of trametinib, using the calculation method of Nair mentioned above. These data indicate that with these further reduced concentrations of Gefitinib and Trametinib we still have a significant anti-tumor effect *in vivo*. Due to the difficulty in translating drug doses from mice to humans we feel that only a well-designed phase 1 trial can help assess the potential clinical utility of the MLD strategy proposed here.

Even though we focused mostly on EGFR mutant NSCLC, we have also shown that

2

the MLD strategy can potentially be effective in other tumour types. Overall, our findings challenge the current paradigm of using the maximum tolerated dose of single targeted cancer drugs and suggest that, instead, it might be more beneficial to use a combination of multiple drugs that target the oncogenically activated pathway using sub-optimal drug concentrations.

Materials and methods

Cell lines culture and drug-response assays

The PC9 cell line was obtained from ATCC. PC9OR (osimertinib-resistant) and PC9GR (gefitinib-resistant) cells were made by continuous (2 months) drug exposure of PC9 cells to 1 μ M osimertinib (AZD9291) and to 2 μ M gefitinib, respectively. Exome sequencing was performed to determine if any de novo genetic alterations had occurred (Supplemental Table 2). The HCC827, H3255, H3122, H2228, SKBR3, HCC1954, BJ and RPE1 cell lines were obtained from ATCC. And DiFi and Lim1215 cell lines were a gift from A. Bardelli (Torino, Italy). BJ and RPE1 cells were cultured in DMEM (Gibco 41966029). SKBR3 and HCC1954 which were cultured in DMEM/F-12 medium (Gibco 31331028). All the other cell lines were cultured in RPMI medium (Gibco 21875034). All the cell lines media were supplemented with 10% FBS (Serana), 1% penicillin/streptomycin (Gibco 15140122) and 2 mM L-glutamine (Gibco 25030024). All cell lines were cultured at 37°C and with 5% CO₂. All cell lines were validated by STR profiling and mycoplasma tests were performed every 2-3 months.

All drug-response assays were performed in triplicate, using black-walled 384-well plates (Greiner 781091). Cells were plated at the optimal seeding density (Supplemental Table 1) and incubated for approximately 24 hours to allow attachment to the plate. Drugs were then added to the plates using the Tecan D300e digital dispenser. 10 μ M phenylarsine oxide was used as positive control (0% cell viability) and DMSO was used as negative control (100% cell viability). Four days later, culture medium was removed and CellTiter-Blue (Promega G8081) was added to the plates. After 1-4 hours incubation, measurements were performed according to manufacturer's instructions using the EnVision (Perkin Elmer).

Organoid culture and drug-response assays

Colorectal (CRC) and non-small cell lung cancer (NSCLC) organoids were established and handled as previously described¹. All drug-response assays were performed in replicate, each by independent researchers. PDOs were mechanically and enzymatically dissociated into single cells, pipetted through a 40 μ M cell strainer, and re-plated to allow for organoids formation. At day 4 PDOs were collected,

2

Cultrex was removed by incubation of the cell pellet in 1 mg/ml dispase II (Sigma D4693) for 15 minutes. Whole organoids were counted using a hemocytometer and trypan blue. PDOs were resuspended in 1:3 Advanced Dulbecco's Modified Eagles Medium with Nutrient Mixture F-12 Hams (Ad-DF) (Invitrogen 12634), supplemented with 1% penicillin/streptomycin (Invitrogen 15140122), 1% HEPES (Invitrogen 15630056) and 1% GlutaMAX (Invitrogen 35050) (Ad-DF+++):Cultrex at a concentration of 20 organoids/ μ l. Five μ l/well was dispensed in clear-bottomed, white-walled 96-well plates (Greiner Bio-One 655098) and overlaid with 200 μ l CRC or NSCLC culture medium. We generated 10-step dose response curves using the Tecan D300e digital dispenser, interpolated IC₂₀ values and re-screened organoids in presence of a range of concentration around the IC₂₀ of each drug separately and in 3D and 4D Combos. In addition, we re-performed the dose-response curves to control for variation between experiments. Read-out was performed at day 10 in the positive control (10 μ M phenylarsine oxide), negative control (DMSO), and the drug-treated wells. Quantification of cell viability was done by replacing the CRC medium with 50 μ L Cell-TiterGlo 3D (Promega G9681) mixed with 50 μ L Ad-F+++ . Measurements were performed according to manufacturer's instructions on an Infinite 200 Pro plate reader (Tecan Life Sciences) with an integration time of 100 ms.

Compounds, reagents and antibodies

Gefitinib (100140), LY3009120 (206161), trametinib (201458), SCH772984 (406578), osimertinib (206426), crizotinib (202222), lapatinib (100946), BKM120 (204690), MK2206 (201913) and AZD8055 (200312) were purchased from MedKoo Biosciences. Erlotinib (S7786), BGB-283 (S7926), selumetinib (S1008) and LY-3214996 (S8534) were purchased from Selleckchem. Annexin V-FITC Apoptosis Staining Detection Kit was purchased from Abcam (ab14085).

Antibodies against Tubulin (T9026) and Vinculin (V9131) were purchased from Sigma; antibodies against EGFR (4267), pERK (4377), ERK (9102) and RSK (8408) were purchased from Cell Signalling; antibody against pRSK (04-419) was purchased from Millipore; antibody against pEGFR (ab5644) was purchased from Abcam.

Colony formation and IncuCyte cell proliferation assays

Cells were seeded in the appropriate density (Supplemental Table 1) in 6-well plates. Cells were incubated for approximately 24 hours to allow attachment to the plates, after which drugs were added to the cells using the Tecan D300e digital dispenser as indicated. The culture media/drugs were refreshed every 3/4 days. When control wells (DMSO) were confluent (unless otherwise stated in the text) cells were fixed using a solution of 2% formaldehyde (Millipore 104002) diluted

in phosphate-buffered saline (PBS). Two hours later, they were stained, using a solution of 0.1% crystal violet (Sigma HT90132) diluted in water. Not more than 10 minutes later the staining solution was removed, plates were washed with water left to dry overnight. Finally, plates were scanned and stored.

For IncuCyte proliferation assays, cells were seeded in 96-well plates and incubated overnight to allow attachment to the plates. Drugs were added to the cells using the Tecan D300e digital dispenser. Cells were imaged every 4 hours in the IncuCyte ZOOM (Essen Bioscience). Phase-contrast images were collected and analysed to detect cell proliferation based on cell confluence. For cell apoptosis, IncuCyte® Caspase-3/7 green apoptosis assay reagent (Essen Bioscience 4440) was also added to culture medium and cell apoptosis was analysed based on green fluorescent staining of apoptotic cells.

Western Blots

After the indicated culture period, cells were washed with chilled PBS and then lysed with RIPA buffer (25mM Tris - HCl pH 7.6, 150mM NaCl, 1% NP-40, 1% sodium deoxycholate, 0.1% SDS) containing protease inhibitors (Complete (Roche) and phosphatase inhibitor cocktails II and III). Samples were then centrifuged for 10 minutes at 14.000 rpm at 4°C and supernatant was collected. Protein concentration of the samples was normalized after performing a Bicinchoninic Acid (BCA) assay (Pierce BCA, Thermo Scientific), according to the manufacturer's instructions.

Protein samples (denatured with DTT followed by 5 minutes heating at 95°C) were then loaded in a 4-12% polyacrylamide gel. Gels were run (SDS-PAGE) for approximately 60 minutes at 165 volts. Proteins were then transferred from the gel to a polyvinylidene fluoride (PVDF) membrane, using 330 mA for 90 minutes. After the transfer, membranes were placed in blocking solution (5% bovine serum albumin (BSA) in PBS with 0,1% Tween-20 (PBS-T). Subsequently, membranes were probed with primary antibody in blocking solution (1:1000) and left shaking overnight at 4°C. Membranes were then washed 3 times for 10 minutes with PBS-T, followed by one hour incubation at room temperature with the secondary antibody (HRP conjugated, 1:10000) in blocking solution. Membranes were again washed 3 times for 10 minutes in PBS-T. Finally, a chemiluminescence substrate (ECL, Bio-Rad) was added to the membranes and the Western Blot was resolved using the ChemiDoc (Bio-Rad).

Mouse xenografts studies

All animal experiments were approved by the Animal Ethics Committee of the Netherlands Cancer Institute or by the Animal Ethics Committee of the Institut Català d'Oncologia and performed in accordance with institutional, national and European guidelines for Animal Care and Use.

PC9 cell line xenografts: One million PC9 cells were resuspended in PBS and mixed 1:1 with matrigel (Corning 354230). Cells were injected subcutaneously into the posterior flanks of 7-week-old immunodeficient BALB/cAnNRj-Foxn1nu mice (half male and half female; Janvier Laboratories, The Netherlands). Tumour formation was monitored twice a week. Tumour volume, based on calliper measurements, was calculated by the modified ellipsoidal formula (tumour volume = $1/2(\text{length} \times \text{width}^2)$). When tumours reached a volume of approximately 200 mm³, mice were randomized into the indicated treatment arms. Vehicle, gefitinib, LY3009120, trametinib, SCH772984 or the combination of the 4 inhibitors were formulated in DMSO: Kolliphor EL (Sigma 27963): Saline solution, in a ratio of (1:1:8). Mice were treated 5 days a week (Monday to Friday) at the indicated doses by intraperitoneal injection.

Patient-derived xenografts (PDX) and orthotopic xenograft (PDOX): Primary tumours were obtained from Bellvitge Hospital (HUB) and the Catalan Institute of Oncology (ICO) with approval by the Ethical Committee. Ethical and legal protection guidelines of human subjects, including informed consent from the patient to implant the tumour in mice, were followed. PDX-1 was generated from a lung adenocarcinoma biopsy from a patient who was treated with Erlotinib (first line), Gefitinib + Capmatinib (second line) and Cisplatin+Pemetrexed (third line). This tumour has an EGFR mutation (del19) and MET amplification. PDX-2 was generated from a lung adenocarcinoma biopsy from a patient who was treated with Erlotinib (first line), Gefitinib + Capmatinib (second line) and Carboplatin+Gemcitabine and Nivolumab (third line). This tumour has an EGFR mutation (L858R) and MET amplification. PDX-3 was generated from a lung adenocarcinoma biopsy of a brain metastasis from a patient who was treated with Erlotinib (first line) and Osimertinib (second line). PDX-4 was generated from a lung adenocarcinoma biopsy from a patient who was treated with Afatinib (first line) and CBDCA + pemetrexed (second line). This tumour has a germline p53 mutation and an EGFR mutation (del19). Tumours were isolated and implanted subcutaneously (or orthotopically, in the lungs, in the case of PDX-3) into Crl:NU-Foxn1nu mice by following previously reported procedures^{2,3}. In the subcutaneous models, tumour volume was monitored twice a week by a digital caliper. When tumours reached a volume of approximately 200-600 mm³, mice were randomized into the indicated treatment arms. In the orthotopic model, tumours were left to grow for 2 weeks, followed by 26 days of treatment. Vehicle, gefitinib, osimertinib or the 3D and 4D Combos were formulated in DMSO: Kolliphor EL (Sigma 27963): Saline solution, in a ratio of (1:1:8). Mice were treated 5 days a week (Monday to Friday) at the indicated doses by intraperitoneal injection.

In vivo pharmacokinetics and pharmacodynamics studies

Plasma and tumour samples were assayed by liquid chromatography triple quadrupole mass spectrometry (LC-MS/MS) using an API4000 detector (Sciex) for the simultaneous determination of Gefitinib (MRM: 447.4/128.1), LY3009120 (MRM: 425.5/324.2), Trametinib (616.3/491.2) and SCH772984 (MRM: 588.4/320.2). Gefitinib-d8 (MRM: 455.4/136.3) was used as internal standard. LC separation was achieved using a Zorbax Extend C18 column (100 × 2.0 mm; ID). Mobile phase A and B comprised 0.1% formic acid in water and methanol, respectively. The flow rate was 0.4 ml/min and a linear gradient from 20%B to 95%B in 2.5 min, followed by 95%B for 2 min, followed by re-equilibration at 20%B for 10 min was used for elution. Sample pre-treatment was accomplished by mixing 5 µl (plasma) or 25 µl (tumour homogenate) with 30 or 150 µl, respectively, of formic acid in acetonitrile (1+99) containing the internal standard. After centrifugation, the clear supernatant was diluted 1+4 with water and 50 µl was injected into the LC-MS/MS system.

The plasma/tumour samples were harvested at the time points indicated in supplemental figure 5. Blood samples were obtained by tail cut (at 2h and 8h time points) and by cardiac puncture at the 24h time point. Samples were collected on ice in tubes containing potassium EDTA as anticoagulant. The tubes were immediately cooled in melting ice and centrifuged (10 minutes, 5000g, 4°C) to separate the plasma fraction, which was transferred into clean vials. For the tumours samples, the mice were sacrificed by cervical dislocation, the tumour was dissected and frozen at -80°C. Half of the tumour was then lysed mechanically with RIPA buffer and lysates were analysed by Western blot. The other half was weighed and homogenized in 1 ml of ice-cold 1% of BSA in water and stored at -20°C until further analysis.

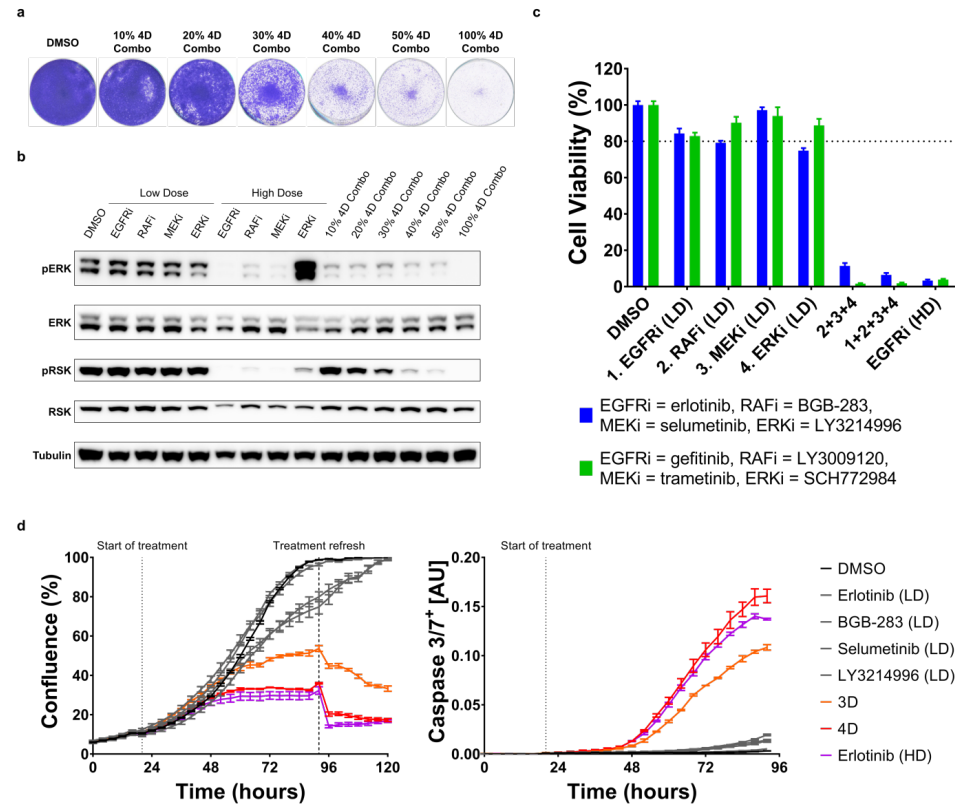
Acknowledgements

We thank A. Bardelli (Torino, Italy) for gift of cell lines and the facilities of The Netherlands Cancer Institute: Mouse Clinic – Intervention Unice (Natalie Proost, Bjorn Siteur, Bas van Gerwen, Charlotte Baak, Renske Grimmerink, Rebecca Theeuwssen and Marieke van de Ven), Robotics and Screening Center (Ben Morris and Roderick Beijersbergen), Clinical Pharmacology (Levi Buil and Artur Burylo), Experimental Animal Pathology, Flow Cytometry and Sequencing. We also thank Richard Marais for discussions. This work was supported by a grant from the Dutch Cancer Society through the OncoCode Institute.

Alberto Villanueva was supported by the Fondo de Investigaciones Sanitarias, FIS (PI16-01898 (to A.V.)), and by the Spanish Association Against Cancer, AECC (CGB14142035THOM) and Ideas Semilla project (IDEAS098VILL-IDEAS16) and

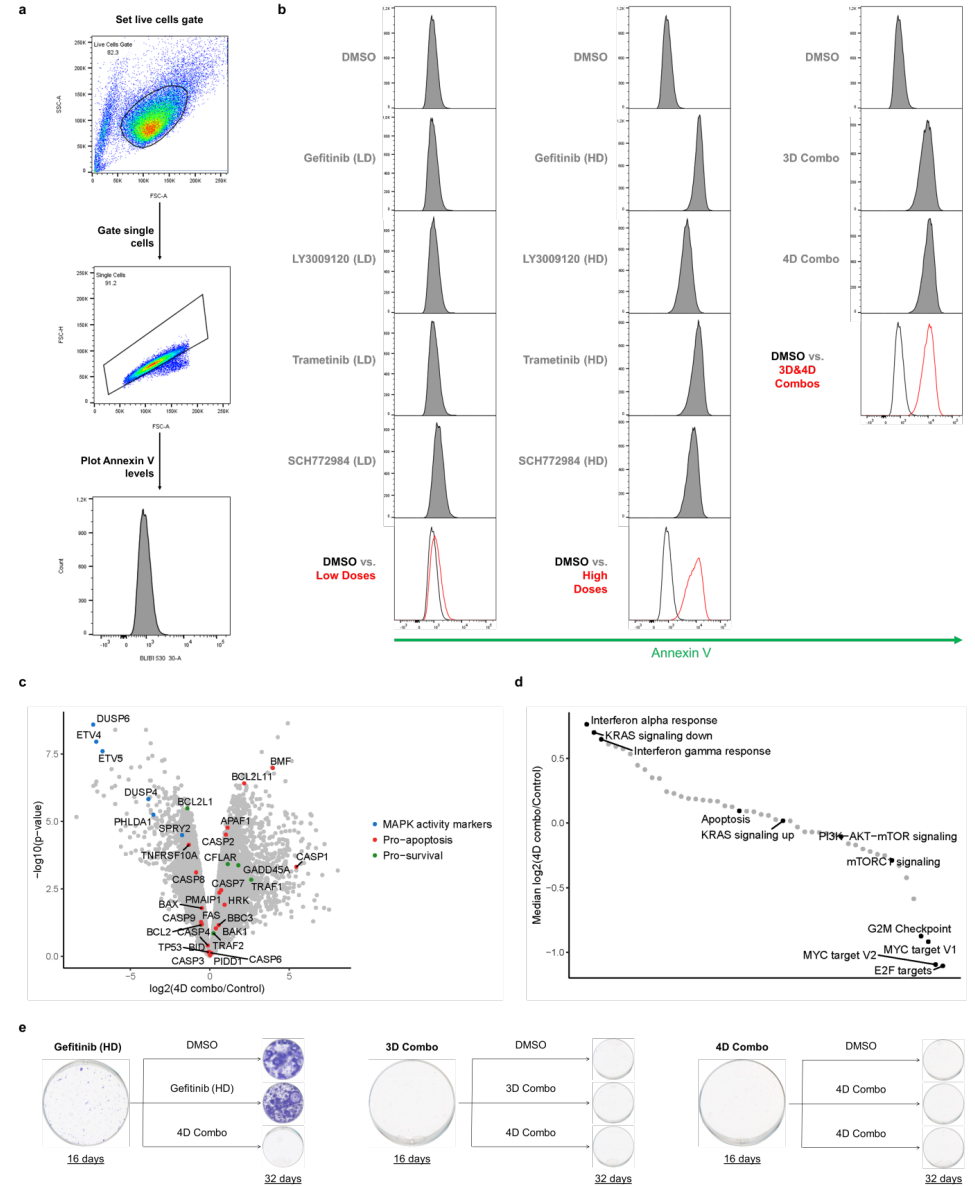
Generalitat de Catalunya (2014SGR364) (to A.V.). L.F. received a European Union's Horizon 2020 research and innovation programme under the Marie Skłodowska-Curie, grant agreement number 799850 (L.F.). E.N. received support from the SLT006/17/00127 grant, funded by the Department of Health of the Generalitat de Catalunya by the call "Acció instrumental d'intensificació de professionals de la salut" and the AECC grant from Junta Provincial de Barcelona. We thank CERCA Program/Generalitat de Catalunya for their institutional support and grant 2017SGR448.

Supplementary Information



Supplementary Figure 1: A drug concentration threshold is necessary for the efficacy of MLD therapy, which is not drug-specific.

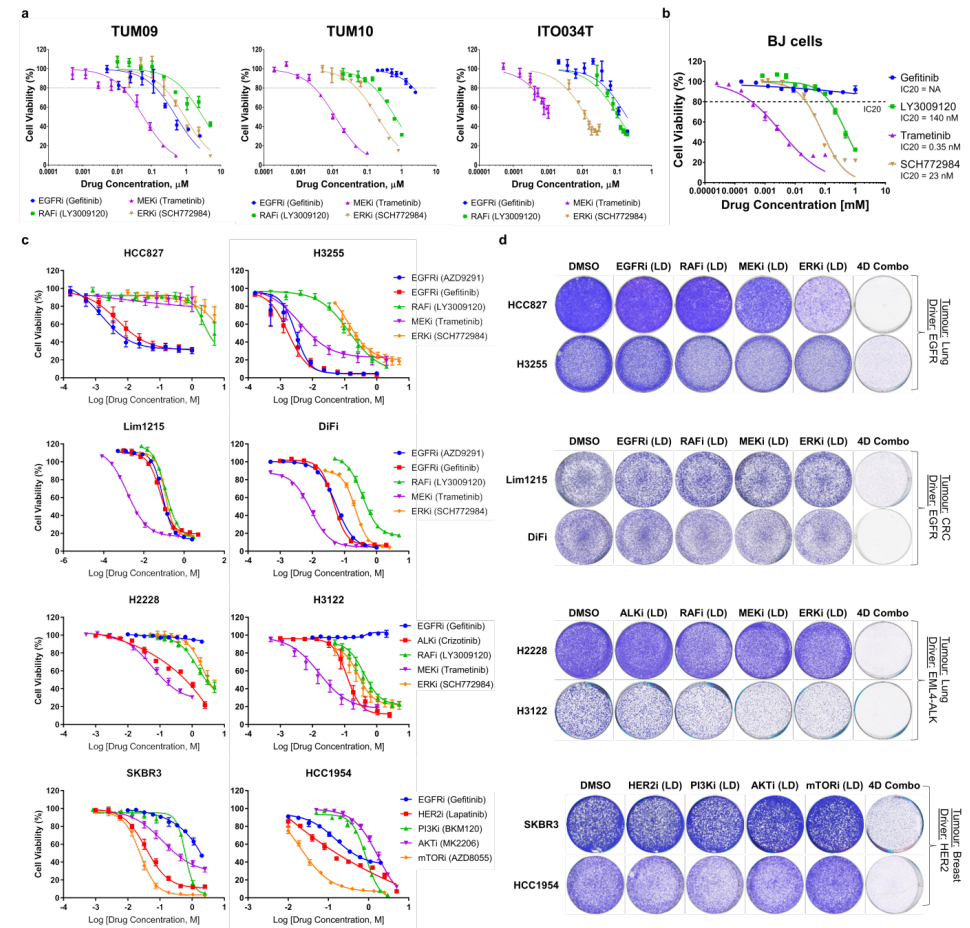
a, Dilution of 4D Combo results in incomplete inhibition of proliferation. PC9 cells were plated and incubated overnight to allow attachment to the plate. Cells were then treated with DMSO, with 4D Combo and with the indicated dilutions of 4D Combo. Cells were cultured for 7 days, after which plates were stained and scanned; A representative image from 3 biologically independent replicates is displayed. b, Dilution of 4D Combo results in incomplete MAPK pathway inhibition. PC9 cells were cultured with DMSO, with EGFR, RAF, MEK and ERK inhibitors both at low and at high doses, with 4D Combo and with different dilutions of 4D combo. Protein for western blotting was harvested after 48 hours of treatment. The level of pathway inhibition was measured by examining pERK and pRSK protein levels; Tubulin was used as loading control. A representative image from 2 biological replicates is displayed. c, d, MLD therapy efficacy is not drug-specific. PC9 cells were plated and incubated overnight to allow attachment to the plate; Cells were then treated with two different inhibitors for each of the nodes in the MAPK pathway (gefitinib or erlotinib as EGFRi, LY3009120 or BGB-283 as RAFi, Trametinib or selumetinib as MEK and SCH772984 or LY-3214996 as ERKi) as indicated. In (d) cell viability was measured using CellTiter-Blue® after 4 days of treatment. Standard deviation (SD) from 3 biologically independent replicates (each with 3 technical replicates) is plotted. In (e) the confluence (left) and caspase 3/7 activation (right) over time was measured by the IncuCyte®; 3 days after the first treatment the drugs and media were refreshed. SEM from 3 replicates is plotted.



Supplementary Figure 2: MLD therapy induces apoptosis and prevents drug resistance.

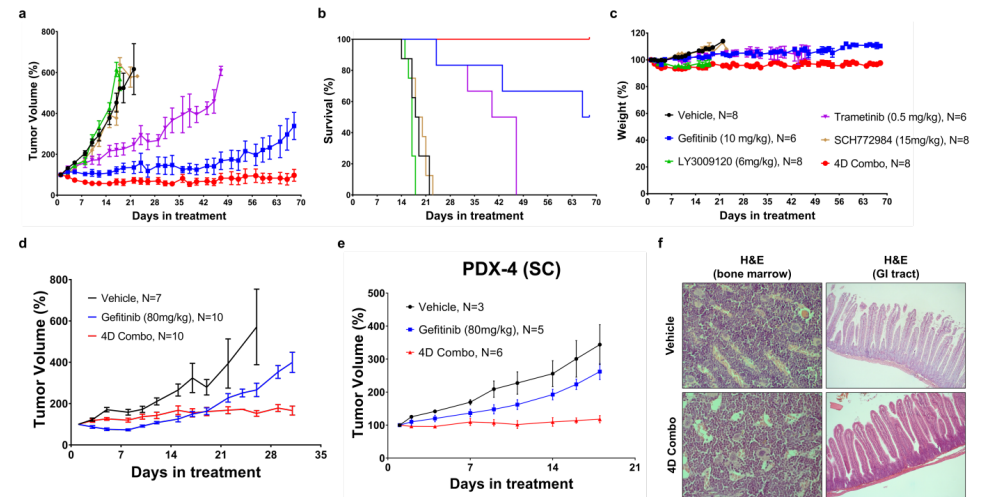
a, Gating strategy used for (b). Live cells were gated from all events; then single cells were gated from the live cells and, finally, Annexin V levels were plotted from the single cells. b, 3D and 4D Combos induce apoptosis at comparable levels as high doses of each inhibitor in PC9 cells. PC9 cells were stained with Annexin V-FITC Apoptosis Staining/Detection kit (ab14085) after 48 hours of drug treatment. The Annexin V levels were measured by flow cytometry (BD LSRFortessa) and analysed using FlowJo 10. c, d, Transcriptome analysis of PC9 cells treated with 4D combo. (c) Volcano plot of differential gene expression analysis. (d) Median log₂-fold change of the MSigDB hallmark gene-sets, ranked from high to low. For (c) and (d) PC9 cells were treated with DMSO for 48 hours or with 4D combo for 48 or 72 hours. Experiments were performed in duplicates. Because the difference between 48 and 72 hour 4D combo

treatment was comparable to the variability between replicates, the four MLD treated samples were considered replicates. Differential expression analysis was performed using the R-package limma (99) and the MSigDB hallmark gene-sets analysis was performed using version 6.2 of MSigDB (100). e, MLD therapy prevents the acquisition of drug resistance in PC9 cells. PC9 cells were cultured with high dose of gefitinib (280 nM) and with 3D and 4D Combos (4 plates per condition). After 16 days in culture, one plate was fixed and stained. From the remaining three plates (per condition) one was switched to DMSO treatment, the other was switched to 4D Combo and the third one continued with the previous treatment. Sixteen days later (after 32 days of “treatment” in total) cells were fixed and stained and then plates were scanned. A representative image from the 3 replicates performed is displayed.



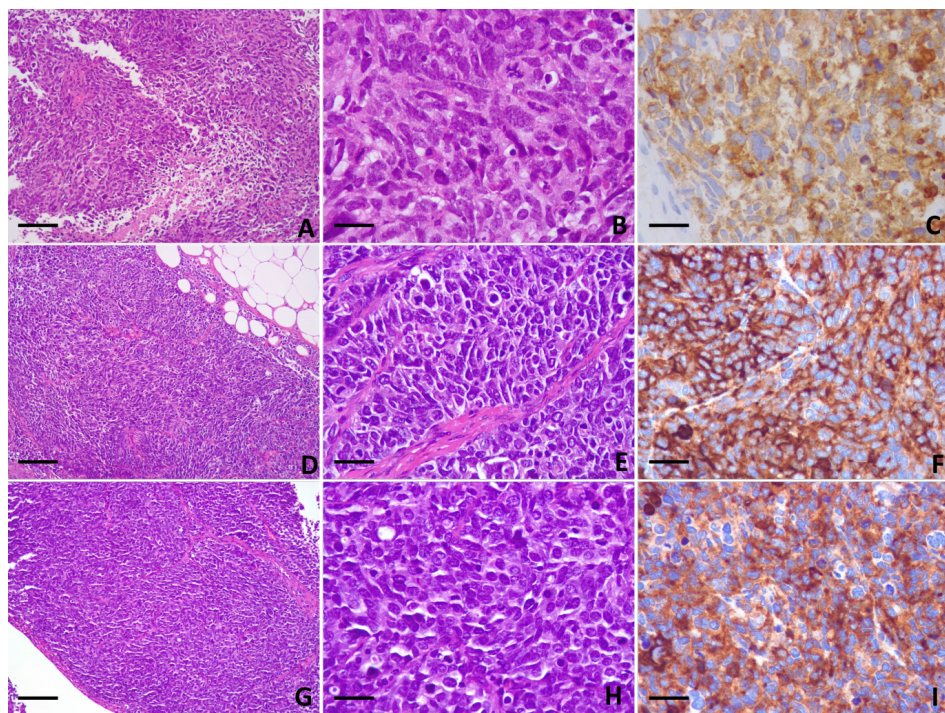
Supplementary Figure 3: MLD therapy is effective in multiple cancer cell lines.

a-c, Dose-response curves across the organoid and cell line panel. (a) Organoids were cultured with DMSO or with the different inhibitors and after 5 days of drug treatment cell viability was measured using CellTiter-Glo®. SEM from 3 biologically independent replicates (each with 3 technical replicates) is plotted. (b, c) Cells were plated in 384-well plates. Drugs were added ~24h after plating; after 4 days of exposure to the drugs cell viability was measured using CellTiter-Blue®. SEM from 3 biologically independent replicates (each with 3 technical replicates) is plotted. Low doses (IC20s) were then determined (see Supplemental Table 1). d, MLD therapy is effective in several cell lines/tumour types. HCC827, H3255, Lim1215, DiFi, H2228, H3122, SKBR3 and HCC1954 cell lines were treated with DMSO, with the indicated pathway inhibitors at low dose and with their combination (4D Combo). After 10 days of treatment plates were stained and scanned; A representative image from 3 biologically independent replicates is displayed.



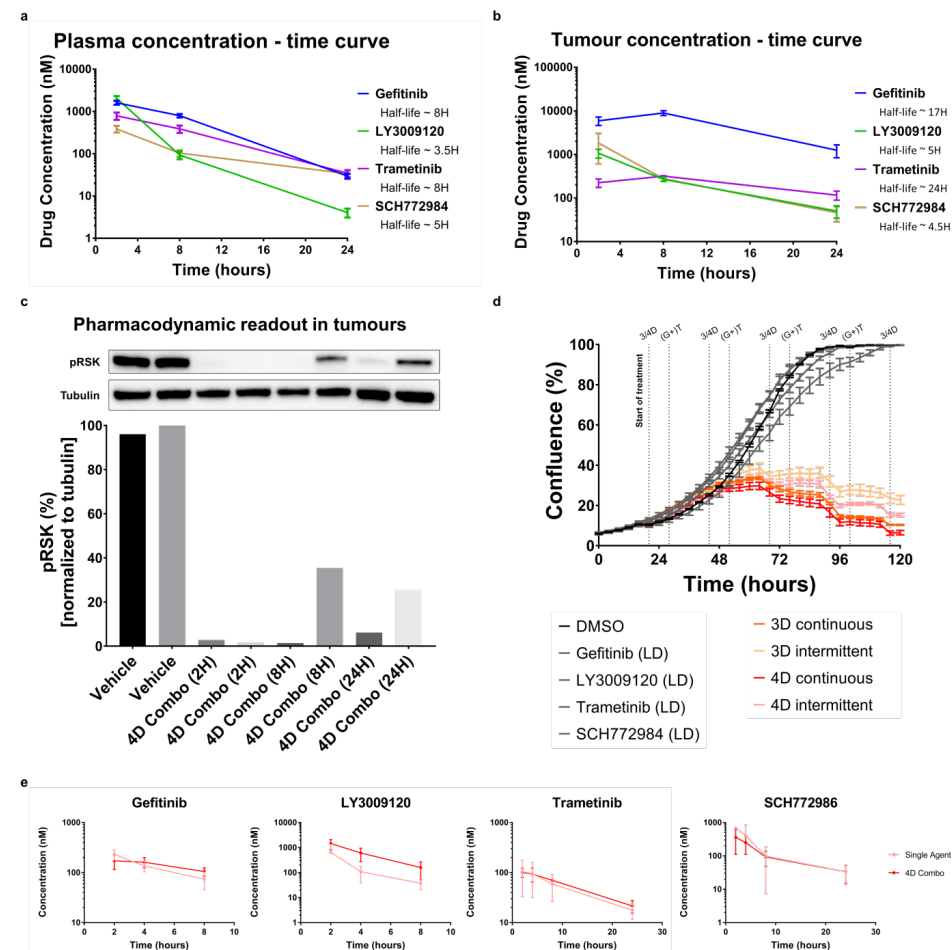
Supplementary Figure 4: MLD therapy reduces tumour volume in vivo without toxicity.

a-d, PC9 xenografts are sensitive to 4D Combo without toxicity. (a-c) PC9 cells were grown as tumour xenografts in BALB/cAnNRj-Foxn1nu mice. After tumour establishment (200–250 mm³), mice were treated 5 days/week with vehicle, gefitinib (10 mg/kg), LY3009120 (6 mg/kg), trametinib (0.5 mg/kg), SCH772984 (15 mg/kg) or the combination of the 4 inhibitors (4D Combo) for 10 weeks. In (a) the mean tumour volume percentages ± SEM is shown; In (b) the Kaplan-Meier survival curve is shown; In (c) the mice weight percentages ± SEM is shown. (d) PC9 cells and PC9GR cells were mixed in a 9:1 ratio, respectively, and were grown as tumour xenografts in BALB/cAnNRj-Foxn1nu mice. After tumour establishment (200–250 mm³), mice were treated 5 days/week with vehicle, with the MTD of gefitinib (80 mg/kg) and with 4D Combo – cocktail containing gefitinib (1 mg/kg), LY3009120 (6 mg/kg), trametinib (0.1 mg/kg), SCH772984 (15 mg/kg) for 30 days. The mean tumour volume percentages ± SEM is shown. e, EGFR and p53 mutant PDX responds to 4D Combo. PDX-4 was generated from a biopsy of patient with EGFR and TP53 mutation that progressed after afatinib and chemotherapy treatment. After tumour establishment, mice were treated 5 days/week with Vehicle (N=3), with gefitinib (80 mg/kg) (N=5) or with 4D combo (N=6) – cocktail containing gefitinib (10 mg/kg), LY3009120 (6 mg/kg), trametinib (0.5 mg/kg) and SCH772984 (15 mg/kg) (N=6) for 18 days. Tumour volume percentages ± SEM is shown. f, Representative H&E stainings from the GI tract and the bone marrow of the PC9 xenografts in a-c are displayed.



Supplementary Figure 5: Small cell lung cancer transformation of PDX4.

Biopsy samples from either the primary human lung cancer (a-c), the subcutaneous xenograft of this tumor (d-f) or the orthotopic xenograft of this tumor (g-i) were fixed and stained with H&E. Immunohistochemical staining with synaptophysin antibody was performed to assess small cell lung cancer transformation. a-c: Small cell carcinoma metastatic to a mediastinal lymph node. The tumor has a sheet-like growth pattern. The tumor cells have ovoid or spindled nuclei and scant cytoplasm. Nuclear chromatin is finely granular and nucleoli are absent. There are brisk mitotic activity with atypical mitotic figures. d-f: subcutaneous xenograft of lung cancer shown in a-c. g-i: orthotopic xenograft of lung cancer shown in a-c. a, d and g: original magnification 100X, scale bars 200 μ m. b, c, e, f, h, i: original magnification 400X, scale bars 50 μ m. a, b, d, e, g, h: H&E stain. c, f, i: immunohistochemical stain for synaptophysin.



Supplementary Figure 6: PK-PD studies in PC9 xenografts reveal different half-lives of the inhibitors. a-d, Pharmacokinetic and pharmacodynamics studies in PC9 xenografts. In (a-c) PC9 cells were injected (bilaterally) subcutaneously in BALB/cAnNRj-Foxn1nu mice. After tumour establishment (~200 mm³), mice were treated with vehicle (N=4) or 4D Combo (N=12). Vehicle mice were sacrificed 2H after treatment; Mice treated with 4D combo were sacrificed 2, 8 and 24h after treatment, respectively; 4 mice were sacrificed per time point. Blood and tumours were harvested; half of the tumour was used for the PD study and the other half was used for biochemical analysis. The drug concentrations in the blood and in the tumours were determined by mass spectrometry. In (a) the concentration of the individual drugs in the plasma is displayed and in (b) the concentration of the individual drugs in the tumours is displayed; SEM is plotted. In (c) the level of pathway inhibition in the tumours was measured by examining pRSK protein levels in the western blot (WB). Tubulin was used as loading control. WB was quantified using the Image Lab software, from Bio Rad. d, Intermittent MLD therapy is less efficient in reducing cell growth in PC9 cells. PC9 cells were plated and incubated overnight to allow attachment to the plate. Cells were then treated with DMSO, with EGFR, RAF, MEK, ERK inhibitors at low dose, with 3D Combo or with 4D Combo. To mimic the availability of the drugs in vivo, in some of the 3D and 4D combo replicates the RAF and ERK inhibitors were removed from the culture media for approximately 8 hours every day (called intermittent MLD therapy). Confluence over time was measured by the IncuCyte®. SEM from 3 replicates is plotted. e, BALB/cAnNRj-Foxn1nu mice were treated with gefitinib (1mg/kg, N=3), LY3009120 (6mg/kg, N=3), trametinib (0,1mg/kg, N=3), SCH72984 (15mg/kg, N=3) or 4D Combo (N=3) and blood was harvested 2, 4, 8 and 24h after treatment. The drug concentrations in the blood was determined by mass spectrometry. The concentration of the drugs in the plasma given as single agent or in the 4D Combo is displayed.

Table with columns: Cell Line Name, Tissue of Origin, Driver, Plating density (384-well plates), Plating density (96-well plates), Plating density (6-well plates), EGFRi, RAFI, MEK1i, ERK1i, EGFRi, RAFI, MEK1i, ERK1i, EGFRi, RAFI, MEK1i, ERK1i, EGFRi, RAFI, MEK1i, ERK1i, EGFRi, RAFI, MEK1i, ERK1i, EGFRi, RAFI, MEK1i, ERK1i. Includes cell lines like PC9/PC9GR, HCC827, H3255, H3122, H2228, DFI, Lim1215, SKBR3, HCC1954, ITO034T, TUM09, TUM110.

Supplementary Table 1: Compendium of drivers, plating density, low doses and high doses of the cell lines and organoids used in the study.

Table with columns: #, Gene, Mutation, #, Gene, Mutation, #, Gene, Mutation, #, Gene, Mutation. Lists 55 genes with their respective mutations in PC9OR and PC9GR cell lines.

Supplementary Table 2: Compendium of de novo mutations found in PC9OR and PC9GR by Exome Sequencing

Table with columns: Age, Gender, Smoking info, Diagnostic, EGFR mutation, Treatment 1 (T1), Alterations after T1, Treatment 2, Treatment 3, Source of PDX, Known alterations in the PDX. Summarizes patient and treatment data for four PDX lines (PDX-1 to PDX-4).

Supplementary Table 3: Compendium of patient, tumour, treatments and mutations information for all the PDXs used in the study.

3

Identifying selective multi-drug combinations using Comparative Network Reconstruction

Evert Bosdriesz^{1,2}, João M. Fernandes Neto², Anja Sieber^{3,4}, René Bernards²,
Nils Blüthgen^{3,4,5}, and Lodewyk F.A. Wessels^{2,6}

¹Computer Science Department, Center for Integrative Bioinformatics (IBIVU), Vrije Universiteit
Amsterdam, The Netherlands

²Division of Molecular Carcinogenesis, The Oncode Institute, The Netherlands Cancer Institute,
Amsterdam, the Netherlands

³Institute of Pathology, Charité Universitätsmedizin, Berlin, Germany

⁴IRI Life Sciences, Humboldt University of Berlin, Berlin, Germany

⁵Berlin Institute of Health, Berlin, Germany

⁶Faculty of EEMCS, Delft University of Technology, Delft, the Netherlands

Abstract

Inhibition of aberrant signalling with targeting inhibitors is an important treatment strategy in cancer. Unfortunately, due to compensatory mechanisms, response to single drug treatment is often short-lived. Multi-drug combinations have the potential to mitigate compensatory mechanisms, but to avoid toxicity such combinations must be selective and the dosage of the individual drugs should be as low as possible. Since the search space of possible multi-drug combinations and their optimal dosage is enormous, this calls for an efficient approach to identify the most promising drug combinations and dosages. To meet this challenge, we developed a combined experimental and computational pipeline. For the experimental component, we perform, for a given isogenic cell line pair, a limited set of drug perturbations and record pre- and post-treatment signalling states and longer term viability. In the computational component we employ these to reconstruct cell line specific signalling networks and map changes in signalling output to changes in cell viability. We then employ these models to prioritize selective low-dose, multi-drug combinations *in silico*, based on the mutation status of the cell line. As proof of principle, we applied this approach to a breast cell line and an isogenic clone with an activating PI3K mutation, for which we predicted and validated multiple selective multi-drug combinations. Remarkably, of the 30 combinations predicted to be selective, we were able to validate 25 (83%). Applying this pipeline to suitably chosen model systems will allow for the identification of biomarker-specific combination treatment regimens.

Introduction

The dependency of tumors on activated signaling pathways results in therapeutic responses to inhibitors that block pathway activity (74). However, resistance to such targeted inhibitors inevitably develops (42,101). Combinations of two targeted inhibitors can give more lasting clinical benefit, but resistance nonetheless emerges (43,102). Combining more than two drugs might further extend the duration of the response (103), but toxicity becomes a major concern when multiple drugs are combined at their maximum tolerated dose (MTD). Recently, we found that partial inhibition of three or four kinases by combining Multiple drugs at Low Dose (MLD) is surprisingly effective in receptor tyrosine kinase (RTK) driven tumors in multiple cancer types. It prevents the development of resistance, and it is well tolerated by mice (47). Others have also shown the potential of multi-drug (low dose) combinations in pre-clinical (48,79,104,105) and clinical (106,107) settings. These findings warrant further exploration of multiple-drug combination strategies and call for a systematic way to explore the opportunities, including optimizing the dosing of the different drugs. The combinatorial explosion of the search space – there are more than 2 million possible 4-way combinations of the 89 (as of 2017 (108)) FDA approved targeted inhibitors, and 24 billion if each drug is to be tested at 10 different concentrations – means that *in-vitro* testing of all combinations is infeasible and hence computational approaches are required to prioritize promising combinations. Nowak-Sliwinska and collaborators presented a “Feedback Systems Control” approach to explore the search-space of possible multi-drug combinations (105,109,110). While this approach is promising, the method does not optimize for selectivity and the obtained results lack a mechanistic underpinning, making it hard to assess to what extent the results will generalize. Another promising approach is building mathematical models of cellular signaling, based on a limited set of (perturbation) experiments (111–118). Unfortunately, current approaches suffer from two major shortcomings. First, only a very limited number of such modeling approaches focus on the difference between cells with different mutation profiles (111,119), which is critical for optimizing selectivity. Second, how inhibition of oncogenic signaling affects proliferation and apoptosis quantitatively, remains underexplored (117,118,120).

We therefore set out to establish and validate a combined experimental and computational pipeline to prioritize multi-drug low-dose combinations based on mathematical models of drug response (Fig 1). Importantly, we aimed to find combinations that are selective for cells with or without a particular mutation. To isolate the effect of the mutation, we used an isogenic cell line pair with and without a mutation. Specifically, we used MCF10A, a cell line derived from epithelial breast tissue (121), and an isogenic clone with the activating PI3K^{H1047R}-mutation

knocked in under its endogenous promoter (122). We measured the response of the MAPK and AKT pathway and cell viability after drug perturbations, and used the measurement to build mutant specific signaling networks models using Comparative Network Reconstruction, a method we recently developed (111). In addition, we parameterized the relation between signaling response and cell viability. Combining this allowed us to simulate the effect of arbitrary multi- drug combinations and thus to prioritize promising ones. Our models indicated that no drug combination would likely be selective for the PI3K-mutant cells, but low-dose multi-drug combinations that we predicted to be selective for the parental cells were indeed selective, which validated our computational pipeline.

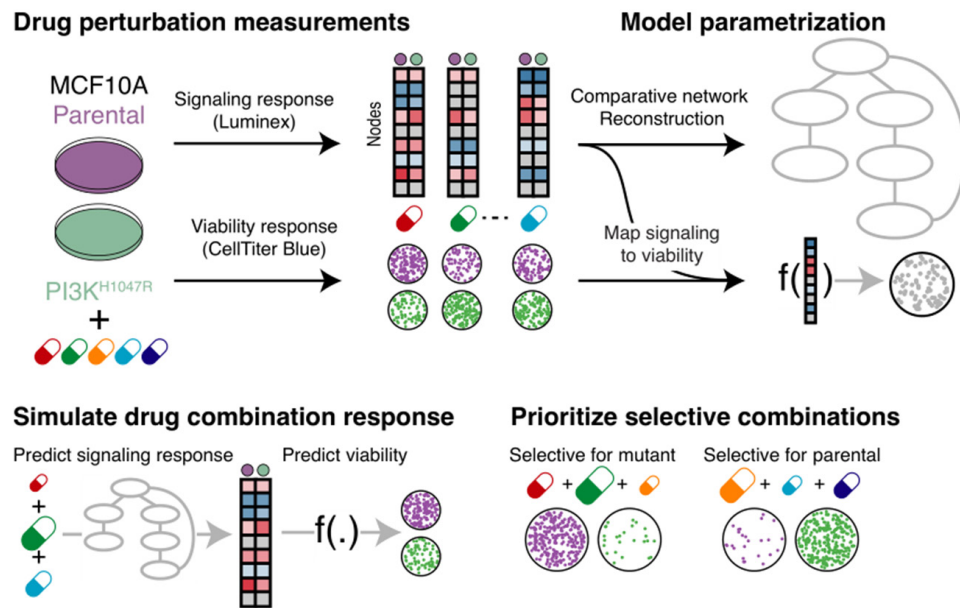


Figure 1: Overview of pipeline to prioritize promising selective low-dose multi-drug combinations. Top: MCF10A parental and PI3KH1047R cells are treated with inhibitors targeting the MAPK and AKT pathways. The signaling and cell viability responses are measured and used to build mutant specific models of signal-transduction networks and to parametrize the relationship between signaling response and cell viability. Bottom: These models are used to simulate the response to unobserved multi-drug combinations, at arbitrary concentrations, of the signaling networks and how this affects cell viability. In this way, low-dose multi-drug combinations that are likely selective for a particular cell type can be prioritized.

Results

The signaling and viability response to drug perturbations in MCA10A parental and PI3K^{H1047R} mutated cells

To test how oncogenic mutations affect signal transduction networks and their downstream effects on cellular phenotypes such as cell viability, we used the MCF10A cell line (121) and an isogenic clone with the activating PI3K^{H1047R} mutation knocked in under its endogenous promoter (122). In the absence of drug perturbations, PI3K^{H1047R}-mutant MCF10A cells have a comparable growth rate as their parental cells (122). As expected, the baseline signaling activity of AKT and PRAS40, both downstream of PI3K, is elevated, but the other signaling nodes do not show significant differences in activity (Fig 2A). Dose response curves of selected PI3K and the MAPK pathway inhibitors showed subtle differences in sensitivities between the parental and the mutant cells (Fig S1A).

To study how the signaling of these cells respond to drug-perturbations and if the PI3K^{H1047R} mutation influences this, we perturbed both cell lines with inhibitors of the PI3K and MAPK pathways, and selected 2-drug combinations of these. Single drugs were tested at two different concentrations, corresponding roughly to their IC₅₀ and IC₉₀ values (except RAFi, which was only tested at IC₉₀) and drug-combinations were tested with both drugs at their IC₅₀ values, to obtain a total of 34 different perturbations. We measured the response (log₂ fold change relative to DMSO control) of nine main nodes in the PI3K and MAPK signaling pathway using a multiplexed luminex assay in both cell lines to obtain more than 600 signaling drug-response measurements (Fig 2B, Table S1,S2). In addition we measured the effect on cell viability using CellTiter Blue (Fig 2C, Table S3,S4). Luminex quantification showed excellent concordance with Western Blots (Fig S1B). Generally, the differences in both signaling response and cell viability between the parental and PI3K-mutant cells were subtle but consistent. For instance, while the responses of the signaling nodes of the parental and PI3K^{H1047R} cells are strongly correlated (Fig 2B and Fig S1C), phospho-AKT shows a strong negative response to growth-factor receptor inhibition (EGFRi or IGF1Ri) that is nearly absent in the PI3K^{H1047R} mutant cells (Fig 2B, highlighted).

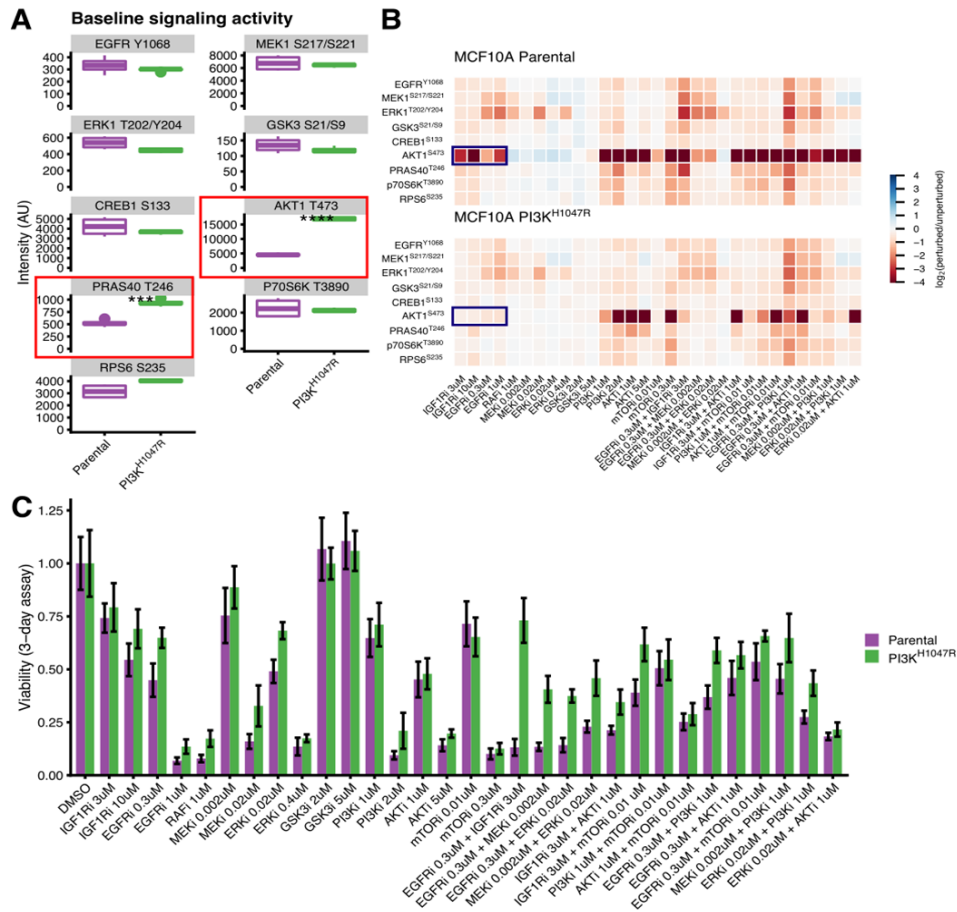


Figure 2: Profiling signaling and viability response of MCF10A Parental en PI3K^{H1047R} cells to drug perturbations.

A. Node activity in the unperturbed cells. Most nodes have similar activity in the parental and PI3K^{H1047R} cells, except AKT and PRAS40 (highlighted) which are downstream of PI3K. B. Heatmap representing log₂-fold changes compared to DMSO controls of the signaling nodes in response to drug treatment. Signaling response is measured after 2 hours of drug treatment. The color scale is capped between -4 and 4 for visualization purposes. C. Cell viability under the same drug treatments as reported in panel B. Cell viability is measured after 3 days of drug treatment.

Network reconstructions identify relevant differences between parental and PI3K-mutant cells

To establish how the PI3K^{H1047R} mutation affects the signal transduction network, we used the drug- response measurements to perform Comparative Network Reconstruction (CNR) (111) of the MAPK and AKT pathways. CNR is a method we recently developed to reconstruct and quantify signaling networks and identify

the most important quantitative differences between two or more cell lines. Prior knowledge about the network topology can be included, but the algorithm can also propose edges to be added to the network. The edge-weights are interpreted as the percent change in the downstream node activity in response to a 1% change in activity of the upstream node. Importantly, CNR identifies which edges are quantitatively different between the two cell lines.

We used the canonical MAPK and PI3K pathway interactions as prior information, and extended the network topology with 4 edges that were added in a leave-one-out cross validation loop (Fig 3A and Fig S2A). The model gave a good fit to the data (Pearson correlation = 0.91) (Fig 3B). As expected, most of these differences are located close to AKT in the network (note, PI3K is not measured) (Fig 3A). Specifically, in the PI3K^{H1047R} cells, AKT is less sensitive to changes in EGFR and unresponsive to IGF1R inhibition (Fig 3A,C), which is consistent with PI3K being constitutively activated. Additionally, AKT is less responsive to PI3K and mTOR inhibition (Fig 3D,E). At the IC₅₀, AKT is also less sensitive to AKT inhibition, but when AKTi is applied at its IC₉₀, the PI3K^{H1047R} cells show a larger response (Fig 3F). This last observation might be explained by the higher baseline AKT activity of PI3K^{H1047R} cells, since if AKT activity is reduced to a similar absolute level, the fold-change of AKT in the mutant is higher.

In order to be able to predict the signaling-response to drugs combined at arbitrary concentrations, we used the direct target-inhibition estimates for drug *k* on node *i* ($S_{i,k}$) for the IC₅₀ and IC₉₀ to parameterize the general relation between target inhibition and drug concentration. To this end, we modelled the response as $S_{i,k}([I_k]) - I_{max,ik} * [I_k]/(K_{i,ik} + [I_k])$, where $[I_k]$ is concentration of inhibitor *k*, $I_{max,ik}$ the maximal response of node *i* to inhibitor *k* (as $[I_k]$ goes to infinity) and $K_{i,ik}$ the inhibitor concentration where the half-maximal response is attained (Fig 3C-F and Fig S2B, dashed lines, c.f. Materials and Methods equation (4)).

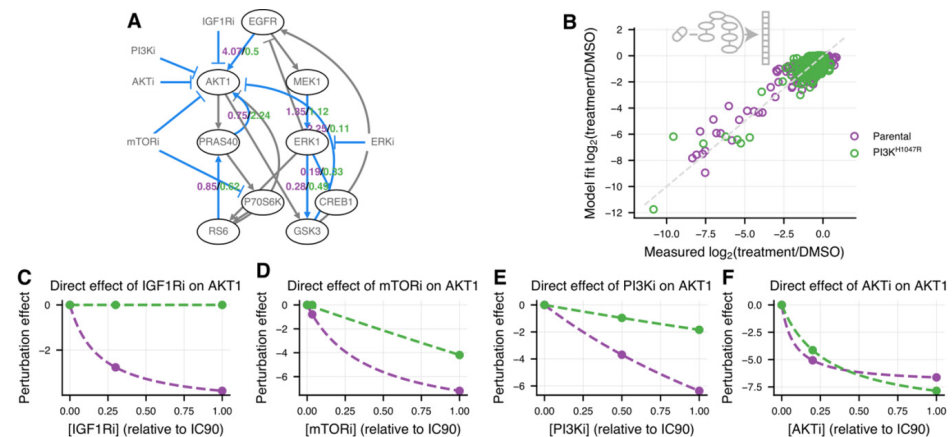


Figure 3: Mutant specific network reconstructions show expected differences.

A. Comparative Network Reconstruction (CNR) of MCF10A parental and PI3K^{H1047R} cells. Edges and direct perturbation effects that differ between the two cell lines are highlighted in blue. Ovals indicate nodes. As expected, the most and the strongest differences between the cell lines are located close to AKT in the network (note that PI3K is not measured). B. Comparison of network model fit with measured signaling response shows that the network model can explain the signaling response data well (Pearson correlation 0.91). C-F. The estimated direct effect of IGF1R (C), mTOR (D), PI3K (E) and AKT (F) inhibition on AKT activity as a function of applied inhibitor concentration. Points indicate the estimated effects of the concentrations used in the CNR reconstruction, the dashed lines indicate the interpolated curves between these points (c.f. Materials and Methods, equation (4)). IGF1R PI3K, and mTOR inhibition were modelled as directly affecting AKT because their actual targets were not measured.

Short-term signaling response is informative for long-term cell viability

To prioritize multi-drug combinations, the response of the signaling network to a drug perturbation needs to be related to its effect on cell viability. Important open questions here are: Is the short-term signaling response predictive to longer term cell viability? If so, which signaling outputs are most predictive?

The association between the individual node-responses and cell viability were moderate even for the most strongly associated nodes, phospho-AKT and phospho-ERK, which had a Pearson correlation with cell viability of 0.36 and 0.42, respectively (Fig 4A). The responses of all other nodes also correlated somewhat with cell viability (Fig S3A), but clearly no single node alone is a good predictor for cell viability. We therefore investigated whether a model combining the phospho-AKT and phospho-ERK response could fit the cell viability data better. We used a model with the property that cell viability goes to 0 if either phospho-ERK or phospho-AKT are fully inhibited (c.f. Materials and Methods, equation (3)). The biological assumption behind this is that both ERK and AKT activation are required for cell survival and growth. This model gave a good fit to the data (Fig 4B), with a Pearson correlation between fitted and measured viability of 0.71. Importantly, this means that the short-term signaling response is predictive for longer-term cell

viability. The fitted parameters (KM,ERK and KM,AKT) differ slightly between the two cell lines, but the bootstrapped 95% confidence intervals strongly overlap (Fig S3B), so we do not want to over interpret these differences.

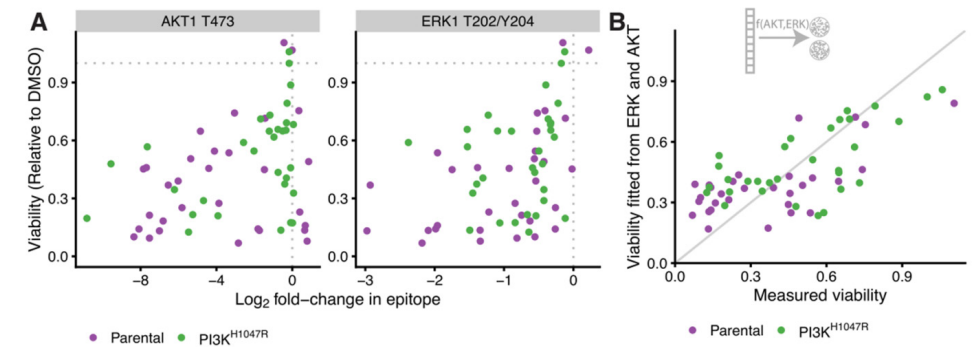


Figure 4: Short term signaling response is predictive for longer term cell viability.

A. Scatterplot of cell viability against log₂-fold changes in AKT (left panel) and ERK (right panel) activity in response to drug treatments. The Pearson correlations are 0.36 and 0.42 respectively. B. Scatterplot of model fit against measured cell viability based on a model where both ERK and AKT response are used to explain cell viability (c.f. Materials and Methods, equation (3)). The Pearson correlation between fit and measurement is 0.71.

Prediction and validation of selective multi-drug-combinations

We then combined the network models (Fig 3A) with the parametrization of the signaling-viability model (Fig 4A) to simulate the effect on cell viability of any multi-drug combination at any concentration. When applying this model to the training data, the Pearson correlation between measured and fitted cell viability was 0.78 (Fig 5A). We decided that this was accurate enough to make predictions about unseen multi-drug combinations. Hence, we used our model to prioritize multi-drug combinations and dosings that maximize the selectivity, defined as the difference in viability between the two cell lines.

We first tried to optimize for PI3K^{H1047R}-selectivity. To do this, for all possible 3-drug combinations we optimized the concentrations such that the viability of the PI3K^{H1047R} mutants is minimized, under the constraint that the viability of the parental cells remains above 0.8 relative to DMSO control (c.f. Materials and Methods, equation (6)). To look for low-dose drug combinations, we also added the constraint that each drug can be used maximally at its IC₁₀. However, no drug-combination was predicted to be selective for the PI3K^{H1047R} cells at any combination of concentrations. Since none of the single drugs shows selectivity towards the PI3K^{H1047R} cells (Fig 2C), this is not very surprising. Moreover, our

network reconstructions indicated that the main effect of the PI3K^{H1047R} mutation is to render the MCF10A parental line independent of growth-factor stimulation. Indeed, when we grew MCF10A parental and PI3K^{H1047R} cells in the media without growth-factor, this is what we observed (Fig 4).

We then looked for drug-combinations that we predicted to be selective for the parental cells. In our optimizations, we found 30 such combinations with a selectivity > 0.1 (Fig 4B). Interestingly, IGF1R inhibition was part of all of the 17 combinations that we predict to be most selective, while its selectivity in the training data was only modest (Fig 2C). However, the difference in signaling response, and specifically phospho-AKT, was much more pronounced (Fig 2B), and this latter aspect gets picked up in the network reconstructions (Fig 3A). A particularly interesting example is the combination IGF1Ri + PI3Ki + GSK3i, since both PI3Ki and GSK3i at their lower dose (IC50) show no selectivity towards the parental cells, and yet this combination is predicted to be one of the more selective ones (Fig 5B, highlighted). As a control, we also selected 44 combinations that we predicted to be non-selective for either cell line (Fig 5C). We then treated the parental and PI3K^{H1047R} cells with the 30 predicted to be selective and 44 control combinations and measured their viability (Table S5). Combinations that we predicted to be selective were indeed so, and this was highly significant when compared to the non-selective control combinations (Wilcoxon signed-rank test $p < 10^{-7}$) (Fig 5D). Individually, 25 of the 30 combinations predicted to be selective were indeed significantly selective (one-sided t-test $p < 0.05$) (Table S6).

As mentioned above, of the 30 predicted-to-be-selective combinations we tested, 17 contain the IGF1R inhibitor, which is also mildly selective for parental cells as monotherapy. (None of the other inhibitors showed selectivity as a monotherapy at their IC10, Fig S5). To rule out the possibility that our result is mainly driven by the selectivity of IGF1R mono-therapy, we compared the 17 IGF1Ri containing drug combinations with IGF1Ri monotherapy. Figure 5E shows that each of the IGF1Ri containing combinations we tested (red boxplot) is more selective than IGF1Ri treatment alone (indicated by horizontal gray line). This effect is highly significant (one-sample t-test $p < 10^{-7}$). When looking at the individual drug combinations, we found that 11 of the 17 IGF1Ri containing combination treatments are significantly more selective than IGF1Ri monotherapy (one sided t-test $p < 0.05$) (Fig 5E, Table S7). This also includes the IGF1Ri + PI3Ki + GSK3i combination highlighted above, which is amongst the second most selective combinations when ranked by effect size.

These results indicate that our pipeline is capable of making an accurate prioritization of selective low-dose multi-drug combinations. Importantly, these predictions are not always obvious, and would not have been possible without the help of mathematical models of the signal transduction networks and its relation to cell viability.

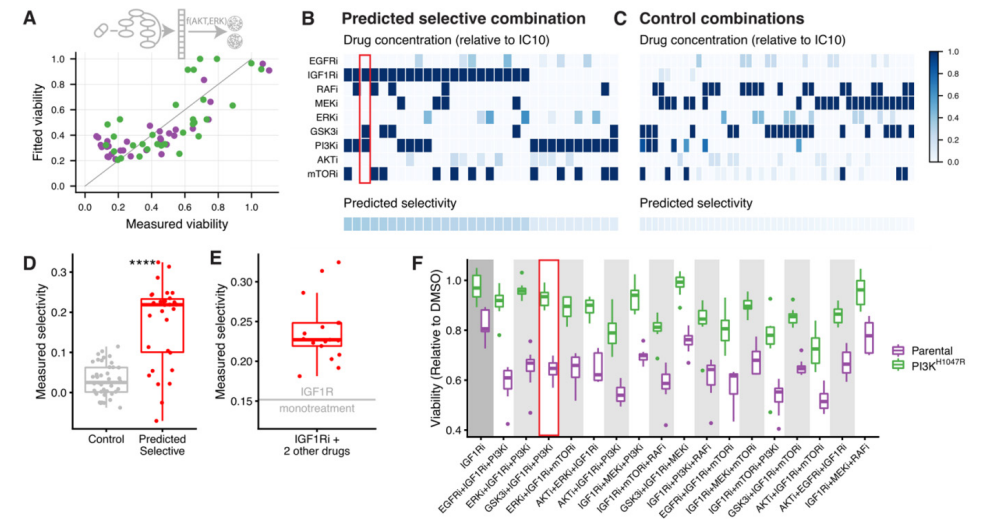


Figure 5: Experimental validation of selective drug combination predictions. A. Scatterplot comparing full model fit (network model combined with signaling response-viability mapping) to the training data. The Pearson correlation between fit and measurement is 0.78. B-C. Overview of drug combinations that we predicted to be selective (B) and non-selective (C) based on this model. Drug concentrations are color-coded relative to their IC10. Bottom row indicates predicted selectivity (defined as the difference in viability between PI3K^{H1047R} and parental cells) of the combination. These combinations were subsequently tested in the validation experiments. D. Boxplot comparing the measured selectivity of the drug combinations predicted to be selective (panel B) or non-selective (panel C). Each point represents the mean selectivity of one drug combination, which were each tested in 8 replicates. The difference is highly significant (Wilcoxon signed-rank test $p < 10^{-7}$). E. Comparison of the measured selectivity of IGF1Ri mono treatment, indicated by the horizontal gray line, with the selected IGF1Ri-containing 3-drug combinations (red boxplot). IGF1Ri containing combinations are significantly more selective than IGF1Ri mono treatment (one-sample t-test $p < 10^{-7}$). F. Box plots comparing cell-viability of Parental and PI3K^{H1047R} cells of the 11 (out of 17) IGF1Ri containing drug-combinations that are significantly more selective than IGF1Ri mono treatment.

Discussion

In this study, we have shown that it is possible to prioritize promising multiple low dose (MLD) drug combinations based on a combination of single and 2-drug response measurements and mathematical modeling. We have used drug-perturbation experiments to reconstruct, quantify and compare signal-transduction networks of an isogenic cell line pair, and linked the responses of these networks to cell viability. This showed that the short-term signaling response is predictive for cell viability, which is measured in longer-term experiments. Based on the so-obtained models we were able to predict and validate drug combinations that are selective for a particular cell line, even though the differences between the cell lines were subtle.

According to our model, no drug combination is likely to be selective for the PI3K^{H1047R}-mutant MCF10A cells compared to their parental counterparts. The absence of oncogene-specific sensitivities is presumably due to an absence of “oncogene addiction” (74) to the PI3K mutation (or any other) in the PI3K^{H1047R} MCF10A cells. In the absence of drug-treatment the mutation has no effect on proliferation (under the growth conditions we used), and this mutation therefore presumably does not induce any vulnerabilities. Our network reconstruction suggests that the main effect of the PI3K^{H1047R} mutation on MCF10A cells is to make them growth-factor independent, consistent with previous observations (123) and likely the reason that IGF1R inhibition selectively affects the parental cells. Interestingly, while as monotherapy low-dose IGF1Ri is mildly selective, combinations of IGF1Ri with selected other drugs are strongly selective for the parental cells. Importantly, which combinations are most selective is often far from obvious. For instance, while in the training data PI3Ki and GSK3i at their lower dose (IC50) individually show no selectivity towards the parental cells at all, the combination IGF1Ri + PI3Ki + GSK3i is one of the most selective drug combinations, both as predicted by our model and as measured validation experiments. This underscores the need for mathematical modelling in prioritizing promising combinations.

While isogenic cell line pairs with a mutation knocked in are interesting models because they allow study of the effect of the mutation in isolation, they may not always be the best model to study oncogene-specific sensitivities due to their lack of oncogene addiction. An interesting alternative approach might be to use cancer cell lines of which one of the driver mutations is removed (124–126). Alternatively, a larger, more heterogeneous panel of cell lines with and without a particular biomarker could be used (113,116,127,128). In this scenario, one would look at commonalities in the signaling network response of the cell lines with the biomarker compared to the lines without out, and use this to propose combinations that are selective of the biomarker carrying cell lines. Finally, the use of matched tumor and normal organoids from the same patient could be used for truly personalized models.

In conclusion, we have shown here that it is feasible to make accurate, non-trivial predictions about selectivity of multi-drug combinations based on mathematical models of signaling transduction networks. In combination with suitable model systems, this framework therefore makes it possible to rationally design biomarker-selective low-dose multidrug combinations.

Materials and Methods

Cells and cell culture

Human parental and PI3K^{H1047R}/+ MCF10A cell lines were obtained from Horizon discovery (HD PAR- 003 and HD 101-011). Cells were cultured in DMEM/F-12 including 2.5 mM L-glutamine and 15 mM HEPES, supplemented with 5% horse serum, 10 µg/mL insulin, 0.5 µg/mL hydrocortisone and 0.1 µg/mL cholera toxin. Mycoplasma tests were performed every 2 months.

Reagents and compounds

The following inhibitors were used in this study: EGFRi (Gefitinib), IGF1Ri (OSI-906), RAFi (LY3009120), MEKi (Trametinib), ERKi (SCH772984), PI3Ki (BKM120), AKTi (MK-2206), mTORi (AZD8055). All inhibitors were purchased from MedKoo Biosciences. The luminex antibodies against CREB1S133, EGFRY1068, ERK1T202/Y204, GSK3S21/S9, MEK1S217/S221, p70RSKT389, PRAS40T246 and RPS6S235 were purchased from ProtATonce Ltd. The luminex antibody against AKT1T473 was purchased from BioRad.

Drug perturbation and validation experiments

All the cell-viability measurements were performed in biological triplicates, each with 2 technical replicates, using black-walled 384-well plates (Greiner 781091). Cells were plated at the optimal seeding density (200 cells per well) and incubated for approximately 24 hours to allow attachment to the plate. Drugs were then added to the plates using the Tecan D300e digital dispenser. 10 µM phenylarsine oxide was used as positive control (0% cell viability) and DMSO was used as negative control (100% cell viability). Three days later, culture medium was removed and CellTiter-Blue (Promega G8081) was added to the plates. After 2 hours incubation, measurements were performed according to manufacturer’s instructions using the EnVision (Perkin Elmer). Viabilities were normalized per cell line according to (treatment - PAOmean)/(DMSOmean - PAOmean). IC50 and IC90 values were fitted using the R-package MixedIC50 (129) (code available at <https://github.com/NKI-CCB/MixedIC50>).

The signaling response measurements were performed using 6-well plates (Greiner 657165). 300K cells per well were plated and incubated for approximately 24 hours to allow attachment to the plate. Drugs were then added to the plates and protein was harvested after 2 hours using the Bio-Plex Pro Cell Signaling Reagent Kit (BioRad 171304006M) according to the manufacturer’s instructions. Protein concentration of the samples was normalised after performing a Bicinchoninic Acid (BCA) assay (Pierce BCA, Thermo Scientific), according to the manufacturer’s instructions. Cell lysates were analyzed using the Bio-Plex Protein Array system

(Bio-Rad, Hercules, CA) according to the suppliers protocol as described previously (113). Intensities were normalized by subtracting blanks for each epitope and correcting for protein concentration.

Computational pipeline and data analysis

Comparative network reconstruction

MAPK and AKT signaling networks of the parental and PI3K^{H1047R} mutant cell lines were reconstructed based on the Luminex drug-response data using Comparative Network Reconstruction (CNR) (111). Briefly, CNR is a network reconstruction method based on Modular Response Analysis (130). It links the matrix of measured node responses to a set of perturbations, R (where R_{ik} is defined as log2 fold change in node i in response to perturbation k) to the matrix unobserved interaction strengths r (where r_{ij} is the logarithmic partial derivative of node i with respect to node j) and direct perturbation effects s (with s_{ik} the scaled direct effect of perturbation k on node i). These matrices are related through

$$r \cdot R = -s \quad (1)$$

CNR solves this equation using an optimization procedure with penalties on the number of edges (non-zero entries in r) and differences between cell lines (entries in r that are quantitatively different between the cell lines). The optimization problem reads:

$$\begin{aligned} \text{Minimize:} \quad & \sum_n \sum_{i,j} \sum_x \epsilon_{in}^x{}^2 + \eta \cdot I_{ij}^{\text{edge}} + \theta \cdot (I_{ij}^{\text{diff}} + I_{in}^{\text{sdiff}}) \\ \text{Subject to:} \quad & \sum_k r_{ik}^x \cdot R_{kn}^x + s_{in}^x = \epsilon_{in}^x & \forall i, j, n, x \\ & I_{ij}^{\text{edge}} = 0 \Rightarrow r_{ij}^x = 0 & \forall i, j, x \\ & I_{ij}^{\text{diff}} = 0 \Rightarrow r_{ij}^x - r_{ij}^{\text{mean}} = 0 & \forall i, j, x \\ & I_{in}^{\text{sdiff}} = 0 \Rightarrow s_{in}^x - s_{in}^{\text{mean}} = 0 & \forall i, n, x \\ & r_{ij}^{\text{mean}} = 1/N_{\text{cell lines}} \sum_x r_{ij}^x & \forall i, j \\ & s_{in}^{\text{mean}} = 1/N_{\text{cell lines}} \sum_x s_{in}^x & \forall i, n \\ & I_{\text{edge}}, I_{\text{diff}}, I_{\text{sdiff}} \in \{0,1\} \\ & n \in \{\text{perturbations}\}; i, j, k \in \{\text{nodes}\}; x \in \{\text{parental, PI3K}^{\text{H1047R}}\} \end{aligned} \quad (2)$$

Solving this optimization problem gives the matrices r and s from a given

R.

Additional constraints reflecting the experimental design were added to the CNR problem.

- s_{ik} is negative and stronger for higher drug concentrations, i.e. $0 > s_{ik}([IC_{50}]) > s_{ik}([IC_{90}])$.
- Each inhibitor-target pair has a single indicator for both inhibitor

concentrations for the difference in perturbations strengths, i.e. if $I_{ik}^{\text{sdiff}} = 0 \Rightarrow s_{ik}^{\text{parental}}([IC_{50}]) = s_{ik}^{\text{PI3K}}([IC_{50}])$ and $s_{ik}^{\text{parental}}([IC_{90}]) = s_{ik}^{\text{PI3K}}([IC_{90}])$.

- The MEK inhibitor interferes not only with MEK phosphorylation, but also its catalytic efficiency. Hence, MEK inhibition was modelled as a direct effect on both MEK and its downstream proteins.
- Some inhibitors target kinases that were not measured in our assay. The effect of these inhibitors was modelled as a perturbation to the (canonical) downstream nodes of the kinases being inhibited. Specifically, IGF1R inhibition was modelled as a perturbation to MEK1 and AKT1, PI3K inhibition as a perturbation to AKT1, RAF inhibition as a perturbation to MEK1, and mTOR inhibition as a perturbation to AKT1 and p70S6K.

Prior information about network topology was added by setting the indicators of a set of canonical MAPK and PI3K pathway interactions to 1. Hyperparameter were set to $\eta = 0.1$ and $\theta = 2.0$ based on a leave one out cross validation loop. Single drug treatments were not included in the leave one out cross validation because each drug concentration needs to be present in at least one perturbation to estimate the corresponding parameter. The final model was obtained by restricting the topology to the prior network information with addition of the 4 edges that were identified in the leave one out cross-validation, and then performing the optimization with $\theta = 2.0$.

The relation between signaling output and cell viability

The viability (relative to DMSO control) upon perturbation k , v_k , were fitted to the following function:

$$v_k = \frac{1}{1 - R_{\text{AKT},k}/K_{\text{M,AKT}} - R_{\text{ERK},k}/K_{\text{M,Erk}}} \quad (3)$$

Where $R_{\text{AKT},k}$ and $R_{\text{ERK},k}$ are the log2-fold changes of phospho-AKT and phospho-ERK relative to DMSO control upon perturbation k , respectively. Fitting was performed using the nls function of R. Bootstraps were performed using the function bootstrap from the “rsample” package (131).

Simulation and prediction of selective 3-drug combinations

The relations between the applied concentration of drug k , $[I_k]$, and target inhibition of node i in response to this, s_{ik} were fitted to the following function for each inhibitor-target pair,

$$s_{ik}([I_k]) = \frac{I_{\text{max},ik} \cdot [I_k]}{(K_{i,ik} + [I_k])} \quad (4)$$

The parameters $I_{\max,ik}$ and $K_{i,ik}$ were fitted to this function using the s_{ik} -values for the $[I_k] = IC_{50}$ and IC_{90} obtained from the CNR optimizations with the curve_fit function from the python package “scipy.optimize” package (132). For convenience all drug concentrations were normalized to the highest concentration applied (the IC_{90}), and in all analyses only interpolations and not extrapolations are used ($0 \leq [I] \leq 1$).

R_{A+B+C} , the vector of simulated log2-fold changes in response to a perturbation with 3 drugs A, B and C, at concentration $[I_A]$, $[I_B]$ and $[I_C]$ was calculated as

$$R_{A+B+C} = r^{-1}(s_A([I_A]) + s_B([I_B]) + s_C([I_C])), \quad (5)$$

to obtain $R_{AKT,A+B+C}$ and $R_{ERK,A+B+C}$. These were then used to calculate viability according to equation [eq:viability].

For each possible 3-drug combination, the selectivity for cell line x relative to y was optimized by solving the following optimization problem:

$$\begin{array}{l} \text{Minimize:} \quad v_{A+B+C}^x \\ \text{Subject to:} \quad v_{A+B+C}^y \geq 0.8 \\ \quad \quad \quad 0 < [I_k] < IC_{10} \quad k \in \{A, B, C\} \end{array} \quad (6)$$

Similarly, unselective control combinations were obtained by solving the optimization problem:

$$\begin{array}{l} \text{Minimize:} \quad (v_{A+B+C}^x - 0.8)^2 + (v_{A+B+C}^y - 0.8)^2 \\ \text{Subject to:} \quad 0 < [I_k] < IC_{10} \quad k \in \{A, B, C\} \end{array} \quad (7)$$

for all possible 3-drug combinations.

The optimizations were performed in Wolfram Mathematica (version 12.0) using the NMinimize function.

Data and Code availability

All data and code required to reproduce the results and figures in this paper are available at <https://github.com/evertbosdriesz/cnr-selective-combos>.

Acknowledgements

This work was supported by funding from the Onco Institute and the Gravity Program CGC.nl, funded by The Netherlands Organisation for Scientific Research (NWO).

Supplementary Information

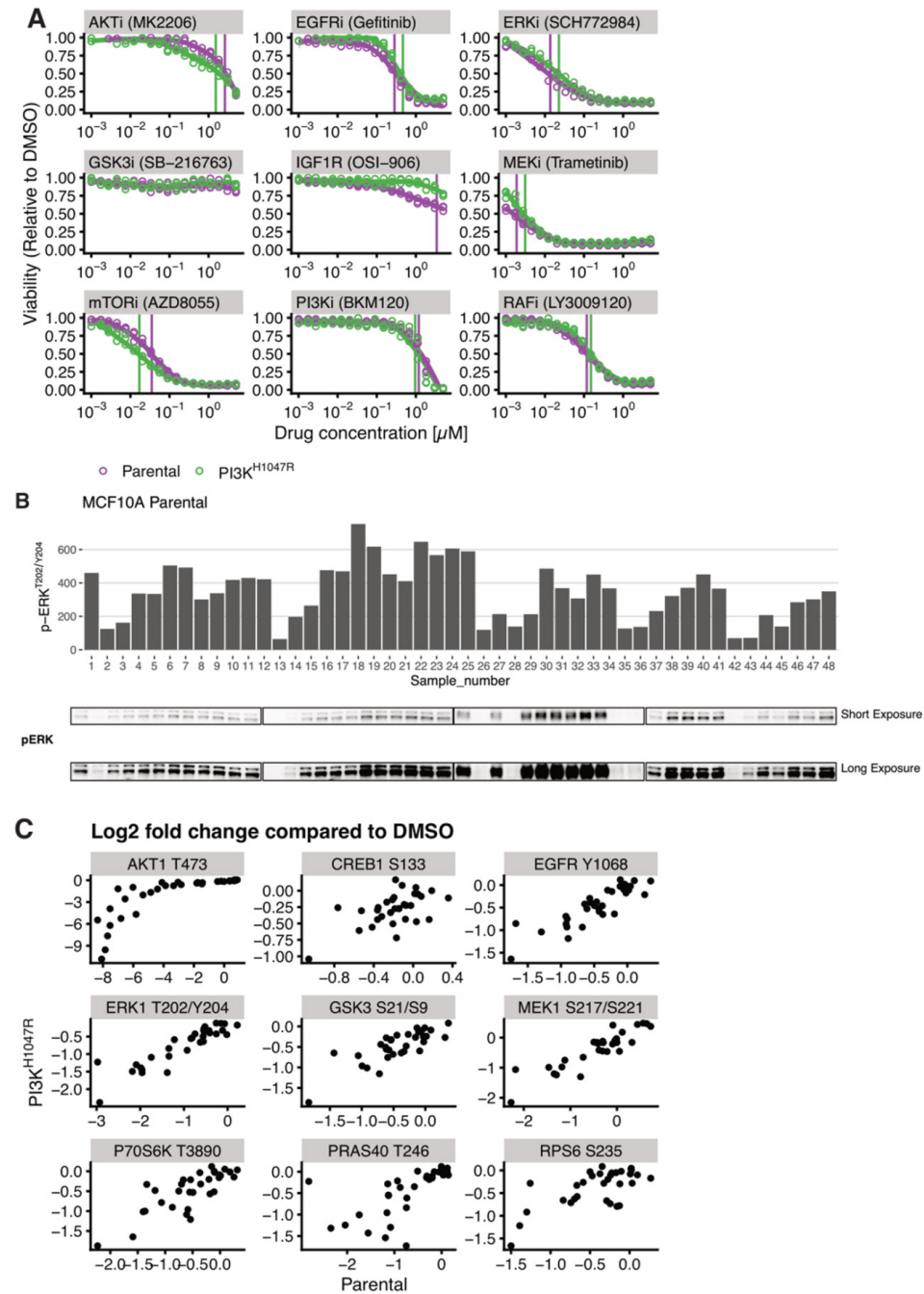


Figure S1: A. Dose-response curves of the inhibitors used in this study. B. Correlation between phospho-ERK quantification using Luminex (top) and Western blot (bottom). C. Correlation between the response in Parental (x-axis) and PI3K^{H1047R} (y-axis) cells. Response is defined as log₂-fold change compared to DMSO controls.

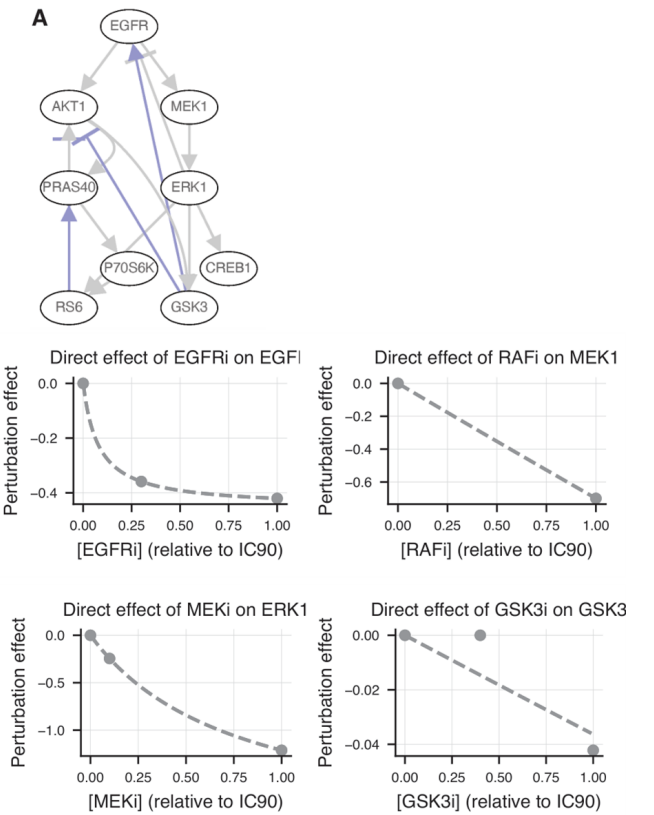


Figure S2: A. Network topology used for modeling. Edges used as prior information are indicated in gray. Edges added in a leave one out cross validation loop are indicated in purple. B. The estimated direct effect of different inhibitors on their target, as a function of applied inhibitor concentration. Points indicate the estimated effects obtained from the CNR reconstruction, at the concentrations used in the perturbation experiments. The dashed lines indicate the interpolated curves between these points. (c.f. Materials and Methods, equation (4))

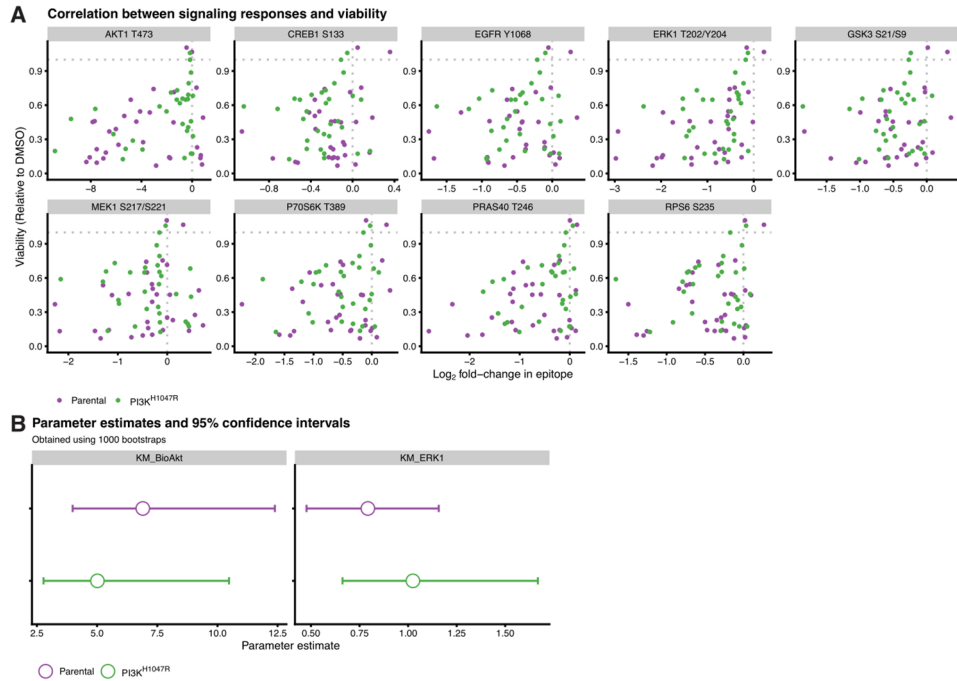


Figure S3: A. Correlation between node response and cell viability of all measured nodes. B. Bootstrapping intervals of the estimated values for the parameters KM,AKT and KM,ERK in equation (3)

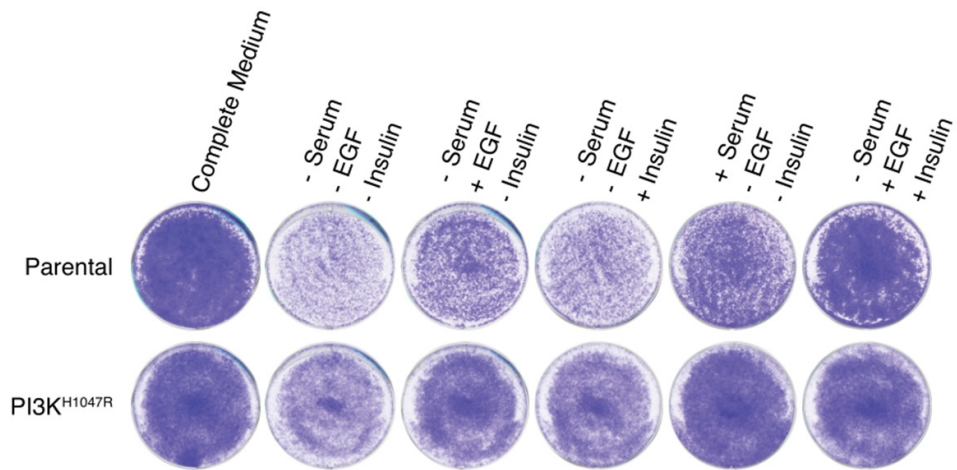


Figure S4: Growth of MCF10A parental and PI3K^{H1047R} cells in different growth media. In contrast to the parental cells the PI3K mutant cells grow well in the absence of serum if either Insulin or EGF is provided.

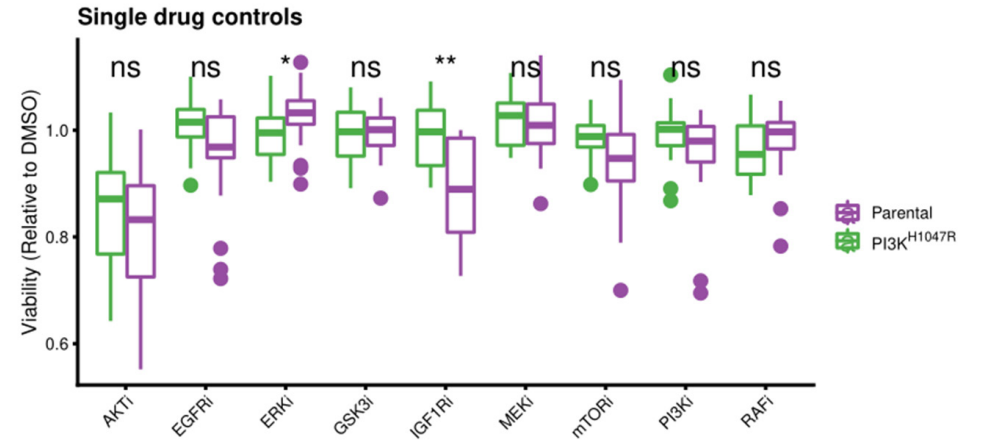


Figure S5: Viability of the low-dose single-drug controls, all measured at their IC₁₀. Except for IGF1Ri, none of the drugs show selectivity towards the parental cells. Treatments were performed in 8 replicates.

4

Using a fluorescent-based sensor to identify microsatellite instability regulators in colon cancer

João M. Fernandes Neto¹, Kaspar Bresser², Cor Liefink¹, Ben Morris¹,
Loredana Vecchione¹, Bastiaan Evers¹, Ferenc Scheeren², Ton Schumacher²,
Roderick L. Beijersbergen¹ and René Bernards¹

¹Division of Molecular Carcinogenesis & Oncode Institute. The Netherlands Cancer Institute,
Plesmanlaan 121, 1066 CX Amsterdam, The Netherlands.

²Division of Cancer immunology, Oncode Institute, The Netherlands Cancer Institute, Plesmanlaan 121,
1066 CX Amsterdam, The Netherlands.

In preparation

Abstract

Inactivation of the DNA mismatch repair (MMR) system, due to (epi)genetic alterations of MMR genes, increases the frequency of mutations across the genome, creating a phenotype known as microsatellite instability (MSI). This phenotype has been associated with a better prognosis for some time, but only since recently it has been recognised as a predictive biomarker (for immunotherapy). Because MSI tumors accumulate more insertions and/or deletions in coding microsatellites regions of the genome, the rate of frameshift neoantigens increases, which promotes immunogenicity. To investigate if additional genes exist that can cause the MSI phenotype, we developed a fluorescent-based sensor to identify genes whose inactivation increases the rate of frameshift mutations in cancer cells. Using CRISPR/Cas9 screens, we found MED12 as a potential new regulator of microsatellite instability.

Introduction

Microsatellites are repetitive DNA tracts in which certain DNA motifs (ranging from one to several base pairs in length) are repeated, typically 5 to 50 times (133,134). Microsatellites are abundant in the genome, however they occur mainly in non-coding DNA. Replication slippage, caused by the transient dissociation of the replicating DNA strands followed by misaligned re-association, occurs frequently in microsatellites but mutations are generally corrected by the mismatch-repair (MMR) system. However, in the absence of a proficient MMR system, due to genetic or epigenetic alterations of MMR genes MLH1, MSH2, MSH6, and PMS2, the rate of mutations will significantly increase, leading to a phenotype known as microsatellite instability (MSI) (135). MMR deficiency, and therefore microsatellite instability, increases the chances of developing cancer (136), but on the other hand, patients with MSI tumors have a better prognosis compared to microsatellite stable (MMS) patients (137). And with the recent advances in immunotherapy, the prognosis has even further improved, as MSI tumors have been shown to respond better to immune checkpoint blockade therapies (138). Because loss of MMR increases the mutation rate in tumors, the rate of putative frameshift peptide neoantigens also increases. Frameshift mutations are genetic mutations caused by insertions or deletions of a number of nucleotides in a DNA sequence that is not divisible by three (139). Due to the triplet nature of gene expression by codons, such a mutation can result in completely different transcripts than the original, which can lead to a more immunogenic tumour microenvironment (140,141).

It has been almost 10 years since the so-called MSI-like phenotype was identified in colorectal cancer (142). Tumors with this phenotype score negative for MSI in a clinical diagnostic assay, but have an expression profile similar to MSI tumors and, like MSI tumors, have a better prognosis. More recently, a study also showed that a fraction of MSS tumors have a high immunoscore and better prognosis (143). Together, these data suggest that there might be additional (currently unknown) genes involved in the regulation of DNA mismatch repair. Because a positive MSI test or dMMR is the eligibility criteria for immunotherapy, some MSS patients who could benefit from immunotherapy are currently not identified. We developed a fluorescent-based sensor in such a way that when cells acquire an increased rate of frameshift mutations, the sensor becomes irreversibly activated. We then performed a whole-genome CRISPR/Cas9 screen to study which genes, when inactivated, could potentiate such a phenotype in an unbiased way.

Results

Microsatellites, because of their repetitive nature, are more prone to frameshift mutations than other genomic regions (144). For this reason, to increase the sensitivity of our frameshift mutation sensor, we cloned an “MSI domain” (i.e., a tract of tandem nucleotide repeats) followed by a protein coding gene (Cre recombinase). We designed the MSI domain in such a way that the protein coding gene would be out-of-frame, and thereby would not be expressed, unless a frameshift mutation that would make it in-frame would occur. We called this vector the MSI activator. Because of the high mutation rate in microsatellites, it would be possible that, after being mutated in-frame, a subsequent mutation could place it again out-of-frame. To ensure that if the MSI activator was ever mutated in-frame we could detect it irreversibly, we cloned a second vector – called the MSI reporter. Here, a selection marker (neomycin) and a red fluorescent protein (Katushka) were cloned in-frame, after a transcriptional STOP cassette flanked by loxP sites. With this double system, upon activation of the MSI activator, Cre would get expressed which would lead to the excision of the transcriptional STOP cassette, making the cells irreversibly resistant to neomycin and Katushka-positive (Fig. 1A). We also included selection markers in these reporters (hygromycin and blasticidin, respectively) to facilitate selection of cells with the double integration.

We used the MSS colorectal cancer cell line SW480 (145) to validate our MSI sensor. We first transfected the cells with the MSI reporter and tested its activation by expressing Cre recombinase in the cells. This resulted in a heterogeneous activation of the reporter, possibly due to the different integration sites of the reporter. However, after single-cell sorting we were able to pick a clone (called SW#8) which became completely activated upon Cre induction (Fig. 1B). Next, we transfected the SW#8 cells with the MSI activator (SW#8_G23) and then knocked-out MMR genes MLH1 or MSH2. We observed that the KO of MLH1 or MSH2 significantly increased the activation of our MSI sensor over time, compared to the control (Figs. 1C-D). Additionally, all the Katushka positive cells were resistant to G418 (Sup. Fig. 1A). However, it is important to notice that it took a significant amount of time (>3 weeks) to see a significant difference. This is not unexpected, as a frameshift mutation needs to occur within our MSI domain (23 bp region), out of the many other microsatellites in the genome, to be activated. Therefore, the longer the cells are cultured for, the higher the chances of activating the sensor. We also validated our sensor using a MSI cell line (Sup. Fig. 1B). To find potential new regulators of microsatellite instability we performed a whole-genome (WG) CRISPR/Cas9 screen. We hypothesised that regulators of microsatellite instability would, in some way, deregulate the MMR system. Because MMR deficient cells are resistant to Temozolomide (146) (Sup. Fig. 2A), we also included an arm in the screen where the cells were treated with Temozolomide

(TMZ), to enrich for MMR deficient cells. We generated high Cas9 expressing SW#8_G23 cells and transduced them with the Brunello gRNA library. To increase the chances of activating the sensor we kept the cells in culture for 36 days. We then selected the cells which had activated the sensor with G418 for 12 days (Fig. 2A). In the TMZ arm we also harvested cells before selection with G418, to rule out any side-effect from G418. The screen performed well technically, as judged by the depletion of essential genes over non-essential genes (Sup. Fig. 2B). As expected, treating the cells with TMZ enriched for sgRNAs targeting MMR genes (Fig. 2B). And not surprisingly, these genes were also enriched after selecting the cells which activated our sensor with G418 (Sup. Fig. 2C). However, in the unbiased arm (untreated), only PMS2 scored as a potential hit (Fig. 2C).

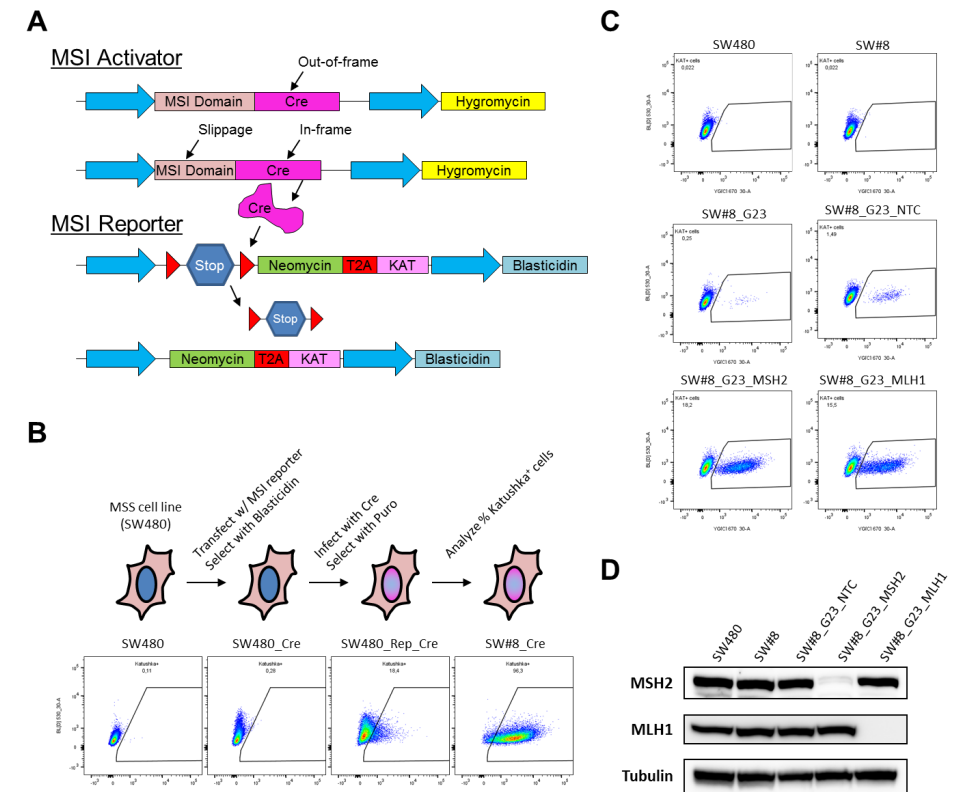


Figure 1: Development of the fluorescent-based sensor to study microsatellite instability. A. Schematic representation of the MSI sensor. B-D. Validation of the MSI sensor in MSS cell line SW480. In (B) SW480 cells were transduced with the MSI reporter and with Cre. Activation of the reporter was measured by flow cytometry and the best clone (SW#8) was selected for further studies. In (C) SW#8 cells were transduced with the MSI activator (G23) and with sgRNAs targeting positive control genes (MSH2 and MLH1) or a non-targeting control (NTC). Activation of the reporter was measured by flow cytometry after 3 weeks in culture. In (D) protein was isolated from the cell lines, as indicated, to assess levels of MSH2 and MLH1 by western blot. Tubulin was used as a loading control. A representative image from two biological replicates is displayed.

The other MMR genes scored within the top 500, but far from being significant. This indicates that, in such a complex screening system, using a whole-genome library creates too much “noise”, which hinders the chances of identifying hits. To potentially increase those chances, we would have to increase the representation of the library as well as the time given to the cells to activate the reporter, but such conditions would be very difficult to achieve logistically with a whole genome library. To overcome the “noise” problem and the logistical hurdles, we decided to re-screen our cells with a smaller “MSI-focused” sgRNA library, comprised of sgRNAs targeting the top enriched genes from our WG screens, as well as candidate genes from literature and control genes. This time, we transduced the high Cas9 expressing SW#8_G23 cells with the “MSI-focused” gRNA library, using a 2000-fold library representation. To further increase the chances of activating the sensor we kept the cells in culture for 85 days. We also harvested cells at day 7, to assess the depletion of essential genes over non-essential genes and proliferation differences, and at day 44, to assess if the extra time was beneficial (Sup. Fig. 2D). With these screening conditions, all MMR genes scored as hits in the screen, as well as MED12 (Fig. 2D). Culturing the cells for longer than 44 days didn’t make a significant difference, as the top 5 hits (MLH1, MSH2, MSH6, PMS2 and MED12) were the same after 44 and 85 days in culture.

To study further whether MED12 regulates microsatellite instability, we generated MED12 KO in SW#8_G23 cells, as well as KO of MSH2 and MLH1 as positive controls. We observed that, after 3 months in culture, loss of MED12 led to an increase in the activation of our MSI sensor approximately 4-fold as compared to control cells, but very far from the 145-fold increase observed in the positive controls (Figs. 3A, B). We also observed that MED12 KO cells acquired resistance to Temozolomide, albeit to a lesser extent than knockout of MLH1 or MSH2 (Fig. 3C). We also tested the MSI status of the MED12 clones using the Promega MSI Analysis System, which is the gold standard MSI assay in clinical research. Using this PCR-based method, we tested five nearly monomorphic mononucleotide repeat markers (BAT-25, BAT-26, MONO-27, NR-21 and NR-24). By evaluating the length of these markers it is possible to detect contractions or expansions. Scoring positive for at least 2 markers is the criteria for classifying a sample as MSI positive. In our samples, the positive controls MLH1 and MSH2 scored positive for 2 markers (BAT-25 and Mono-27), but only one of the four MED12 KO clones scored positive for 2 markers (Fig. 3D). Finally, we observed that MED12 KO cells slightly downregulated MLH1 and MSH2 expression (Fig. 3B).

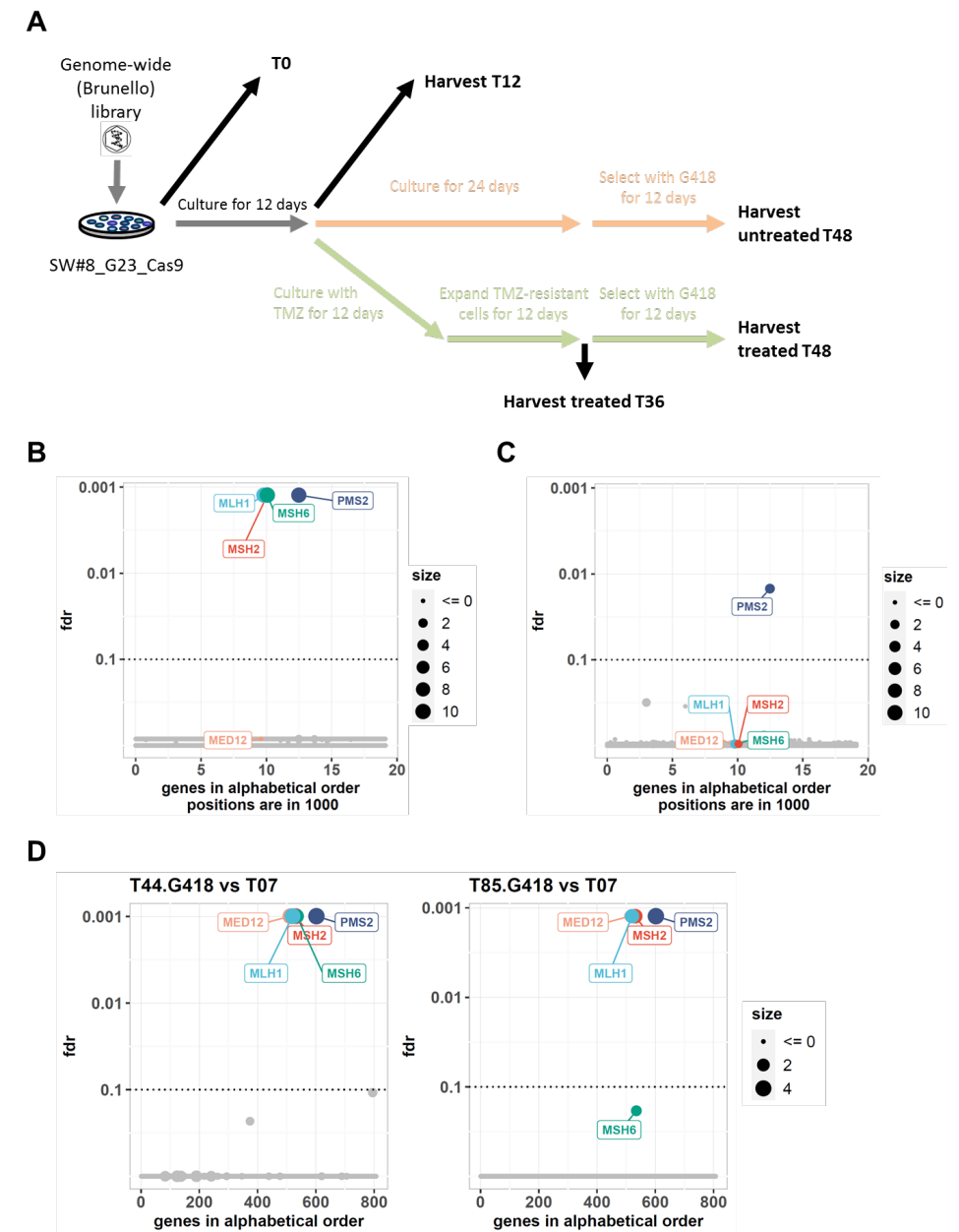


Figure 2: Identification of MED12 as a potential regulator of microsatellite instability. A. Schematic representation of the genome-wide CRISPR screen. B, C. Robust rank analysis of the sgRNAs enrichment in the genome-wide screen. Cas9 expressing SW#8 cells were screened with the Brunello whole-genome sgRNA library. In (B) the Robust rank distribution of the enriched sgRNAs in the Temozolomide treated arm (T36) compared to the reference (T12) is displayed. In (C) the Robust rank distribution of the enriched sgRNAs in the untreated arm (T48) compared to the reference (T12)

is displayed. D. Robust rank analysis of the sgRNAs enrichment in the MSI-focused library screen. Cas9 expressing SW#8 cells were screened with the MSI-focused library. The Robust rank distribution of the enriched sgRNAs after 44 and 85 days in culture (left and right, respectively) compared to the reference (T7) is displayed.

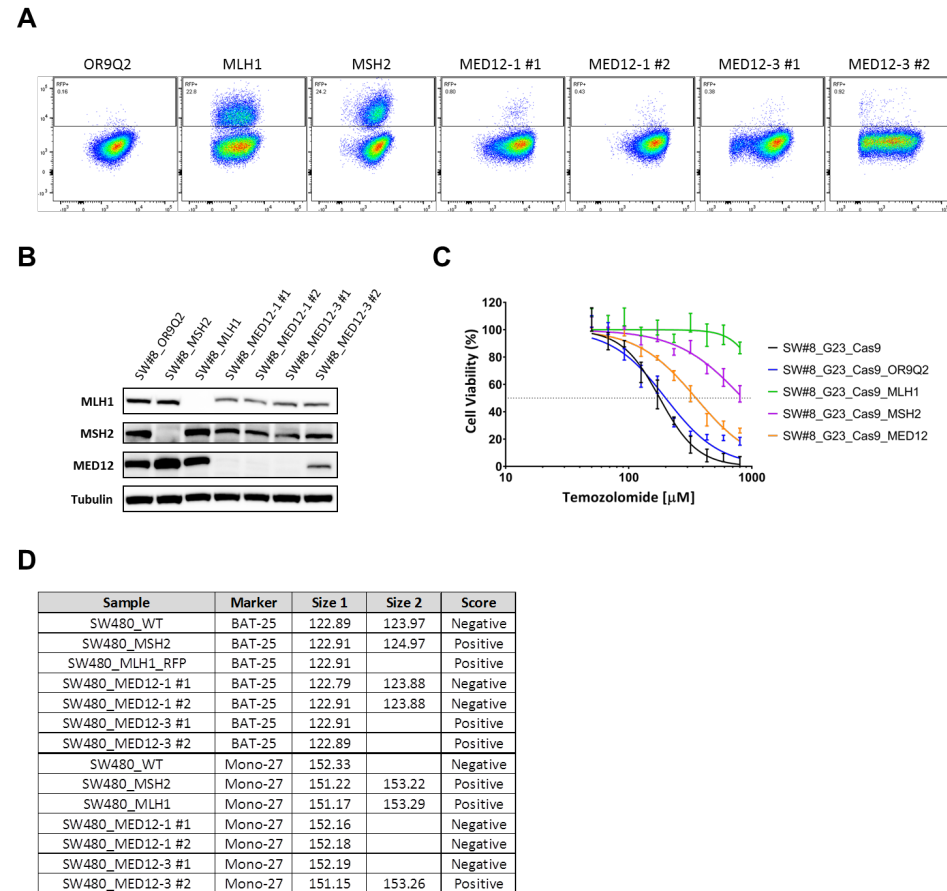


Figure 3: Validation of MED12 as a potential regulator of microsatellite instability. A-D. SW#8_G23_Cas9 cells were transduced with sgRNAs targeting positive control genes (MSH2 and MLH1), a negative control gene (OR9Q2) and with 2 different sgRNAs targeting MED12. For each MED12 sgRNA 2 different clones were generated (#1 and #2). In (A) activation of the reporter was measured by flow cytometry after 3 months in culture. In (B) protein was isolated from the cell lines, as indicated, to assess levels of MSH2, MLH1 and MED12 by western blot. Tubulin was used as a loading control. A representative image from three biological replicates is displayed. In (C) cells were cultured with increasing concentrations of Temozolomide for 4 days, after which cell viability was measured using CellTiter-Blue®. Standard deviation (SD) from 3 biologically independent replicates (each with 3 technical replicates) is plotted. In (D) the MSI status of the cells was tested by PCR. The results for the BAT-25 and Mono-27 markers are displayed.

Conclusions and future perspectives

This study aimed to identify new regulators of microsatellite instability using a fluorescent-based sensor and CRISPR screens. Our findings suggest that MED12 might play a role in microsatellite instability by downregulating members of the MMR system. MED12 is a component of the mediator of RNA polymerase II transcription (MEDIATOR) complex. As an essential component of the RNA polymerase II general transcriptional machinery it plays a crucial part in the activation and repression of transcription initiation (147,148). This can potentially explain how MED12 could be involved with microsatellite instability regulation, i.e. MED12 loss might impair the transcription of the MMR genes, causing expression downregulation. However, this downregulation is only “mild”, explaining why the MSI phenotype takes longer to appear, in line with the differences observed in the activation of the MSI sensor in the MED12 KO cells compared to the KO of MSH2 or MLH1. A closer look into the analysis of the Temozolomide arm of the genome-wide CRISPR screen revealed that MED12 was actually a top hit, but only in one of the biological replicates. It is unclear why that was the case but that explains why it didn’t score as a hit in the analysis. Additionally, EP300, which is also a regulator of MLH1 expression (149) was also in the top 8 genes, which were enriched in the MSI-focused screen. The link between MED12 and MMR raises the question whether MED12 could indeed contribute to microsatellite instability in CRC tumors, but more work is necessary to better understand this link. Additional cell lines should be included in validation studies as well as bioinformatics analysis to see whether there’s a correlation between MED12 mutations and MSI status in patients. Lynch syndrome is a hereditary condition caused by germline inactivation in one of the MMR genes. This condition increases the chances of developing cancer, and because of the accumulation of multiple mutations over time patients also develop MSI tumors. Another condition that causes MSI tumors are Lynch-like syndrome patients. Cancers from Lynch-like syndrome patients show MSI but the mechanism for the generation of MSI is unknown because they have no germline mutations in the DNA MMR genes (150). In a clinical study which analyzed tumors from patients with Lynch-like syndrome, MED12 was found to be mutated in 29% of the tumors (151), which is significantly higher than the 5% mutation frequency observed in CRC patients (152), providing some clinical evidence linking MED12 and MSI. Similarly to Lynch-like tumors, MSI-like tumors display a MSI signature but have no germline mutations in the DNA MMR genes (142). This is in line with the finding from our study in which only one clone scored as MSI positive, but all clones downregulated the MMR genes. As a transcriptional regulator, it is plausible that alterations in MED12 could cause this. In future work, we should analyze the transcriptome of MED12 KO cells and compare it to that of MSI cell lines.

Recently, Bardelli's lab has shown that inactivation of MMR genes triggered neoantigen generation and increased response to immunotherapy (153). It would be interesting to replicate this study using MED12 KO cells, to address if loss of MED12 contributes to an increase in immunogenicity *in vivo*.

In the clinic, MSI status can be assessed by 3 methods: immunohistochemistry (IHC) for the MMR proteins MLH1, MSH2, MSH6 and PMS2, (PCR)-based assessment of microsatellite alterations using five microsatellite markers including at least BAT-25 and BAT-26, and next-generation sequencing (154). The first two are significantly cheaper, therefore it is not surprising that in the majority of hospitals the latter is not performed. However, there is increasing evidence suggesting that a subset of patients which score negative for dMMR and MSI could also benefit from immunotherapy. Due to economic reasons it is not possible to perform next-generation sequencing on every patient that comes into the clinic to identify such a patient subset. In our study we tried to identify markers which could help identify this subset of patients without the need for next generation sequencing approaches. Overall, we developed a new system to study, in real time, the development of microsatellite instability. Using this system together with CRISPR screening technology we could identify MED12 as a potential new MSI regulator. Since in most hospitals MSI testing is done by immunohistochemistry our findings indicate that it could be relevant to also assess the expression of MED12 by immunohistochemistry in tumors which score negative for dMMR and MSI. In case patients have low expression of MED12 they should then be further evaluated. This would give more patients the opportunity to receive the best possible treatment.

Materials and methods

Cell culture and drug response assays

SW480 cells were cultured in RPMI medium (Gibco 21875034). All the cell lines media were supplemented with 10% FBS (Serana), 1% penicillin/streptomycin (Gibco 15140122) and 2 mM L-glutamine (Gibco 25030024). All cell lines were cultured at 37°C and with 5% CO₂. All cell lines were validated by STR profiling and mycoplasma tests were performed every 2-3 months.

All drug-response assays were performed in triplicate, using black-walled 384-well plates (Greiner 781091). Cells were plated at the optimal seeding density and incubated for approximately 24 hours to allow attachment to the plate. Drugs were then added to the plates using the Tecan D300e digital dispenser. 10 μM phenylarsine oxide was used as positive control (0% cell viability) and DMSO was used as negative control (100% cell viability). Four days later, culture medium was removed and CellTiter-Blue (Promega G8081) was added to the plates. After 1-4

hours incubation, measurements were performed according to manufacturer's instructions using the EnVision (Perkin Elmer).

Western Blots

After the indicated culture period, cells were washed with chilled PBS and then lysed with RIPA buffer (25mM Tris - HCl pH 7.6, 150mM NaCl, 1% NP-40, 1% sodium deoxycholate, 0.1% SDS) containing protease inhibitors (Complete (Roche) and phosphatase inhibitor cocktails II and III). Samples were then centrifuged for 10 minutes at 14,000 rpm at 4°C and supernatant was collected. Protein concentration of the samples was normalized after performing a Bicinchoninic Acid (BCA) assay (Pierce BCA, Thermo Scientific), according to the manufacturer's instructions.

Protein samples (denatured with DTT followed by 5 minutes heating at 95°C) were then loaded in a 4-12% polyacrylamide gel. Gels were run (SDS-PAGE) for approximately 60 minutes at 165 volts. Proteins were then transferred from the gel to a polyvinylidene fluoride (PVDF) membrane, using 330 mA for 90 minutes. After the transfer, membranes were placed in blocking solution (5% bovine serum albumin (BSA) in PBS with 0,1% Tween-20 (PBS-T). Subsequently, membranes were probed with primary antibody in blocking solution (1:1000) and left shaking overnight at 4°C. Membranes were then washed 3 times for 10 minutes with PBS-T, followed by one hour incubation at room temperature with the secondary antibody (HRP conjugated, 1:10000) in blocking solution. Membranes were again washed 3 times for 10 minutes in PBS-T. Finally, a chemiluminescence substrate (ECL, Bio-Rad) was added to the membranes and the Western Blot was resolved using the ChemiDoc (Bio-Rad).

CRISPR/Cas9 screen

The appropriate number of cells to achieve 250-fold representation of the library, multiplied by five to account for 20% transduction efficiency, were transduced at approximately 40-60% confluence in the presence of polybrene (8 μg/mL) with the appropriate volume of the lentiviral-packaged sgRNA library. Cells were incubated overnight, followed by replacement of the lentivirus-containing medium with fresh medium containing puromycin (2-4 μg/mL). The lentivirus volume to achieve a MOI of 0.2, as well as the puromycin concentration to achieve a complete selection in 3 days was previously determined for each cell line. Transductions were performed in triplicate. After puromycin selection, cells were split into the indicated arms (for each arm, the appropriate number of cells to keep a 250-fold representation of the library was plated at approximately 10-20% confluence) and a T0 (reference) time point was harvested. Cells were maintained as indicated. In case a passage was required, cells were reseeded at the appropriate number to keep at least a 500-fold representation of the library. Cells (enough to keep at least a 500-fold

representation of the library, to account for losses during DNA extraction) were collected when indicated, washed with PBS, pelleted and stored at -80°C until DNA extraction.

DNA extraction, PCR amplification and Illumina sequencing

Genomic DNA (gDNA) was extracted (Zymo Research, D3024) from cell pellets according to the manufacturer's instructions. For every sample, gDNA was quantified and the necessary DNA to maintain a 250-fold representation of the library was used for subsequent procedures (for this we assumed that each cell contains 6.6 pg genomic DNA). Each sample was divided over 50 µl PCR reactions (using a maximum of 1 µg gDNA per reaction) using barcoded forward primers to be able to deconvolute multiplexed samples after next generation sequencing (for primers and barcodes used, see Supplementary Table 3). PCR mixture per reaction: 10 µl 5x HF Buffer, 1 µl 10 µM forward primer, 1 µl 10 µM reverse primer, 0.5 µl Phusion polymerase (Thermo Fisher, F-530XL), 1 µl 10mM dNTPs, adding H₂O and template to 50 µl. Cycling conditions: 30 sec at 98°C, 20× (30 sec at 98°C, 30 sec at 60°C, 1 min at 72°C), 5 min at 72 °C. The products of all reactions from the same sample were pooled and 2 µl of this pool was used in a subsequent PCR reaction using primers containing adapters for next generation sequencing (Supplementary Table 2). The same cycling protocol was used, this time for 15 cycles. Next, PCR products were purified using the ISOLATE II PCR and Gel Kit (Bioline, BIO-52060) according to the manufacturer's instructions. DNA concentrations were measured and, based on this, samples were equimolarly pooled and subjected to Illumina next generation sequencing (HiSeq 2500 High Output Mode, Single-Read, 65 bp). Mapped read-counts were subsequently used as input for the further analyses.

Bioinformatics Analysis

For each CRISPR screen the sgRNA count data for each sample was normalized for sequence depth using DESeq2, with the difference that the median instead of the total value of a sample was used. Then we took the results from the DESeq2 analysis, and sorted it on the DESeq2 statistic. We then sorted the results by alphabetical order of the gene. We then ran the MAGeCK Robust Rank (RRA) tool on this list to generate a multiple testing corrected pvalue (FDR).

Generation of custom MSI-focused sgRNA library

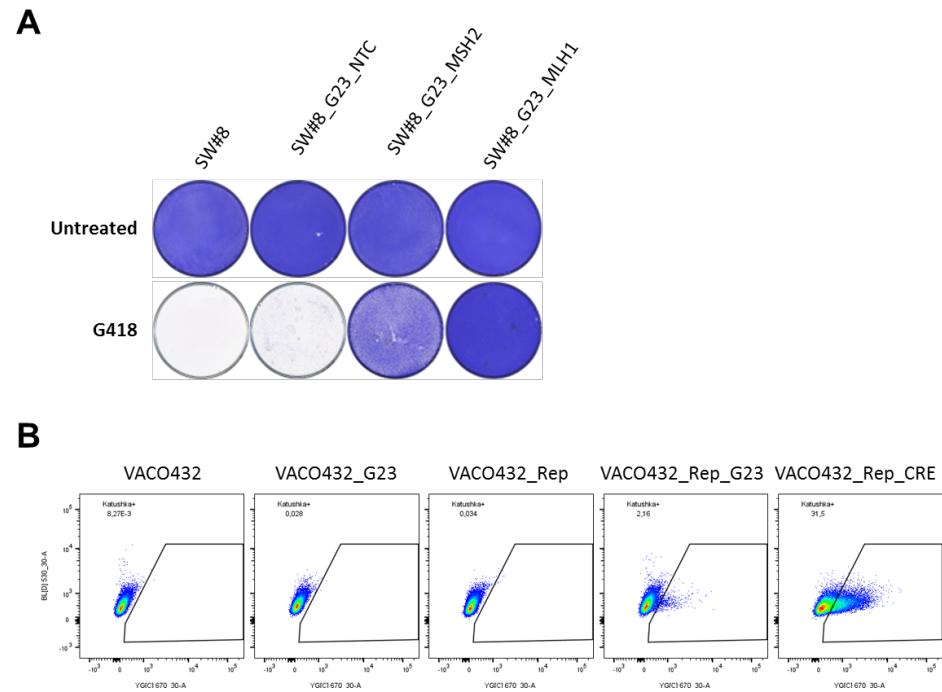
For the design of the custom sgRNA library we used the Broad GPP sgRNA design portal. The sgRNA sequences were ordered as a pool of oligonucleotides (Agilent) with flanking sequences to enable PCR amplification and Gibson assembly into pLentiGuide-Puro (pLG, addgene #52963). The pooled oligo library was amplified using pLG_U6_foward 5'- GGCTTTATATATCTTGTGGAAAGGACGAAACACCG-3' and

pLG-TRACR_Reverse 5'-GACTAGCCTTATTTTAACTTGCTATTTCTAGCTCTAAAAC-3'. The fragments were purified and cloned into pLG. The representation of the custom sgRNA library was validated by next generation sequencing.

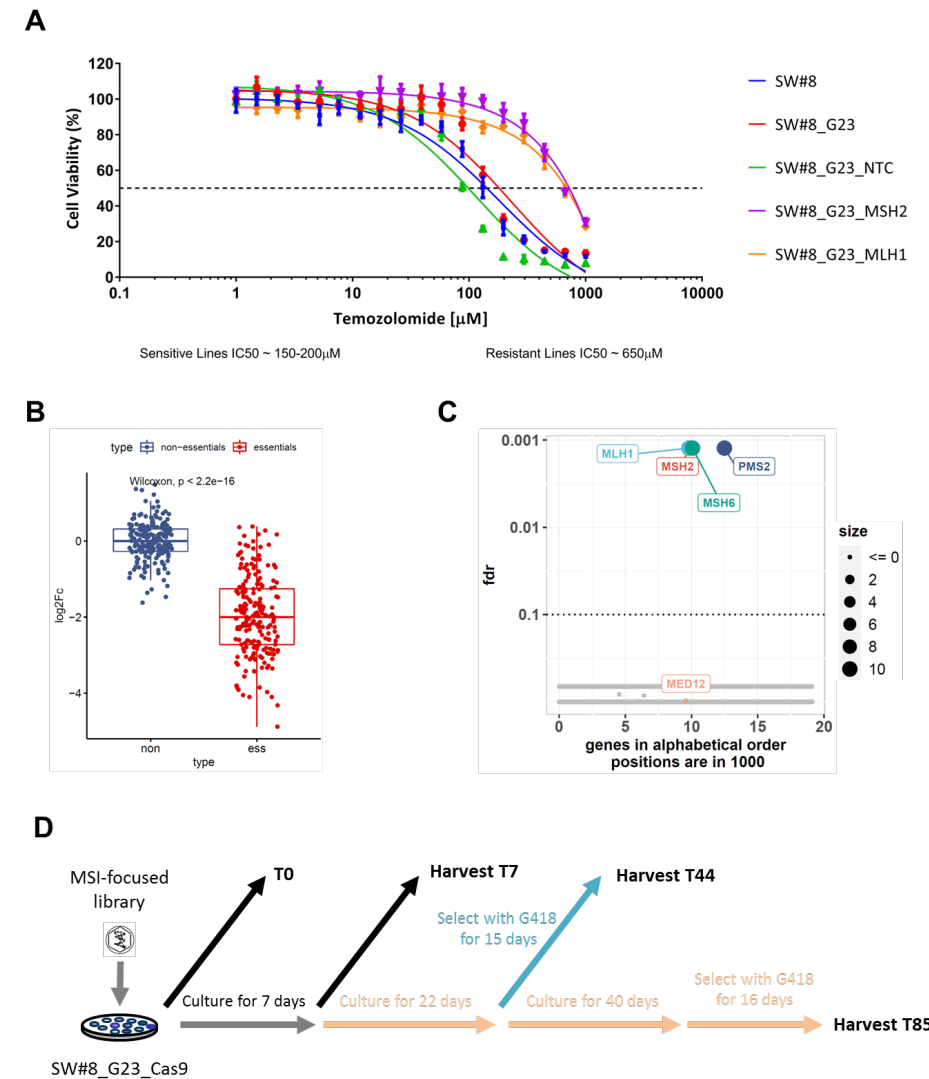
MSI PCR test

MSI status was determined using the MSI Analysis kit (MD1641, Promega) according to the manufacturer's instructions.

Supplementary Information



Supplementary Figure 1: Development of the fluorescent-based sensor to study microsatellite instability. A. Validation of the MSI reporter. SW#8 cells were transduced with the MSI activator (G23) and with sgRNAs targeting positive control genes (MSH2 and MLH1) or a non-targeting control (NTC). After 3 weeks in culture, G418 (200µg/mL) was added to the cells. 10 days later plates were fixed and stained. B. Validation of the MSI sensor in MSI cell line VACO432. VACO432 cells were transduced with the MSI reporter and activator (and with Cre as a positive control). Activation of the reporter was measured by flow cytometry after 3 weeks in culture.



Supplementary Figure 2: Using CRISPR screens to identify potential regulators of microsatellite instability.

A. Cells were cultured with increasing concentrations of Temozolomide for 4 days, after which cell viability was measured using CellTiter-Blue®. Standard deviation (SD) from 3 replicates is plotted. B,C. Analysis of the genome-wide screen. Cas9 expressing SW#8 cells were screened with the Brunello whole-genome sgRNA library. In (B) the analysis of the depletion (log2 Fold Change) of the sgRNAs targeting essential genes over non-essential genes is displayed. Box plot shows the median (horizontal line), interquartile range (hinges), and the smallest and largest values no more than 1.5 times the interquartile range (whiskers). Comparisons were made using the Wilcoxon test. In (C) the Robust rank distribution of the enriched sgRNAs in the Temozolomide treated arm (T48) compared to the reference (T12) is displayed. D. Schematic representation of the MSI-focused CRISPR screen.

5

Optimized Cas9 expression improves performance of large-scale CRISPR screening

João M. Fernandes Neto^{1,3}, Katarzyna Jastrzebski^{1,3}, Cor Lieftink^{1,2}, Lenno Krenning^{3,4},
Matheus Dias^{1,3}, Ben Morris^{1,2}, Daimy van der Ven^{1,3}, Hester Heimans^{1,3},
René H. Medema^{3,4}, René Bernards^{1,3}, and Roderick L. Beijersbergen^{1,2}

¹Division of Molecular Carcinogenesis, ²The NKI Robotics and Screening Center, ³Onco Institute,
⁴Division of Cell Biology, The Netherlands Cancer Institute, Plesmanlaan 121, 1066 CX Amsterdam, The
Netherlands.

Submitted

Abstract

CRISPR technology is an invaluable tool for large-scale functional genomic screening. Genome editing efficiency and timing are important parameters impacting the performance of pooled CRISPR screens. Here we show that by optimizing Cas9 expression levels, the time necessary for gene editing can be reduced, contributing to improved performance of CRISPR based screening.

Introduction

The simplicity, speed and low-cost of CRISPR technology has led to its widespread application in biomedical research in recent years. In particular, large scale pooled CRISPR screening technologies have yielded many new discoveries in a variety of research fields (155–158). Since its establishment, the technology has undergone many improvements, and the CRISPR toolbox has been significantly expanded (159,160). sgRNA design has improved to a level where efficient screening is possible with whole-genome (WG) libraries containing only two independent sgRNAs per gene (161). Nevertheless, one aspect that remains rather ambiguous is the optimal method of sgRNA and Cas9 delivery. Most publicly available sgRNA libraries can be purchased in a “1 vector system” (e.g. lentiCRISPRv2 backbone) which delivers both the sgRNA library and Cas9 expression at the same time, or in a “2 vector system” (e.g. lentiGuide-Puro backbone) which delivers only the sgRNA library and requires a Cas9-expressing cell line to be generated first. To date, no comprehensive comparison has been made to address differences in screening efficiencies between the two systems. Here, we demonstrate that the level of Cas9 expression is a crucial determinant of editing speed. Therefore, a system that allows for control of Cas9 expression can significantly reduce the time necessary for editing, thereby increasing screen performance.

Results and discussion

Pooled CRISPR screens generally use a low multiplicity of infection (MOI<1) to prevent the presence of more than one sgRNA per cell. When using a “1 vector system”, most infected cells will integrate a single copy of a sgRNA and Cas9 in a single step (1-step). Depending on the position of the integration, which is unpredictable in pooled screening, this could result in varying levels of sgRNA and Cas9 expression across a population of cells. When using a “2 vector system”, first Cas9-expressing cells are established and subsequently a sgRNA library is introduced at low MOI (2-step) into these cells. Although the expression of sgRNAs can still vary depending on the position of the integration, the expression of Cas9 can be optimized independently to increase screening efficiency. We show experimentally that using a 2-step approach results in higher Cas9 expression levels in MCF10A cells, as compared to a 1-step approach (Fig. 1A).

To test whether Cas9 expression affects the performance of CRISPR screens, we performed two screens using either a 1-step or a 2-step system (Sup. Fig. 1A). For each screening system the same collection of sgRNAs (Brunello library) was used. To evaluate the performance of each screen, we analyzed the depletion of

essential genes over non-essential genes, as previously described (162,163). By using the 2-step system we observe significantly more depletion of essential genes, in comparison to the 1-step system, indicating that increasing the level of Cas9 expression improved screening efficiency (Fig. 1B, Sup. Figs. 1B, C and Sup. Table 1).

To further study the relationship between Cas9 expression and editing timing and efficiency we expressed Cas9 in 3 different cell lines (SW480, A375 and HEK293T), using either constitutively expressed Cas9 (lentiCas9-P2A-EGFP) or an inducible Cas9 expression (lenti-iCas9-P2A-EGFP). With both vectors, the Cas9 expression should be directly proportional to the expression of EGFP. For the constitutively expressed Cas9, we used fluorescence activated cell sorting to select cell populations with low, medium and high levels of Cas9 expression (Sup. Figs. 2A-D). For the inducible system, a range of Cas9 levels was achieved by increasing doses of doxycycline (10ng/mL to 1 ug/mL). We then used these cell lines expressing different levels of CAS9 to measure editing efficiency both indirectly (using pXPR011 – Sup. Fig. 2E) and directly (using TIDE analysis (164) – Fig. 1C and Sup. Figs. 3A-D) in a time-course experiment. These results show that higher Cas9 levels reduce the time required for editing, meaning that higher Cas9 expression resulted in faster editing kinetics. Importantly, this correlation was observed in all cell lines examined. Of note, a low level of CAS9 expression, due to leakiness of the inducible system, led to gene editing for sgRNAs 1 and 2, even in the absence of doxycycline (Figure 1C). To confirm whether the correlation between Cas9 levels and editing efficiency was independent of sgRNA sequence, we generated a sgRNA library (consisting of 486 sgRNAs targeting essential genes and 210 targeting safe-haven regions) and performed screens in all of our cell lines (Sup. Fig. 4A). As expected, we found that the amount of depletion of sgRNAs targeting essential genes was directly proportional to the level of Cas9 expression in the cells (Fig. 1D and Sup. Figs. 4B-D and Sup. Table 2).

There is a general preconception in the CRISPR field that high Cas9 expression can result in toxicity and increasing off-target effects. Indeed, several reports in different model organisms have shown that high Cas9 expression is toxic (165). We also observed that mammalian cell lines expressing very high levels of Cas9 tend to downregulate Cas9 expression over time (data not shown). To address whether high Cas9 expression increases off-target effects, we analyzed the behavior of sgRNAs targeting safe-havens in our screens. We did not observe any increase in the number of outliers in the conditions with high Cas9 (Fig. 1D and Sup. Figs. 4B-D). Instead, the same outliers were found across the different levels of Cas9 expression and, as expected, became more pronounced in the high Cas9 conditions due to the faster editing speed. This indicates that off-targets are predominantly caused by poor sgRNA design and not by high Cas9 expression. However, because

high Cas9 expression exacerbates sgRNA effects, off-target effects affecting cell fitness do become more apparent.

In conclusion, our findings suggest that in a heterogeneous population of cells, gene editing via CRISPR/Cas9 behaves similarly to an enzymatic reaction, i.e. the percentage of edited cells increases over time until it reaches a plateau. Although the editing rate depends on factors such as sgRNA design (specificity of target site selection), target region (open versus closed chromatin) and DNA repair capacity (NHEJ versus HDR) (166), our data show that editing speed is highly dependent on the level of Cas9 expression. The maximum achievable editing efficiency does not seem to be influenced by Cas9 expression, as it accumulates to the same level (Fig. 1C). However, in CRISPR screens increasing editing speed is desirable and therefore also higher levels of Cas9. In addition, due to variation in the characteristics of single cell derived clonal lines, the use of polyclonal populations is preferred (167). The introduction of a construct expressing Cas9 together with GFP, for example, can be used for the polyclonal selection of high Cas9 expressing cells by using GFP as a “selection” marker. This strategy is favored over the generation and subsequent validation of single cell derived clonal lines (168). Our data highlight that Cas9 expression is a crucial parameter that influences the timing of gene editing, and the careful optimization per model system can significantly impact the outcome of large-scale pooled CRISPR screens.

Cell culture

MCF10A, SW480, A375 and HEK293T cell lines were obtained from ATCC. MCF10A cells were cultured in DMEM/F-12 medium containing 2.5 mM L-glutamine and 15 mM HEPES, supplemented with 5% horse serum, 10 µg/mL insulin, 0.5 µg/mL hydrocortisone and 0.1 µg/mL cholera toxin. SW480 cells were cultured in RPMI medium; A375 and HEK293T cells were cultured in DMEM medium. All the media were supplemented with 10% FBS, 1% penicillin/streptomycin and 2 mM L-glutamine. All cell lines were cultured at 37°C and with 5% CO₂. All cell lines were validated by STR profiling and mycoplasma tests were performed every 2-3 months.

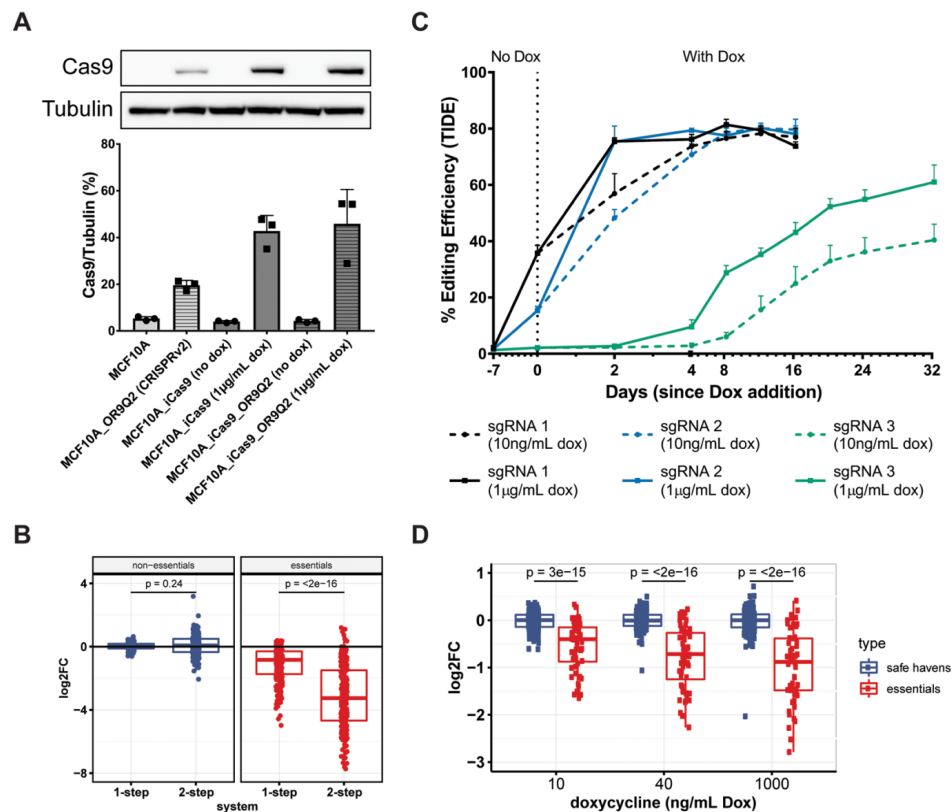


Figure 1: The importance of time and Cas9 expression for efficient gene editing. A, Comparison of 1-step versus 2-step system. MCF10A and MCF10A_iCas9 cells were transduced with a sgRNA targeting a non-essential gene (OR9Q2), cloned in the lentiCRISPRv2 vector (1-step system) and in the lentiGuide-Puro vector (2-step system), respectively. The level of Cas9 expression was measured by examining Cas9 levels in the western blot. Tubulin was used as loading control. The quantification from 3 biological replicates, as well as a representative blot are shown. B, Comparison of depletion of sgRNAs targeting essential genes for 1-step and 2-step systems. MCF10A cells were screened with the same whole-genome sgRNA library (Brunello), using either a 1-step or a 2-step system. The analysis of the depletion (\log_2 Fold Change) of the sgRNAs targeting essential genes over non-essential genes is displayed. Box plot shows the median (horizontal line), interquartile range (hinges), and the smallest and largest values no more than 1.5 times the interquartile range (whiskers). Comparisons were made using the Wilcoxon test. C, Analysis of editing speed in relation to Cas9 expression levels. SW480_iCas9 cells were transduced with 3 different sgRNAs. Cells were kept in puromycin for 7 days. At day 7, a fraction of the cells was harvested as a reference sample, while the rest of the cells were placed back in culture and treated with either 10 ng/mL or 1 μ g/mL doxycycline. Cells were kept in continuous culture with doxycycline and harvested from these two arms at the indicated time-points. Gene editing efficiency was analyzed using TIDE. D, Analysis of editing speed in relation to Cas9 expression levels for a sgRNA library targeting essential genes and safe-havens. SW480_iCas9 cells were screened with a library of essential and safe-haven sgRNAs. To induce different levels of Cas9 expression, cells were treated with 10, 40 or 1000 ng/mL of doxycycline and cultured for 8 population doublings. The analysis of the depletion (\log_2 Fold Change) of the sgRNAs targeting essential genes and safe-havens is displayed. Box plot shows the median, interquartile range and the smallest and largest values no more than 1.5 times the interquartile range. Comparisons were made using the Wilcoxon test.

Methods

Western blots

After the indicated culture period, cells were washed with chilled PBS, then lysed with RIPA buffer (25mM Tris-HCl, pH 7.6, 150 mM NaCl, 1% NP-40, 1% sodium deoxycholate, 0.1% SDS) containing Complete Protease Inhibitor cocktail (Roche) and phosphatase inhibitor cocktails II and III (Sigma). Samples were then centrifuged for 10 min at 15,000 x g at 4°C and supernatant was collected. Protein concentration of the samples was normalized after performing a Bicinchoninic Acid (BCA) assay (Pierce BCA, Thermo Scientific), according to the manufacturer's instructions. Protein samples (denatured with DTT followed by 5 min heating at 95°C) were then loaded in a 4-12% polyacrylamide gel. Gels were run (SDS-PAGE) for approximately 45 min at 175 volts. Proteins were transferred from the gel to a polyvinylidene fluoride (PVDF) membrane at 330 mA for 90 min. After the transfer, membranes were incubated in blocking solution (5% bovine serum albumin (BSA) in PBS with 0.1% Tween-20 (PBS-T)). Subsequently, membranes were probed with primary antibody in blocking solution (1:1000) overnight at 4°C. Membranes were then washed 3 times for 10 min with PBS-T, followed by 1 h incubation at room temperature with the secondary antibody (HRP conjugated, 1:10,000) in blocking solution. Membranes were again washed 3 times for 10 min in PBS-T. Finally, a chemiluminescence substrate (ECL, Bio-Rad) was added to the membranes and signal imaged using the ChemiDoc-Touch (Bio-Rad).

Generation of Cas9-expressing cancer cell lines

MCF10A cells were transduced with a lentivirus containing Edit-R Inducible Cas9 (Horizon CAS11229) at approximately 40% confluence in the presence of polybrene (4 μ g/mL). Cells were incubated overnight, followed by replacement of the lentivirus-containing medium with fresh medium containing Blasticidin (10 μ g/mL). After selection, several single cell clones were generated and Cas9 expression was assessed by Western blot. A clone with high Cas9 expression upon doxycycline treatment, and undetectable Cas9 expression in the absence of doxycycline, (named "MCF10A_iCas9") was used for subsequent experiments.

SW480 cells were transduced with Lenti-iCas9-neo (Addgene 85400) at approximately 60% confluence in the presence of polybrene (8 μ g/mL). Cells were incubated overnight, followed by replacement of the lentivirus-containing medium with fresh medium containing G418 (100 μ g/mL). After selection was completed, a titration of doxycycline (1 to 1000 ng/mL) was performed and the induction of Cas9 expression was assessed by flow cytometry. We determined that 10, 40 and 1000 ng/mL of doxycycline induced low, medium and high levels of Cas9 expression, respectively. Cas9 expression levels were confirmed by Western blot and flow

cytometry one week later. The Cas9-expressing cell line was named “SW480_iCas9”. SW480, A375 and HEK293T cells were transduced with lentiCas9-EGFP (Addgene 63592) at approximately 40-60% confluence in the presence of polybrene (8 µg/mL). Cells were incubated overnight, followed by replacement of the lentivirus-containing medium with fresh medium. After 1 week in culture cells were sorted on low, medium and high GFP levels (BD FACSAria™ Fusion Cell Sorter). Cas9 expression levels were confirmed by Western blot and flow cytometry one week later. The Cas9-expressing cells were named according to their cell line name and Cas9 expression level, i.e. “name_Cas9expression level”.

Editing efficiency assessment by flow cytometry and TIDE analysis

Parental and Cas9-expressing cell lines, as indicated, were transduced with pXPR_011 (Addgene, 59702) at approximately 40-60% confluence in the presence of polybrene (8 µg/mL). Cells were incubated overnight, followed by replacement of the lentivirus-containing medium with fresh medium containing puromycin (2 µg/mL). Cells were harvested 20 h, 3 days (SW480), 6 days and 10 days (HEK293T and A375) after transduction with pXPR_011, GFP levels were assessed by flow cytometry (BD LSRFortessa) and analyzed using FlowJo 10. pXPR_011 results in the expression of both GFP and a sgRNA targeting GFP in the transduced cells. Therefore, editing efficiency can be (indirectly) assessed by analyzing the reduction in GFP signal over time.

SW480_iCas9 cells were transduced with 3 different sgRNAs cloned into pU6-sgRNA-EF1-Puro-T2A-GFP (see sgRNA cloning section below) at approximately 60% confluence in the presence of polybrene (8 µg/mL). Cells were incubated overnight, followed by replacement of the lentivirus-containing medium with fresh medium containing puromycin (2 µg/mL). Cells were kept in puromycin for 7 days. At day 7, a fraction of the cells was harvested, another fraction was analyzed by flow cytometry to confirm equal infection efficiencies indicating similar sgRNA expression levels, and the rest of the cells were placed back in culture and treated with either 10 ng/mL or 1 µg/mL doxycycline. Cells were harvested from these two induction arms after 2, 4, 8, 12, 16, (20, 24 and 32 – only for sgRNA 3) days in continuous culture with doxycycline. DNA was isolated from all samples, Sanger sequencing was performed and editing efficiency was analyzed using TIDE (<https://tide.nki.nl/>). At day 13, cells were also harvested for western blot and flow cytometry analysis, to assess Cas9 expression levels.

sgRNA cloning

To generate OR9Q2 (non-essential gene) sgRNA-expressing MCF10A cells, we cloned OR9Q2 sgRNA (5'-ATAACCGAGAAGGCCCGCTG-3') sequence into lentiCRISPRv2 (Addgene, #52961) and lentiGuide-Puro (Addgene, #52963). Backbones were

digested with BsmBI and cloned using Gibson assembly. sgRNAs targeting 3 different locations in the genome were cloned into a modified version of pU6-sgRNA EF1Alpha-puro-T2A-BFP (Addgene, #60955), where BFP was replaced by superfolder GFP (sfGFP) – named “pU6-sgRNA-EF1-Puro-T2A-GFP”. Puro-T2A-BFP was removed using NheI and EcoRI sites. To introduce Puro-T2A-sfGFP, we amplified Puro-T2A as well as sfGFP, adding homology arms to both PCR products. Puromycin-T2A was amplified using the following oligos: FW: 5'-GTTTTTTTCTCCAT-TTCAGGTGTCGTGAGCTAGCCCACCATGACCGAGTACAAGCCCAC-3', RV: 5'-AACTC-CAGTGAAGATTCTTCTCCTTTGCTGGTGGCGACCGGTGGCCAGGATTCTCCTC-3' sfGFP was amplified using the following oligos: FW: 5'-GAGGAGAATCCTGGCC-CACCGGTGCCACCAGCAAAGGAGAAGAACTTTTCACTGGAGTT-3' RV: 5'-ATGTAT-GCTATACGAAGTTATTAGGTCCCTCGACGAATTCTTATTTGTAGAGCTCATCCA-3' The resulting PCR products were inserted into the open sgRNA vector backbone through Gibson Assembly. To introduce the custom designed sgRNA sequences into the pU6-sgRNA-EF1-Puro-T2A-GFP vector, the vector was digested using BstXI and BamHI. The sgRNAs were PCR-amplified using sgRNA-specific forward primers and a universal reverse primer: FW_1: 5'-TTGGAGAACCACCTTGTTG-GAATATGTTTAAAGCCTAGAGAGTTTAAAGAGCTAAGCTGGAA, FW_2: 5'-TTGGAGAACCACCTTGTTGTTATAGGATAATAGCTGGAAGGTTTAAAGAGCTAAGCTGGAA, FW_3: 5'-TTGGAGAACCACCTTGTTGTTGAGAGGTCTAATTCTAGGGCCGTTTAAAGAGCTAAGCTGGAA, RV: 5'-GTAATACGGTTATCCACGCGCCGCTAATGGATCCTAGTACTCGAGA. The resulting PCR products were isolated and used for Gibson Assembly.

Generation of custom sgRNA library

For the design of the custom sgRNA library targeting essential genes and safe-havens we used the Broad GPP sgRNA design portal and the safe-havens as designed previously (169). The sgRNA sequences (Supplemental Table 2) were ordered as a pool of oligonucleotides (Agilent) with flanking sequences to enable PCR amplification and Gibson assembly into pLentiGuide-Puro (pLG, addgene #52963). The pooled oligo library was amplified using pLG_U6_foward 5'-GGCTTTATATATCTTGTG-GAAAGGACGAAACACCG-3' and pLG-TRACR_Reverse 5'-GACTAGCCTTATTTAACT-TGCTATTTCTAGCTCTAAAAC-3'. The fragments were purified and cloned into pLG as described by Morgens (170). The representation of the custom sgRNA library was validated by next generation sequencing.

sgRNA libraries and screens

Two different versions of the Brunello library were used – a “1 vector system” (backbone expresses both Cas9 and the library – Addgene, 73179) and a “2 vector system” (backbone expresses only the library – Addgene, 73178). In this study we also used our Essential/Safe-havens library described above.

The appropriate number of cells to achieve 250-fold representation of the library, multiplied by five to account for 20% transduction efficiency, were transduced at approximately 40-60% confluence in the presence of polybrene (4-8 $\mu\text{g}/\text{mL}$) with the appropriate volume of the lentiviral-packaged sgRNA library. Cells were incubated overnight, followed by replacement of the lentivirus-containing medium with fresh medium containing puromycin (2-4 $\mu\text{g}/\text{mL}$). The lentivirus volume to achieve a MOI of 0.2, as well as the puromycin concentration to achieve a complete selection in 3 days was previously determined for each cell line. Transductions were performed in triplicate (technical for negative selection screens and biological for positive selection screens). After puromycin selection, cells were split into the indicated arms (for each arm, the appropriate number of cells to keep a 250-fold representation of the library was plated at approximately 10-20% confluence) and a T0 (reference) time point was harvested. Cells were maintained as indicated. In case a passage was required, cells were reseeded at the appropriate number to keep at least a 500-fold representation of the library. Cells (enough to keep at least a 500-fold representation of the library, to account for losses during DNA extraction) were collected when indicated, washed with PBS, pelleted and stored at -80°C until DNA extraction.

DNA extraction, PCR amplification and Illumina sequencing

Genomic DNA (gDNA) was extracted (Zymo Research, D3024) from cell pellets according to the manufacturer's instructions. For every sample, gDNA was quantified and the necessary DNA to maintain a 250-fold representation of the library was used for subsequent procedures (for this we assumed that each cell contains 6.6 pg genomic DNA). Each sample was divided over 50 μl PCR reactions (using a maximum of 1 μg gDNA per reaction) using barcoded forward primers to be able to deconvolute multiplexed samples after next generation sequencing (for primers and barcodes used, see Supplementary Table 3). PCR mixture per reaction: 10 μl 5x HF Buffer, 1 μl 10 μM forward primer, 1 μl 10 μM reverse primer, 0.5 μl Phusion polymerase (Thermo Fisher, F-530XL), 1 μl 10mM dNTPs, adding H₂O and template to 50 μl . Cycling conditions: 30 sec at 98°C , 20 \times (30 sec at 98°C , 30 sec at 60°C , 1 min at 72°C), 5 min at 72°C . The products of all reactions from the same sample were pooled and 2 μl of this pool was used in a subsequent PCR reaction using primers containing adapters for next generation sequencing (Supplementary Table 2). The same cycling protocol was used, this time for 15 cycles. Next, PCR products were purified using the ISOLATE II PCR and Gel Kit (Bioline, BIO-52060) according to the manufacturer's instructions. DNA concentrations were measured and, based on this, samples were equimolarly pooled and subjected to Illumina next generation sequencing (HiSeq 2500 High Output Mode, Single-Read, 65 bp). Mapped read-counts were subsequently used as input for the further analyses.

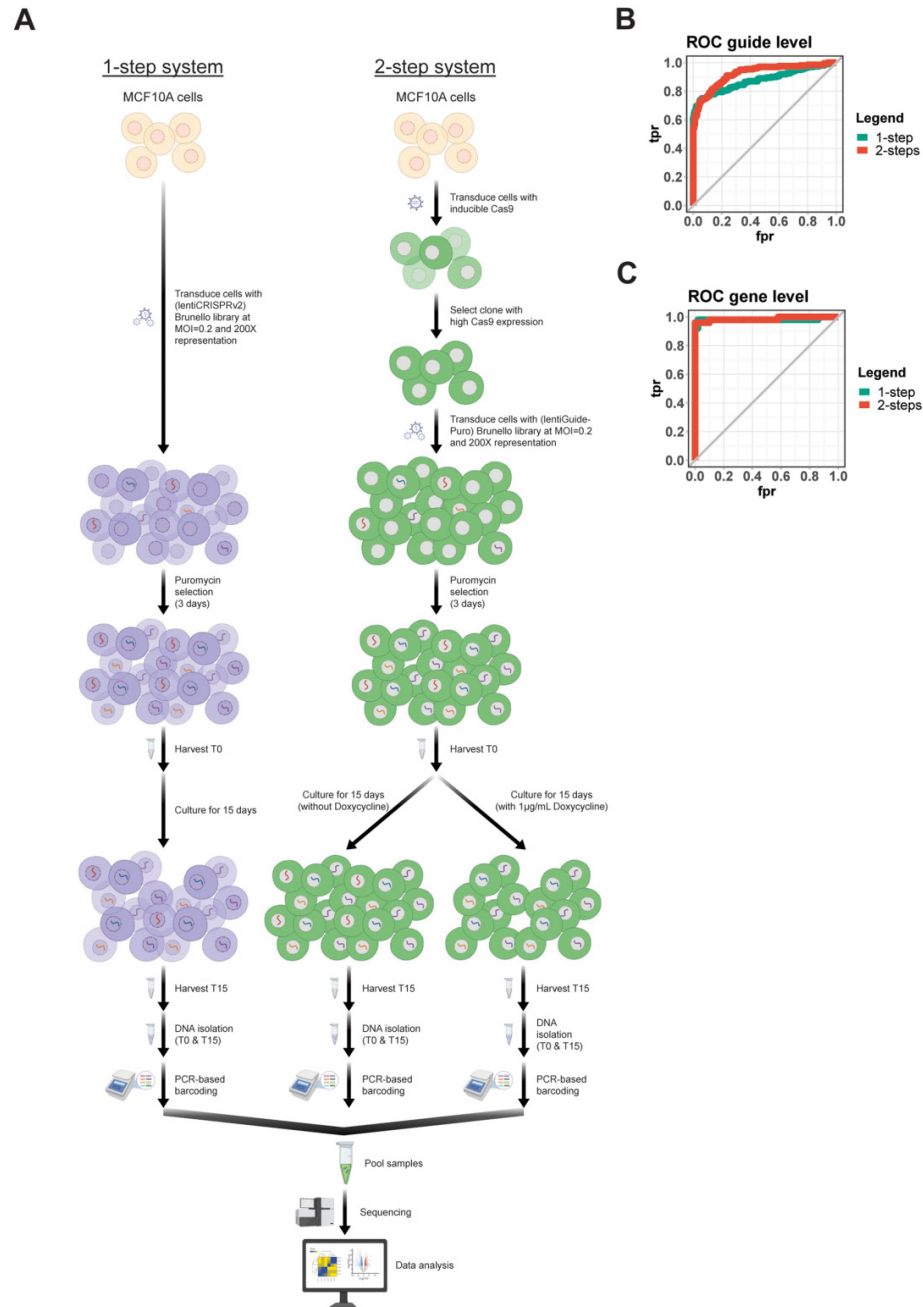
Bioinformatics Analysis

For each CRISPR screen the sgRNA count data for each sample was normalized for sequence depth using the method described by DESeq23 with the difference that the total value instead of the median of a sample was used. Because of the composition of the sgRNA library with a large fraction of sgRNAs targeting essential genes, the T1 samples were corrected by dividing with the median of T1/T0 ratios for the population of non-essential sgRNAs. For the genome-wide CRISPR screen comparing the efficiency of the 1-step and 2-step systems, a differential analysis was performed using DESeq2 (171). The output was sorted on the DESeq2 test statistic with the most depleted sgRNA at the top. We then used MAGeCK Robust Rank Algorithm to determine enrichment of sgRNAs targeting each gene (172). For the ROC curves in supplemental Fig. 1B and 1C the output of these two analyses were filtered for 50 positive and 50 negative controls genes as described by Evers and colleagues (162). The Comparisons of the distribution of different groups of sgRNAs were performed using the Wilcoxon test.

Reagents

Primary antibodies: Tubulin (Sigma, T9026) and Cas9 (Cell Signaling, 14697). Secondary antibody: Goat Anti-Mouse IgG (H + L)-HRP Conjugate (BioRad, 1706516).

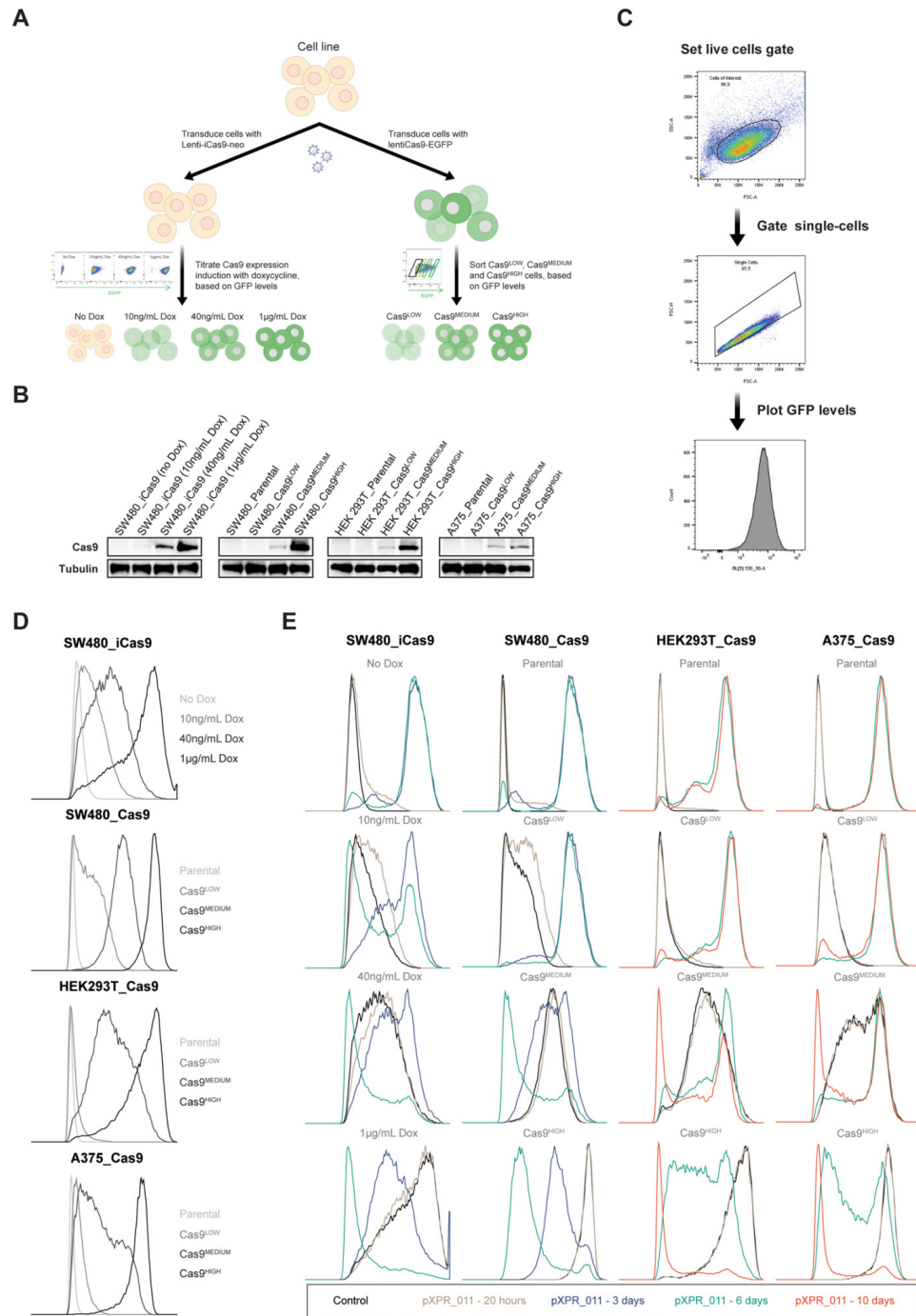
Supplementary Information



Supplementary Figure 1: Genome-wide CRISPR screen to compare the efficiency of the 1-step and 2-step systems.

A, Schematic of the screen layout. 1-step system: $\sim 120 \times 10^6$ MCF10A cells were transduced with the lentiCRISPRv2 Brunello library. After 3 days of puromycin selection, a reference

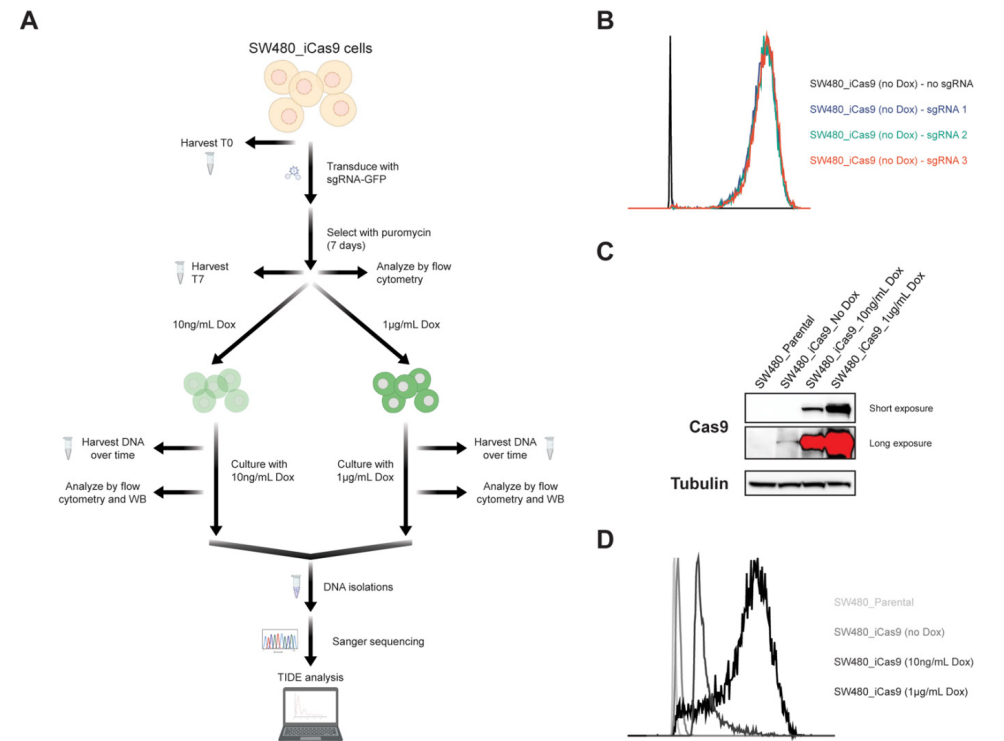
sample was harvested and 1.6×10^7 cells were plated (in triplicate). At day 6 and 11 cells were split and 1.6×10^7 cells were reseeded per replicate. At day 15, all cells were harvested. Abundance of sgRNA for each sample was analyzed by sequencing. 2-steps system: $\sim 150 \times 10^6$ MCF10A_iCas9 cells were transduced with the lentiGuide-Puro Brunello library. After 3 days of puromycin selection, a reference sample was harvested and 2×10^7 cells were plated (in 6 replicates). Three replicates were cultured in the absence of doxycycline, while the other 3 replicates were cultured in the presence of $1 \mu\text{g}/\text{mL}$ doxycycline. At day 6 and 11 cells were split and 4×10^7 cells were reseeded per replicate. At day 15, all cells were harvested. Abundance of sgRNAs for each sample was analyzed by sequencing. B-C, ROC curves for sgRNAs based on the DESeq2 results sorted on the DESeq2 statistic (B) and for genes based on the rank column in the RRA output, both in increasing order (C) p-values for essential genes. FPR, false-positive rate; TPR, true-positive rate.



Supplementary Figure 2: Editing speed is proportional to Cas9 expression level.

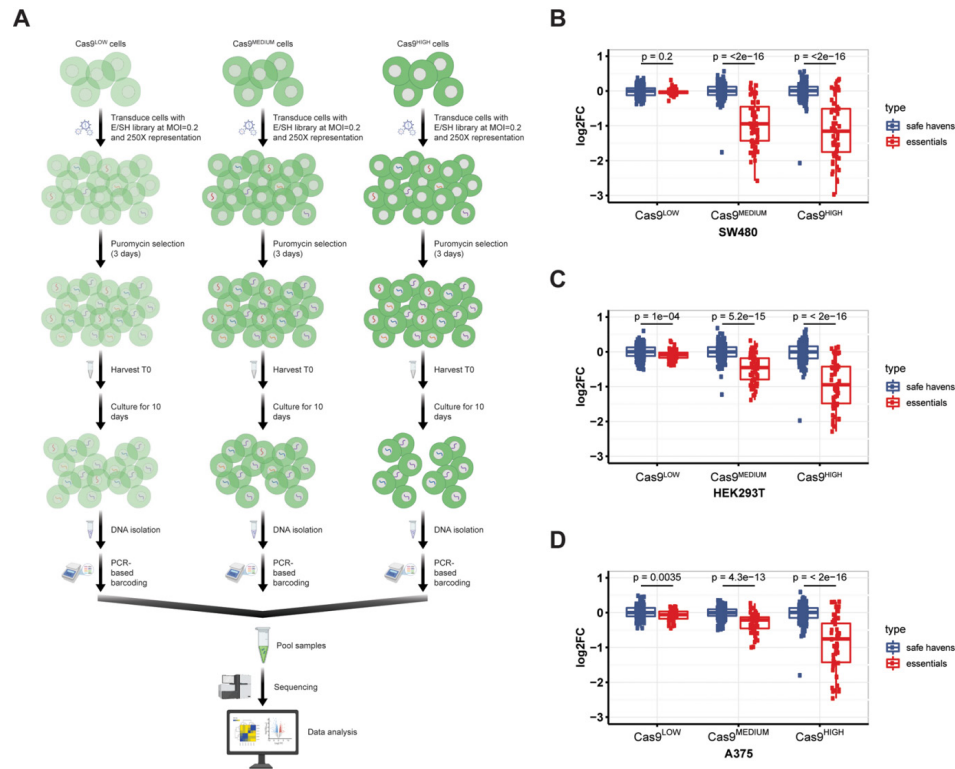
A, Schematic of the generation of Cas9 expressing cell lines. Cell lines were transduced using either lentiCas9-P2A-EGFP or lenti-iCas9-P2A-EGFP. Cells transduced with lenti-iCas9-P2A-EGFP were selected

with G418 and then treated with increasing concentrations of doxycycline. Then, using flow cytometry, we selected cell populations with different levels of Cas9 expression (low, medium or high), based on EGFP expression. B, Validation of the Cas9 expressing lines using western blot. The level of Cas9 expression was measured by examining Cas9 levels by Western blotting. Tubulin was used as loading control. Representative blots from 2 biological replicates are shown. C, Gating strategy used for all flow cytometry experiments. All events were gated on live cells, these were then gated on single cells, and EGFP levels were finally plotted on the single cells. D, Validation of the Cas9-expressing lines using flow cytometry. The level of Cas9 expression was measured (indirectly) by examining EGFP levels (x-axis) by flow cytometry. E, Editing speed is proportional to Cas9 expression level. Parental and Cas9-expressing cell lines were transduced with pXPR_011. Cells were harvested at the indicated time-points after transduction with pXPR_011 and GFP levels (x-axis) were assessed by flow cytometry and analysed using FlowJo 10.



Supplementary Figure 3: Editing speed is proportional to Cas9 expression level.

A, Schematic of editing efficiency assessment by TIDE analysis. SW480_iCas9 cells were transduced with 3 different sgRNAs. Cells were incubated overnight, followed by replacement of the lentivirus-containing medium with fresh medium containing puromycin (2 µg/mL). Cells were kept in puromycin for 7 days. At day 7, a fraction of the cells was harvested as reference sample, (B) another fraction was analyzed by flow cytometry to confirm equal infection efficiency indicating similar sgRNA expression levels, while the rest of the cells were placed back in culture and treated with either 10ng/mL or 1µM/mL doxycycline. Cells were harvested from these two arms at different time-points over time. DNA was isolated from all samples, Sanger sequencing was performed and editing efficiency was analyzed using TIDE. At day 13, cells were also harvested for Western blotting (C) and flow cytometry analysis (D) to assess Cas9 expression levels.



Supplementary Figure 4: Editing speed is proportional to Cas9 expression, independent of sgRNA sequence.

A, Schematic of the screen layout. For each Cas9 expressing subline 2.5×10^6 cells were transduced with the essential/safe-haven library using a MOI of 0.2. Cells were incubated overnight, followed by replacement of the lentivirus-containing medium with fresh medium containing puromycin ($2 \mu\text{g/mL}$). After 3 days of puromycin selection, a reference sample was harvested and 2×10^8 cells were plated (in triplicate). Cells were cultured for 8 population doublings (~ 10 days), after which 5×10^8 cells per replicate were harvested, DNA was extracted, samples were barcoded using PCR and sent for sequencing. B-D, Editing speed is proportional to Cas9 expression, independent of sgRNA sequence. Cells screened as outlined above were analyzed for the depletion (\log_2 Fold Change) of the sgRNAs targeting essential genes and safe-havens. $\log_2\text{FC}$ depicts the \log_2 fold change sgRNA counts T1/T0. Box plot shows the median (horizontal line), interquartile range (hinges), and the smallest and largest values no more than 1.5 times the interquartile range (whiskers). Comparisons were made using the Wilcoxon test.

6

General discussion

Cancer therapy has improved significantly in the last 10-20 years but there is still a long road ahead... Chemotherapy has been the backbone of cancer treatment for decades but the discovery that cancer is a consequence of genetic mistakes and that inhibition of oncogenic proteins elicits therapeutic responses fueled the development of targeted strategies. As a result of technological developments such as next generation sequencing, which expanded our knowledge about cancer biology, the targeted therapy field exploded in the last years. But the initial hype quickly faded, as we discovered that most advanced tumors are intrinsically resistant or develop resistance in a short period of time. In my PhD thesis, I aimed to address the problem of drug resistance with rational but innovative approaches. Here, I will discuss the impact of our findings and share my view on some of the obstacles that we need to overcome to implement them in the clinic, or in standard laboratory practice.

It is well established that drug combinations are more effective than single agent targeted drugs. However, combining drugs is often associated with toxicity. We reasoned that this toxicity could be, at least in some cases, due to the drug administration model, i.e. the delivery of a drug to patients at the maximum tolerated dose (MTD). One recent example of this is the recent BEACON trial(10), where patients with BRAF V600E-Mutated Colorectal Cancer received triple therapy (EGFR+BRAF+MEK inhibition) or double therapy (BRAF+EGFR inhibition). Here, even though the overall survival of the triplet therapy was superior, this combination was not approved because the increased toxicity did not justify the added benefits to the double therapy. This drug administration model has remained virtually unchanged for decades, despite some evidence that MTD is not always necessary to achieve a clinical response (173). We reasoned that if we reduced the concentration of drugs we might eliminate the toxicity problem when using drug combinations while maintaining efficacy. In **chapter 2** of this thesis we show that partial inhibition of multiple components of cancer-activated signalling pathways results in complete pathway inhibition, which is more difficult to circumvent than by a single drug at MTD, therefore reducing chances of resistance. The promising pre-clinical data in mice propelled us to start a clinical trial but we quickly realized one translational disadvantage of using multiple drugs - it is impossible to find companies which have all the inhibitors in their portfolio. This means that agreements between several companies are needed. It's been over 2 years since we started the process of initiating a clinical trial to bring the MLD strategy to the clinic and this bureaucratic nightmare is nowhere near the end. This collaboration problem stems from economic and regulatory reasons, but one underlying culprit is the reliance of most large pharmaceutical companies on an archaic drug development model, as discussed in **chapter 1**. Even though this is starting to change, as evidenced by the recent efforts of Revolution Medicines, who

is testing their SHP2 inhibitor in combination with MEK inhibitors early in the process of clinical development rather than putting their focus on demonstrating single agent activity. Changing this drug development model requires a different approach to how we develop cancer treatments, but it also requires some regulatory changes. The most important one being that new investigative agents should not need to show single agent efficacy in patients before combination therapies are considered, if there is a sound rationale and strong pre-clinical efficacy data. Single agent toxicity studies will still be required to understand if the compound is toxic when used alone before testing drug combinations, but this process requires less patients and therefore it is relatively quick. When companies start to develop drug combinations from the get-go it will become clear that collaboration is necessary, as evidenced by the above-mentioned example of Revolution Medicines, who is collaborating with Genentech to supply the MEK inhibitor Cobimetinib. As this becomes more common, the whole process will speed up, which ultimately will benefit everyone.

Even with improvements in the drug development model, most likely, there will still be a high attrition rate of early-stage investigational agents. One of the reasons for this is the models we currently use to predict response to cancer treatments. The majority of pre-clinical efficacy studies are done using xenograft models. They are the quickest way to analyze the response of a human tumor to therapeutic regimens and they provide realistic heterogeneity of tumor cells. However, these mice are immunocompromised, therefore providing a less realistic tumor microenvironment. With the notion that the immune system and the tumor microenvironment are of utmost importance to treatment outcome, it becomes clear that using only xenografts is not enough. To provide the immune context, including also GEMMs in pre-clinical efficacy studies should become common practice. The biggest limitation to these models used to be the time involved in their development. But nowadays, with CRISPR technology, that's no longer an issue. Another challenge, commonly overlooked, is drug delivery and pharmacokinetics. Most treatment regimens are discovered using in vitro methods, where drugs are in general stable for several days. However, in vivo, liver enzymes degrade most compounds in a matter of hours, as we've shown in chapter 2, making it difficult to maintain constant target inhibition, which is necessary for efficacy. These are some of the reasons why exciting lab discoveries too often don't make it to the clinic. The increasing number of cancer compounds, together with the notion that drug combinations deliver more benefit has created another challenge. The number of possible drug combinations is becoming enormous, making it impossible to test all possible combinations experimentally. CRISPR screens offer an unbiased way to tackle this issue. However, they are mostly limited to identifying 2-drug combinations. And, as we've shown in chapter 2, using multi-drug combinations at low doses

might be a better approach to prevent drug resistance. This multidimensional information (targets and dose) is something CRISPR screens cannot offer. One way to overcome this problem is to develop computational pipelines that reconstruct signaling networks based on experimental perturbation experiments, connect changes in signaling output to changes in cell viability, and use these models to prioritize multi-drug combinations in silico. In **chapter 3** we developed such an approach and we were able to predict and validate drug combinations that were selective for a particular cell line. One limitation of our approach is that the experimental model where experimental perturbation experiments were performed played a key role in the outcome. Unfortunately, there are no perfect models and heterogeneity will always be present in experimental approaches. But nowadays, with the increasing amount of publicly available data, particularly in the characterization of human cancer cell lines it becomes possible to include the effects of mutations and expression levels of genes in cancer-related pathways, per cell line, in the computational pipeline (174). To overcome this hurdle experimentally we would have to use large cell line panels, which would be extremely laborious, expensive and time consuming. For all these reasons, I believe that computational modelling is the way forward in cancer research, but the number of collaborations between “dry” and “wet” labs must increase so that in silico discoveries don’t end up in the “literature pile” with no experimental or clinical follow-up. Finally, large sequencing and screening efforts, such as the Cancer Cell Line Encyclopedia and DepMap have provided critical data for developing more advanced computational pipelines and therefore it will only be a matter of time until in silico discoveries will make it to the clinic.

Cancer immunotherapy has been the “hottest” topic in cancer research in recent years. It revolutionized cancer therapy because, for the first time, a large number of patients with (previously) incurable cancers now stay in remission for a large number of years or even get cured. Deficient MMR and MSI was one of the first predictive biomarkers to be approved for selecting patients for immunotherapy. Importantly, there is evidence suggesting that a subset of patients with MSS tumors could also benefit from immunotherapy (142,143), but because they don’t meet the eligibility criteria they are not treated with immunotherapy. Since induction of MSI increases the immunogenicity of tumors and consequently the response to immunotherapy (153), we reasoned that if we could identify novel genes which regulate MSI we could potentially use them as additional predictive biomarkers for immunotherapy treatment. To that end, in **chapter 4** we tried to find new regulators of microsatellite instability by performing CRISPR screens in a MSS cell line carrying a fluorescent-based MSI sensor. Remarkably, after more than 20 years of research into colon cancer, we were the first to identify a novel candidate MSI gene: MED12. MED12 is a member of the MEDIATOR complex, an essential

component of the transcriptional machinery and therefore it was not surprising to observe that MED12 suppression led to a downregulation of the expression of MMR genes MLH1 and MSH2. Induction of MSI by inactivation of MMR has recently been proposed as a potential treatment strategy to sensitize tumors to immunotherapy (153). We found that MED12-induced MMR downregulation is only mild and therefore induction of MSI by MED12 inhibition would take a long time. Additionally, since MED12 is part of a large complex involved in transcription, which makes it virtually impossible to “drug”, using MED12 as a drug target should not be considered. However, it would be particularly interesting to look into the status of MED12 in the so-called MSI-like tumors. These are tumors which display an MSI expression profile, respond to treatment like MSI tumors but test negative for MSI. If we find a link between MED12 and this phenotype, MED12 could become a predictive biomarker, allowing more patients who should benefit from immunotherapy to become eligible to receive it.

Technology has revolutionized the modern world and the incredible pace at which cancer biology has progressed in the last decade is mostly thanks to a few technological advances. One of them, which transformed genetic studies from time consuming, expensive and specialized into a routine lab technique is CRISPR. Thanks to CRISPR we can now edit genomes in a matter of days, virtually for free. But, just like with every technique, there are always some tweaks that can improve efficiency. And after using CRISPR for a while I noticed that the editing time could be significantly improved by increasing the expression of Cas9. In **chapter 5** we performed a comprehensive study to address this issue and provide evidence which indicates that optimizing Cas9 expression can improve the efficiency of CRISPR screens. One particular example where decreasing editing time is of major importance is in drug-resistance screens. Here, one wants to ensure that all genes are edited before the drug is added to the cells. Adding the drug too early (before editing occurs) can potentially result in the death of cells carrying a sgRNA which would confer resistance to the drug; and adding the drug too late will increase the logistical hurdles of CRISPR screens. Ensuring high Cas9 expression is very simple and with some expression vectors it can be done in less than a week. This modest time investment at the early stage of a project will be paid back later with interest. Ultimately, it will reduce the length of the experiments, and therefore also the costs. CRISPR screens are used in a variety of research fields and therefore this small tweak can potentially influence many future discoveries.

With this thesis I tried to develop new strategies to address the problem of drug resistance. One of the things I learned during this process is that we don’t always have to “reinvent the wheel” to make a difference, as shown in chapter 5, and that using rational approaches with strong mechanistic basis is the best way to discover novel treatment strategies, as exemplified by the high failure rate of the hundreds

of “trial and error” PD1 trials. Despite all the advances in the cancer field in recent years, there are still infinite challenges that need to be addressed. Nevertheless, as a scientific community, we are making steady progress in our understanding of drug resistance and such findings are reaching the clinic faster than ever before. As one example, Jin et al uncovered the resistance mechanism to lenvatinib using a CRISPR screen and, in less than 2 years, were able to demonstrate clinical proof-of-concept of the drug combination that overcomes lenvatinib resistance (175). Findings like this suggest that the pace at which patients can benefit from scientific discoveries will continue to increase in years to come, which is enough reason to be optimistic about the future of cancer treatment.



Appendix

References

Nederlandse samenvatting

Curriculum vitae

Publication list

Acknowledgements

References

1. Dimasi JA. Risks in new drug development: approval success rates for investigational drugs. *Clin Pharmacol Ther.* 2001 May;69(5):297–307.
2. Kopetz S, Desai J, Chan E, Hecht JR, O'Dwyer PJ, Maru D, et al. Phase II pilot study of vemurafenib in patients with metastatic BRAF-mutated colorectal cancer. *J Clin Oncol.* 2015;33(34):4032.
3. Chapman PB, Hauschild A, Robert C, Haanen JB, Ascierto P, Larkin J, et al. Improved survival with vemurafenib in melanoma with BRAF V600E mutation. *N Engl J Med.* 2011;364(26):2507–16.
4. Tsai J, Lee JT, Wang W, Zhang J, Cho H, Mamo S, et al. Discovery of a selective inhibitor of oncogenic B-Raf kinase with potent antimelanoma activity. *Proc Natl Acad Sci.* 2008;105(8):3041–6.
5. Davies H, Bignell GR, Cox C, Stephens P, Edkins S, Clegg S, et al. Mutations of the BRAF gene in human cancer. *Nature.* 2002;417(6892):949–54.
6. Gyawali B, Prasad V. Drugs that lack single-agent activity: are they worth pursuing in combination? *Nat Rev Clin Oncol.* 2017;14(4):193–4.
7. Tol J, Koopman M, Cats A, Rodenburg CJ, Creemers GJM, Schrama JG, et al. Chemotherapy, bevacizumab, and cetuximab in metastatic colorectal cancer. *N Engl J Med.* 2009 Feb;360(6):563–72.
8. Prahallad A, Sun C, Huang S, Di Nicolantonio F, Salazar R, Zecchin D, et al. Unresponsiveness of colon cancer to BRAF(V600E) inhibition through feedback activation of EGFR. *Nature.* 2012 Mar;483(7387):100–3.
9. Corcoran RB, Ebi H, Turke AB, Coffee EM, Nishino M, Cogdill AP, et al. EGFR-mediated reactivation of MAPK signaling contributes to insensitivity of BRAF-mutant colorectal cancers to RAF inhibition with vemurafenib. *Cancer Discov.* 2012;2(3):227–35.
10. Kopetz S, Grothey A, Yaeger R, Van Cutsem E, Desai J, Yoshino T, et al. Encorafenib, Binimetinib, and Cetuximab in BRAF V600E-Mutated Colorectal Cancer. *N Engl J Med.* 2019 Sep;
11. Harrington PE, Biswas K, Malwitz D, Tasker AS, Mohr C, Andrews KL, et al. Unfolded protein response in cancer: IRE1 α inhibition by selective kinase ligands does not impair tumor cell viability. *ACS Med Chem Lett.* 2015;6(1):68–72.
12. Xue JY, Zhao Y, Aronowitz J, Mai TT, Vides A, Qeriqi B, et al. Rapid non-uniform adaptation to conformation-specific KRAS (G12C) inhibition. *Nature.* 2020;577(7790):421–5.
13. Hallin J, Engstrom LD, Hargis L, Calinisan A, Aranda R, Briere DM, et al. The KRASG12C inhibitor MRTX849 provides insight toward therapeutic susceptibility of KRAS-mutant cancers in mouse models and patients. *Cancer Discov.* 2020;10(1):54–71.
14. Molina-Arcas M, Moore C, Rana S, van Maldegem F, Mugarza E, Romero-Clavijo P, et al. Development of combination therapies to maximize the impact of KRAS-G12C inhibitors in lung cancer. *Sci Transl Med.* 2019;11(510).
15. Santana-Codina N, Chandhoke AS, Yu Q, Małachowska B, Kuljanin M, Gikandi A, et al. Defining and targeting adaptations to oncogenic KRASG12C inhibition using quantitative temporal proteomics. *Cell Rep.* 2020;30(13):4584–99.
16. Amodio V, Yaeger R, Arcella P, Cancelliere C, Lamba S, Lorenzato A, et al. EGFR blockade reverts resistance to KRASG12C inhibition in colorectal cancer. *Cancer Discov.* 2020;10(8):1129–39.
17. Lou K, Steri V, Alex YG, Hwang YC, Yogodzinski CH, Shkedi AR, et al. KRASG12C inhibition produces a driver-limited state revealing collateral dependencies. *Sci Signal.* 2019;12(583).
18. Fang Y, McGrail DJ, Sun C, Labrie M, Chen X, Zhang D, et al. Sequential therapy with PARP and WEE1 inhibitors minimizes toxicity while maintaining efficacy. *Cancer Cell.* 2019;35(6):851–67.
19. Lee MJ, Albert SY, Gardino AK, Heijink AM, Sorger PK, MacBeath G, et al. Sequential application of anticancer drugs enhances cell death by rewiring apoptotic signaling networks. *Cell.* 2012;149(4):780–94.
20. Rothschilds AM, Wittrup KD. What, why, where, and when: bringing timing to immuno-oncology. *Trends Immunol.* 2019;40(1):12–21.
21. Hernandez-Segura A, Nehme J, Demaria M. Hallmarks of cellular senescence. *Trends Cell Biol.* 2018;28(6):436–53.
22. Lee S, Schmitt CA. The dynamic nature of senescence in cancer. *Nat Cell Biol.* 2019;21(1):94–101.
23. Mikuła-Pietrasik J, Niklas A, Uruski P, Tykarski A, Książek K. Mechanisms and significance of therapy-induced and spontaneous senescence of cancer cells. *Cell Mol Life Sci.* 2020;77(2):213–29.
24. Bodnar AG, Ouellette M, Frolkis M, Holt SE, Chiu C-P, Morin GB, et al. Extension of life-span by introduction of telomerase into normal human cells. *Science (80-).* 1998;279(5349):349–52.
25. Wang L, de Oliveira RL, Wang C, Neto JMF, Mainardi S, Evers B, et al. High-throughput functional genetic and compound screens identify targets for senescence induction in cancer. *Cell Rep.* 2017;21(3):773–83.
26. Triana-Martínez F, Picallos-Rabina P, Da Silva-Álvarez S, Pietrocola F, Llanos S, Rodilla V, et al. Identification and characterization of Cardiac Glycosides as senolytic compounds. *Nat Commun.* 2019;10(1):1–12.
27. Guerrero A, Herranz N, Sun B, Wagner V, Gallage S, Guiho R, et al. Cardiac glycosides are broad-spectrum senolytics. *Nat Metab.* 2019;1(11):1074–88.
28. Wang C, Vegna S, Jin H, Benedict B, Lieftink C, Ramirez C, et al. Inducing and exploiting vulnerabilities for the treatment of liver cancer. *Nature.* 2019;574(7777):268–72.
29. Fleury H, Malaquin N, Tu V, Gilbert S, Martinez A, Olivier M-A, et al. Exploiting interconnected synthetic lethal interactions between PARP inhibition and cancer cell reversible senescence. *Nat Commun.* 2019;10(1):1–15.
30. Glück S, Guey B, Gulen MF, Wolter K, Kang T-W, Schmacke NA, et al. Innate immune sensing of cytosolic chromatin fragments through cGAS promotes senescence. *Nat Cell Biol.* 2017;19(9):1061–70.
31. Ruscetti M, Morris IV JP, Mezzadra R, Russell J, Leibold J, Romesser PB, et al. Senescence-induced vascular remodeling creates therapeutic vulnerabilities in pancreas cancer. *Cell.* 2020;181(2):424–41.
32. Voorwerk L, Slagter M, Horlings HM, Sikorska K, van de Vijver KK, de Maaker M, et al. Immune induction strategies in metastatic triple-negative breast cancer to enhance the sensitivity to PD-1 blockade: the TONIC trial. *Nat Med.* 2019;25(6):920–8.

33. Kroemer G, Galluzzi L, Kepp O, Zitvogel L. Immunogenic cell death in cancer therapy. *Annu Rev Immunol*. 2013;31:51–72.
34. Ewald JA, Desotelle JA, Wilding G, Jarrard DF. Therapy-induced senescence in cancer. *JNCI J Natl Cancer Inst*. 2010;102(20):1536–46.
35. Hutchison DJ. Cross resistance and collateral sensitivity studies in cancer chemotherapy. *Adv Cancer Res*. 1963;7:235–350.
36. Wang L, Leite de Oliveira R, Huijberts S, Bosdriesz E, Pencheva N, Brunen D, et al. An Acquired Vulnerability of Drug-Resistant Melanoma with Therapeutic Potential. *Cell* [Internet]. 2018;173(6):1413–1425.e14. Available from: <https://www.sciencedirect.com/science/article/pii/S0092867418305051>
37. Shah KN, Bhatt R, Rotow J, Rohrberg J, Olivas V, Wang VE, et al. Aurora kinase A drives the evolution of resistance to third-generation EGFR inhibitors in lung cancer. *Nat Med* [Internet]. 2019;25(1):111–8. Available from: <https://doi.org/10.1038/s41591-018-0264-7>
38. Bertran-Alamillo J, Cattani V, Schoumacher M, Codony-Servat J, Giménez-Capitán A, Cantero F, et al. AURKB as a target in non-small cell lung cancer with acquired resistance to anti-EGFR therapy. *Nat Commun* [Internet]. 2019;10(1):1812. Available from: <https://doi.org/10.1038/s41467-019-09734-5>
39. Kuczynski EA, Sargent DJ, Grothey A, Kerbel RS. Drug rechallenge and treatment beyond progression—implications for drug resistance. *Nat Rev Clin Oncol* [Internet]. 2013;10(10):571–87. Available from: <https://doi.org/10.1038/nrclinonc.2013.158>
40. Das Thakur M, Salangsang F, Landman AS, Sellers WR, Pryer NK, Levesque MP, et al. Modelling vemurafenib resistance in melanoma reveals a strategy to forestall drug resistance. *Nature* [Internet]. 2013;494(7436):251–5. Available from: <https://doi.org/10.1038/nature11814>
41. Algazi AP, Othus M, Daud A, Mehnert JM, Lao CD, Kudchadkar RR, et al. SWOG S1320: A randomized phase II trial of intermittent versus continuous dosing of dabrafenib and trametinib in BRAFV600E/k mutant melanoma. *J Clin Oncol* [Internet]. 2015 May 20;33(15_suppl):TPS9093–TPS9093. Available from: https://doi.org/10.1200/jco.2015.33.15_suppl.tps9093
42. Konieczkowski DJ, Johannessen CM, Garraway LA. A Convergence-Based Framework for Cancer Drug Resistance. *Cancer Cell*. 2018 May;33(5):801–15.
43. Flaherty KT, Robert C, Hersey P, Nathan P, Garbe C, Milhem M, et al. Improved survival with MEK inhibition in BRAF-mutated melanoma. *N Engl J Med*. 2012 Jul;367(2):107–14.
44. Khunger A, Khunger M, Velcheti V. Dabrafenib in combination with trametinib in the treatment of patients with BRAF V600-positive advanced or metastatic non-small cell lung cancer: clinical evidence and experience. *Ther Adv Respir Dis*. 2018;12:1753466618767611.
45. Xue Y, Martelotto L, Baslan T, Vides A, Solomon M, Mai TT, et al. An approach to suppress the evolution of resistance in BRAFV600E-mutant cancer. *Nat Med* [Internet]. 2017;23(8):929–37. Available from: <https://doi.org/10.1038/nm.4369>
46. Bock C, Lengauer T. Managing drug resistance in cancer: lessons from HIV therapy. *Nat Rev Cancer* [Internet]. 2012;12(7):494–501. Available from: <https://doi.org/10.1038/nrc3297>
47. Fernandes Neto JM, Nadal E, Bosdriesz E, Ooft SN, Farre L, McLean C, et al. Multiple low dose therapy as an effective strategy to treat EGFR inhibitor-resistant NSCLC tumours. *Nat Commun* [Internet]. 2020;11(1):3157. Available from: <https://doi.org/10.1038/s41467-020-16952-9>
48. Ozkan-Dagliyan I, Diehl JN, George SD, Schaefer A, Papke B, Klotz-Noack K, et al. Low-Dose Vertical Inhibition of the RAF-MEK-ERK Cascade Causes Apoptotic Death of KRAS Mutant Cancers. *Cell Rep* [Internet]. 2020;31(11):107764. Available from: <https://www.sciencedirect.com/science/article/pii/S2211124720307440>
49. Hamid AB, Petreaca RC. Secondary Resistant Mutations to Small Molecule Inhibitors in Cancer Cells. Vol. 12, *Cancers*. 2020.
50. Phan TG, Croucher PI. The dormant cancer cell life cycle. *Nat Rev Cancer* [Internet]. 2020;20(7):398–411. Available from: <https://doi.org/10.1038/s41568-020-0263-0>
51. Schaefer DJ, Klemt C, Zhang XH, Stark GB. [Tissue engineering with mesenchymal stem cells for cartilage and bone regeneration]. *Chirurg* [Internet]. 2000;71(9):1001–8. Available from: <http://europepmc.org/abstract/MED/11043116>
52. Singh A, Settleman J. EMT, cancer stem cells and drug resistance: an emerging axis of evil in the war on cancer. *Oncogene* [Internet]. 2010;29(34):4741–51. Available from: <https://doi.org/10.1038/onc.2010.215>
53. Wilson MM, Weinberg RA, Lees JA, Guen VJ. Emerging Mechanisms by which EMT Programs Control Stemness. *Trends in Cancer* [Internet]. 2020;6(9):775–80. Available from: <https://www.sciencedirect.com/science/article/pii/S2405803320301205>
54. Sharma S V, Lee DY, Li B, Quinlan MP, Takahashi F, Maheswaran S, et al. A chromatin-mediated reversible drug-tolerant state in cancer cell subpopulations. *Cell*. 2010 Apr;141(1):69–80.
55. Skrypek N, Goossens S, De Smedt E, Vandamme N, Berx G. Epithelial-to-Mesenchymal Transition: Epigenetic Reprogramming Driving Cellular Plasticity. *Trends Genet* [Internet]. 2017;33(12):943–59. Available from: <https://www.sciencedirect.com/science/article/pii/S0168952517301361>
56. Wainwright EN, Scaffidi P. Epigenetics and Cancer Stem Cells: Unleashing, Hijacking, and Restricting Cellular Plasticity. *Trends in Cancer* [Internet]. 2017;3(5):372–86. Available from: <https://www.sciencedirect.com/science/article/pii/S240580331730081X>
57. Swanson EC, Manning B, Zhang H, Lawrence JB. Higher-order unfolding of satellite heterochromatin is a consistent and early event in cell senescence. *J Cell Biol* [Internet]. 2013 Dec 16;203(6):929–42. Available from: <https://doi.org/10.1083/jcb.201306073>
58. Guler GD, Tindell CA, Pitti R, Wilson C, Nichols K, KaiWai Cheung T, et al. Repression of Stress-Induced LINE-1 Expression Protects Cancer Cell Subpopulations from Lethal Drug Exposure. *Cancer Cell* [Internet]. 2017;32(2):221–237.e13. Available from: <https://www.sciencedirect.com/science/article/pii/S1535610817302945>
59. Pham V, Pitti R, Tindell CA, Cheung TK, Masselot A, Stephan J-P, et al. Proteomic Analyses Identify a Novel Role for EZH2 in the Initiation of Cancer Cell Drug Tolerance. *J Proteome Res* [Internet]. 2020 Apr 3;19(4):1533–47. Available from: <https://doi.org/10.1021/acs.jproteome.9b00773>
60. Jin X, Kim LJY, Wu Q, Wallace LC, Prager BC, Sanvoranart T, et al. Targeting glioma stem cells through combined BMI1 and EZH2 inhibition. *Nat Med* [Internet]. 2017;23(11):1352–61. Available from: <https://doi.org/10.1038/nm.4415>

61. Gupta PB, Onder TT, Jiang G, Tao K, Kuperwasser C, Weinberg RA, et al. Identification of Selective Inhibitors of Cancer Stem Cells by High-Throughput Screening. *Cell* [Internet]. 2009;138(4):645–59. Available from: <https://www.sciencedirect.com/science/article/pii/S0092867409007818>
62. Wilson C, Nicholes K, Bustos D, Lin E, Song Q, Stephan J-P, et al. Overcoming EMT-associated resistance to anti-cancer drugs via Src/FAK pathway inhibition. *Oncotarget*. 2014;5(17):7328.
63. Raha D, Wilson TR, Peng J, Peterson D, Yue P, Evangelista M, et al. The cancer stem cell marker aldehyde dehydrogenase is required to maintain a drug-tolerant tumor cell subpopulation. *Cancer Res*. 2014;74(13):3579–90.
64. Hangauer MJ, Viswanathan VS, Ryan MJ, Bole D, Eaton JK, Matov A, et al. Drug-tolerant persister cancer cells are vulnerable to GPX4 inhibition. *Nature*. 2017. p. 247–50.
65. Kurppa KJ, Liu Y, To C, Zhang T, Fan M, Vajdi A, et al. Treatment-Induced Tumor Dormancy through YAP-Mediated Transcriptional Reprogramming of the Apoptotic Pathway. *Cancer Cell* [Internet]. 2020;37(1):104–122.e12. Available from: <https://www.sciencedirect.com/science/article/pii/S1535610819305768>
66. Gerlinger M, Rowan AJ, Horswell S, Larkin J, Endesfelder D, Gronroos E, et al. Intratumor Heterogeneity and Branched Evolution Revealed by Multiregion Sequencing. *N Engl J Med* [Internet]. 2012 Mar 7;366(10):883–92. Available from: <https://doi.org/10.1056/NEJMoa1113205>
67. Cameron D, Piccart-Gebhart MJ, Gelber RD, Procter M, Goldhirsch A, de Azambuja E, et al. 11 years' follow-up of trastuzumab after adjuvant chemotherapy in HER2-positive early breast cancer: final analysis of the HERceptin Adjuvant (HERA) trial. *Lancet* [Internet]. 2017;389(10075):1195–205. Available from: <https://www.sciencedirect.com/science/article/pii/S0140673616326162>
68. Schadendorf D, Hodi FS, Robert C, Weber JS, Margolin K, Hamid O, et al. Pooled Analysis of Long-Term Survival Data From Phase II and Phase III Trials of Ipilimumab in Unresectable or Metastatic Melanoma. *J Clin Oncol* [Internet]. 2015/02/09. 2015 Jun 10;33(17):1889–94. Available from: <https://pubmed.ncbi.nlm.nih.gov/25667295>
69. Schoenfeld AJ, Hellmann MD. Acquired Resistance to Immune Checkpoint Inhibitors. *Cancer Cell* [Internet]. 2020;37(4):443–55. Available from: <https://www.sciencedirect.com/science/article/pii/S1535610820301574>
70. Dardaei L, Wang HQ, Singh M, Fordjour P, Shaw KX, Yoda S, et al. SHP2 inhibition restores sensitivity in ALK-rearranged non-small-cell lung cancer resistant to ALK inhibitors. *Nat Med* [Internet]. 2018;24(4):512–7. Available from: <https://doi.org/10.1038/nm.4497>
71. Ruess DA, Heynen GJ, Ciecieski KJ, Ai J, Berninger A, Kabacaoglu D, et al. Mutant KRAS-driven cancers depend on PTPN11/SHP2 phosphatase. *Nat Med* [Internet]. 2018;24(7):954–60. Available from: <https://doi.org/10.1038/s41591-018-0024-8>
72. Mainardi S, Mulero-Sánchez A, Prahallad A, Germano G, Bosma A, Krimpenfort P, et al. SHP2 is required for growth of KRAS-mutant non-small-cell lung cancer in vivo. *Nat Med* [Internet]. 2018;24(7):961–7. Available from: <https://doi.org/10.1038/s41591-018-0023-9>
73. Wong GS, Zhou J, Liu J Bin, Wu Z, Xu X, Li T, et al. Targeting wild-type KRAS-amplified gastroesophageal cancer through combined MEK and SHP2 inhibition. *Nat Med* [Internet]. 2018;24(7):968–77. Available from: <https://doi.org/10.1038/s41591-018-0022-x>
74. Weinstein IB. Addiction to Oncogenes--the Achilles Heal of Cancer. *Sci* [Internet]. 2002 Jul 5;297(5578):63–4. Available from: <http://www.sciencemag.org/content/297/5578/63.short>
75. Sun C, Bernards R. Feedback and redundancy in receptor tyrosine kinase signaling: relevance to cancer therapies. *Trends Biochem Sci*. 2014 Oct;39(10):465–74.
76. Flaherty KT, Infante JR, Daud A, Gonzalez R, Kefford RF, Sosman J, et al. Combined BRAF and MEK inhibition in melanoma with BRAF V600 mutations. *N Engl J Med*. 2012 Nov;367(18):1694–703.
77. Corcoran RB, Andre T, Atreya CE, Schellens JHM, Yoshino T, Bendell JC, et al. Combined BRAF, EGFR, and MEK Inhibition in Patients with BRAF(V600E)-Mutant Colorectal Cancer. *Cancer Discov*. 2018 Apr;8(4):428–43.
78. Xue Y, Martelotto L, Baslan T, Vides A, Solomon M, Mai TT, et al. An approach to suppress the evolution of resistance in BRAF(V600E)-mutant cancer. *Nat Med*. 2017 Aug;23(8):929–37.
79. Caumanns JJ, van Wijngaarden A, Kol A, Meersma GJ, Jalving M, Bernards R, et al. Low-dose triple drug combination targeting the PI3K/AKT/mTOR pathway and the MAPK pathway is an effective approach in ovarian clear cell carcinoma. *Cancer Lett*. 2019 Oct;461:102–11.
80. Peng S-B, Henry JR, Kaufman MD, Lu W-P, Smith BD, Vogeti S, et al. Inhibition of RAF Isoforms and Active Dimers by LY3009120 Leads to Anti-tumor Activities in RAS or BRAF Mutant Cancers. *Cancer Cell*. 2015 Sep;28(3):384–98.
81. Morris EJ, Jha S, Restaino CR, Dayananth P, Zhu H, Cooper A, et al. Discovery of a novel ERK inhibitor with activity in models of acquired resistance to BRAF and MEK inhibitors. *Cancer Discov*. 2013 Jul;3(7):742–50.
82. Anjum R, Blenis J. The RSK family of kinases: emerging roles in cellular signalling. *Nat Rev Mol Cell Biol*. 2008 Oct;9(10):747–58.
83. Russ D, Kishony R. Additivity of inhibitory effects in multidrug combinations. *Nat Microbiol* [Internet]. 2018;3(12):1339–45. Available from: <https://doi.org/10.1038/s41564-018-0252-1>
84. Brant R, Sharpe A, Liptrot T, Dry JR, Harrington EA, Barrett JC, et al. Clinically Viable Gene Expression Assays with Potential for Predicting Benefit from MEK Inhibitors. *Clin Cancer Res*. 2017 Mar;23(6):1471–80.
85. Hata AN, Niederst MJ, Archibald HL, Gomez-Caraballo M, Siddiqui FM, Mulvey HE, et al. Tumor cells can follow distinct evolutionary paths to become resistant to epidermal growth factor receptor inhibition. *Nat Med* [Internet]. 2016/02/01. 2016 Mar;22(3):262–9. Available from: <https://www.ncbi.nlm.nih.gov/pubmed/26828195>
86. Eberlein CA, Stetson D, Markovets AA, Al-Kadhimi KJ, Lai Z, Fisher PR, et al. Acquired Resistance to the Mutant-Selective EGFR Inhibitor AZD9291 Is Associated with Increased Dependence on RAS Signaling in Preclinical Models. *Cancer Res*. 2015 Jun;75(12):2489–500.
87. Park SR, Davis M, Doroshow JH, Kummar S. Safety and feasibility of targeted agent combinations in solid tumours. *Nat Rev Clin Oncol*. 2013 Mar;10(3):154–68.
88. Mendoza MC, Er EE, Blenis J. The Ras-ERK and PI3K-mTOR pathways: cross-talk and compensation. *Trends Biochem Sci* [Internet]. 2011/04/30. 2011 Jun;36(6):320–8. Available from: <https://www.ncbi.nlm.nih.gov/pubmed/21531565>
89. Fey D, Croucher D, Kolch W, Kholodenko B. Crosstalk and Signaling Switches in Mitogen-Activated

- Protein Kinase Cascades [Internet]. Vol. 3, *Frontiers in Physiology*. 2012. p. 355. Available from: <https://www.frontiersin.org/article/10.3389/fphys.2012.00355>
90. Lake D, Correa SAL, Muller J. Negative feedback regulation of the ERK1/2 MAPK pathway. *Cell Mol Life Sci*. 2016 Dec;73(23):4397–413.
91. Martinez-Marti A, Felip E, Matito J, Mereu E, Navarro A, Cedres S, et al. Dual MET and ERBB inhibition overcomes intratumor plasticity in osimertinib-resistant-advanced non-small-cell lung cancer (NSCLC). *Ann Oncol Off J Eur Soc Med Oncol*. 2017 Oct;28(10):2451–7.
92. Hayakawa H, Ichihara E, Ohashi K, Ninomiya T, Yasugi M, Takata S, et al. Lower gefitinib dose led to earlier resistance acquisition before emergence of T790M mutation in epidermal growth factor receptor-mutated lung cancer model. *Cancer Sci*. 2013 Nov;104(11):1440–6.
93. Tricker EM, Xu C, Uddin S, Capelletti M, Ercan D, Ogino A, et al. Combined EGFR/MEK Inhibition Prevents the Emergence of Resistance in EGFR-Mutant Lung Cancer. *Cancer Discov*. 2015 Sep;5(9):960–71.
94. Ichihara E, Hotta K, Kubo T, Higashionna T, Ninomiya K, Ohashi K, et al. Clinical significance of repeat rebiopsy in detecting the EGFR T790M secondary mutation in patients with non-small cell lung cancer. *Oncotarget* [Internet]. 2018 Jun 29;9(50):29525–31. Available from: <https://www.ncbi.nlm.nih.gov/pubmed/30034635>
95. Vendrell JA, Mazieres J, Senal R, Rouquette I, Quantin X, Pujol J-L, et al. Ultra-sensitive EGFR (T790M) Detection as an Independent Prognostic Marker for Lung Cancer Patients Harboring EGFR (del19) Mutations and Treated with First-generation TKIs. *Clin Cancer Res*. 2019 Jul;25(14):4280–9.
96. Kerbel RS, Kamen BA. The anti-angiogenic basis of metronomic chemotherapy. *Nat Rev Cancer*. 2004 Jun;4(6):423–36.
97. Scharovsky OG, Mainetti LE, Rozados VR. Metronomic chemotherapy: changing the paradigm that more is better. *Curr Oncol*. 2009 Mar;16(2):7–15.
98. Nair AB, Jacob S. A simple practice guide for dose conversion between animals and human. *J basic Clin Pharm* [Internet]. 2016 Mar;7(2):27–31. Available from: <https://pubmed.ncbi.nlm.nih.gov/27057123>
99. Ritchie ME, Phipson B, Wu D, Hu Y, Law CW, Shi W, et al. limma powers differential expression analyses for RNA-sequencing and microarray studies. *Nucleic Acids Res*. 2015 Apr;43(7):e47.
100. Liberzon A, Birger C, Thorvaldsdottir H, Ghandi M, Mesirov JP, Tamayo P. The Molecular Signatures Database (MSigDB) hallmark gene set collection. *Cell Syst*. 2015 Dec;1(6):417–25.
101. Holohan C, Van Schaeybroeck S, Longley DB, Johnston PG. Cancer drug resistance: an evolving paradigm. *Nat Rev Cancer*. 2013 Oct;13(10):714–26.
102. Long G V, Stroyakovskiy D, Gogas H, Levchenko E, de Braud F, Larkin J, et al. Combined BRAF and MEK inhibition versus BRAF inhibition alone in melanoma. *N Engl J Med*. 2014 Nov;371(20):1877–88.
103. Boshuizen J, Peeper DS. Rational cancer treatment combinations: an urgent clinical need. *Mol Cell*. 2020;78(6):1002–18.
104. Ryan MB, de la Cruz FF, Phat S, Myers DT, Wong E, Shahzade HA, et al. Vertical pathway inhibition overcomes adaptive feedback resistance to KRASG12C inhibition. *Clin Cancer Res*. 2020;26(7):1633–43.
105. Zoetemelk M, Ramzy GM, Rausch M, Koessler T, van Beijnum JR, Weiss A, et al. Optimized low-dose combinatorial drug treatment boosts selectivity and efficacy of colorectal carcinoma treatment. *Mol Oncol*. 2020;14(11):2894–919.
106. Van Cutsem E, Cuyle P-J, Huijberts S, Yaeger R, Schellens JHM, Elez E, et al. BEACON CRC study safety lead-in (SLI) in patients with BRAF V600E metastatic colorectal cancer (mCRC): Efficacy and tumor markers. *American Society of Clinical Oncology*; 2018.
107. Van Cutsem E, Huijberts S, Grothey A, Yaeger R, Cuyle P-J, Elez E, et al. Binimetinib, encorafenib, and cetuximab triplet therapy for patients with BRAF V600E-mutant metastatic colorectal cancer: safety lead-in results from the phase III BEACON Colorectal Cancer Study. *J Clin Oncol Off J Am Soc Clin Oncol*. 2019;37(17):1460.
108. Sun J, Wei Q, Zhou Y, Wang J, Liu Q, Xu H. A systematic analysis of FDA-approved anticancer drugs. *BMC Syst Biol*. 2017;11(5):1–17.
109. Nowak-Sliwinska P, Weiss A, Ding X, Dyson PJ, Van Den Bergh H, Griffioen AW, et al. Optimization of drug combinations using Feedback System Control. *Nat Protoc*. 2016;11(2):302–15.
110. Weiss A, Berndsen RH, Ding X, Ho C-M, Dyson PJ, Van Den Bergh H, et al. A streamlined search technology for identification of synergistic drug combinations. *Sci Rep*. 2015;5(1):1–11.
111. Bosdriesz E, Prahallad A, Klinger B, Sieber A, Bosma A, Bernards R, et al. Comparative Network Reconstruction using mixed integer programming. *Bioinformatics*. 2018;34(17):i997–1004.
112. Dorel M, Klinger B, Gross T, Sieber A, Prahallad A, Bosdriesz E, et al. Modelling signalling networks from perturbation data. *Bioinformatics*. 2018;34(23):4079–86.
113. Klinger B, Sieber A, Fritsche-Guenther R, Witzel F, Berry L, Schumacher D, et al. Network quantification of EGFR signaling unveils potential for targeted combination therapy. *Mol Syst Biol*. 2013;9(1):673.
114. Halasz M, Kholodenko BN, Kolch W, Santra T. Integrating network reconstruction with mechanistic modeling to predict cancer therapies. *Sci Signal*. 2016;9(455):ra114–ra114.
115. Saez-Rodriguez J, Alexopoulos LG, Epperlein J, Samaga R. A Lauffenburger, D.; Klamt, S.; Sorger, PK Discrete logic modelling as a means to link protein signalling networks with functional analysis of mammalian signal transduction. *Mol Syst Biol*. 2009;5:331.
116. Jastrzebski K, Thijssen B, Kluijn RJC, De Lint K, Majewski IJ, Beijersbergen RL, et al. Integrative modeling identifies key determinants of inhibitor sensitivity in breast cancer cell lines. *Cancer Res*. 2018;78(15):4396–410.
117. Kirouac DC, Du JY, Lahdenranta J, Overland R, Yarar D, Paragas V, et al. Computational modeling of ERBB2-amplified breast cancer identifies combined ErbB2/3 blockade as superior to the combination of MEK and AKT inhibitors. *Sci Signal*. 2013;6(288):ra68–ra68.
118. Nyman E, Stein RR, Jing X, Wang W, Marks B, Zervantonakis IK, et al. Perturbation biology links temporal protein changes to drug responses in a melanoma cell line. *PLoS Comput Biol*. 2020;16(7):e1007909.
119. Saez-Rodriguez J, Alexopoulos LG, Zhang M, Morris MK, Lauffenburger DA, Sorger PK. Comparing signaling networks between normal and transformed hepatocytes using discrete logical models.

- Cancer Res. 2011;71(16):5400–11.
120. Korkut A, Wang W, Demir E, Aksoy BA, Jing X, Molinelli EJ, et al. Perturbation biology nominates upstream–downstream drug combinations in RAF inhibitor resistant melanoma cells. *Elife*. 2015;4:e04640.
121. Soule HD, Maloney TM, Wolman SR, Peterson WD, Brenz R, McGrath CM, et al. Isolation and characterization of a spontaneously immortalized human breast epithelial cell line, MCF-10. *Cancer Res*. 1990;50(18):6075–86.
122. Di Nicolantonio F, Arena S, Gallicchio M, Zecchin D, Martini M, Flonta SE, et al. Replacement of normal with mutant alleles in the genome of normal human cells unveils mutation-specific drug responses. *Proc Natl Acad Sci*. 2008;105(52):20864–9.
123. Gustin JP, Karakas B, Weiss MB, Abukhdeir AM, Lauring J, Garay JP, et al. Knockin of mutant PIK3CA activates multiple oncogenic pathways. *Proc Natl Acad Sci*. 2009;106(8):2835–40.
124. Haagensen EJ, Thomas HD, Mudd C, Tsonou E, Wiggins CM, Maxwell RJ, et al. Pre-clinical use of isogenic cell lines and tumours in vitro and in vivo for predictive biomarker discovery; impact of KRAS and PI3KCA mutation status on MEK inhibitor activity is model dependent. *Eur J Cancer*. 2016;56:69–76.
125. Torrance CJ, Agrawal V, Vogelstein B, Kinzler KW. Use of isogenic human cancer cells for high-throughput screening and drug discovery. *Nat Biotechnol*. 2001;19(10):940–5.
126. Martin TD, Cook DR, Choi MY, Li MZ, Haigis KM, Elledge SJ. A role for mitochondrial translation in promotion of viability in K-Ras mutant cells. *Cell Rep*. 2017;20(2):427–38.
127. de Lint K, Poell JB, Soueidan H, Jastrzebski K, Rodriguez JV, Liefink C, et al. Sensitizing triple-negative breast cancer to PI3K inhibition by cotargeting IGF1R. *Mol Cancer Ther*. 2016;15(7):1545–56.
128. Iorio F, Knijnenburg TA, Vis DJ, Bignell GR, Menden MP, Schubert M, et al. A landscape of pharmacogenomic interactions in cancer. *Cell*. 2016;166(3):740–54.
129. Vis DJ, Bombardelli L, Lightfoot H, Iorio F, Garnett MJ, Wessels LFA. Multilevel models improve precision and speed of IC50 estimates. *Pharmacogenomics*. 2016;17(7):691–700.
130. Kholodenko BN, Kiyatkin A, Bruggeman FJ, Sontag E, Westerhoff H V, Hoek JB. Untangling the wires: a strategy to trace functional interactions in signaling and gene networks. *Proc Natl Acad Sci*. 2002;99(20):12841–6.
131. Kuhn M, Wickham H. *Tidymodels: a collection of packages for modeling and machine learning using tidyverse principles*. Boston, MA, USA [accessed 10 December 2020]. 2020;
132. Virtanen P, Gommers R, Oliphant TE, Haberland M, Reddy T, Cournapeau D, et al. *SciPy 1.0: fundamental algorithms for scientific computing in Python*. *Nat Methods*. 2020;17(3):261–72.
133. Richard G-F, Kerrest A, Dujon B. Comparative genomics and molecular dynamics of DNA repeats in eukaryotes. *Microbiol Mol Biol Rev*. 2008 Dec;72(4):686–727.
134. Ellegren H. Microsatellites: simple sequences with complex evolution. *Nat Rev Genet*. 2004 Jun;5(6):435–45.
135. Schlötterer C, Harr B. Microsatellite Instability [Internet]. eLS. 2004. (Major Reference Works). Available from: <https://doi.org/10.1038/npg.els.0000840>
136. Buecher B, Cacheux W, Rouleau E, Dieumegard B, Mitry E, Lièvre A. Role of microsatellite instability in the management of colorectal cancers. *Dig liver Dis Off J Ital Soc Gastroenterol Ital Assoc Study Liver*. 2013 Jun;45(6):441–9.
137. Popat S, Hubner R, Houlston RS. Systematic review of microsatellite instability and colorectal cancer prognosis. *J Clin Oncol Off J Am Soc Clin Oncol*. 2005 Jan;23(3):609–18.
138. Sahin IH, Akce M, Alese O, Shaib W, Lesinski GB, El-Rayes B, et al. Immune checkpoint inhibitors for the treatment of MSI-H/MMR-D colorectal cancer and a perspective on resistance mechanisms. *Br J Cancer [Internet]*. 2019;121(10):809–18. Available from: <https://doi.org/10.1038/s41416-019-0599-y>
139. Roth JR. Frameshift mutations. *Annu Rev Genet*. 1974;8:319–46.
140. Nebot-Bral L, Coutzac C, Kannouche PL, Chaput N. Why is immunotherapy effective (or not) in patients with MSI/MMRD tumors? *Bull Cancer*. 2019 Feb;106(2):105–13.
141. Ballhausen A, Przybilla MJ, Jendrusch M, Haupt S, Pfaffendorf E, Seidler F, et al. The shared frameshift mutation landscape of microsatellite-unstable cancers suggests immunoeediting during tumor evolution. *Nat Commun [Internet]*. 2020;11(1):4740. Available from: <https://doi.org/10.1038/s41467-020-18514-5>
142. Tian S, Roepman P, Popovici V, Michaut M, Majewski I, Salazar R, et al. A robust genomic signature for the detection of colorectal cancer patients with microsatellite instability phenotype and high mutation frequency. *J Pathol [Internet]*. 2012/10/12. 2012 Dec;228(4):586–95. Available from: <https://pubmed.ncbi.nlm.nih.gov/22926706>
143. Mlecnik B, Bindea G, Angell HK, Maby P, Angelova M, Tougeron D, et al. Integrative Analyses of Colorectal Cancer Show Immunoscore Is a Stronger Predictor of Patient Survival Than Microsatellite Instability. *Immunity*. 2016 Mar;44(3):698–711.
144. Boyer JC, Farber RA. Mutation rate of a microsatellite sequence in normal human fibroblasts. *Cancer Res*. 1998 Sep;58(17):3946–9.
145. Pino MS, Kikuchi H, Zeng M, Herraiz M-T, Sperduti I, Berger D, et al. Epithelial to mesenchymal transition is impaired in colon cancer cells with microsatellite instability. *Gastroenterology*. 2010 Apr;138(4):1406–17.
146. Wojciechowicz K, Cantelli E, Van Gerwen B, Plug M, Van Der Wal A, Delzenne-Goette E, et al. Temozolomide increases the number of mismatch repair-deficient intestinal crypts and accelerates tumorigenesis in a mouse model of Lynch syndrome. *Gastroenterology*. 2014 Nov;147(5):1064-72. e5.
147. Conaway RC, Sato S, Tomomori-Sato C, Yao T, Conaway JW. The mammalian Mediator complex and its role in transcriptional regulation. *Trends Biochem Sci*. 2005 May;30(5):250–5.
148. Soutourina J. Transcription regulation by the Mediator complex. *Nat Rev Mol Cell Biol*. 2018 Apr;19(4):262–74.
149. Zhang M, Hu C, Moses N, Haakenson J, Xiang S, Quan D, et al. HDAC6 regulates DNA damage response via deacetylating MLH1. *J Biol Chem [Internet]*. 2019;294(15):5813–26. Available from: <https://www.sciencedirect.com/science/article/pii/S0021925820366552>
150. Carethers JM. Differentiating Lynch-like from Lynch syndrome. *Gastroenterology [Internet]*.

- 2014/01/24. 2014 Mar;146(3):602–4. Available from: <https://pubmed.ncbi.nlm.nih.gov/24468183>
151. Ganesh K, Middha S, Hechtman JF, Ashraf A, Tran C, Villano D, et al. Somatic tumor profiling of DNA mismatch repair deficient (MMR-D) colorectal cancers (CRC). *J Clin Oncol* [Internet]. 2016 May 20;34(15_suppl):1528. Available from: https://doi.org/10.1200/JCO.2016.34.15_suppl.1528
152. Muzny DM, Bainbridge MN, Chang K, Dinh HH, Drummond JA, Fowler G, et al. Comprehensive molecular characterization of human colon and rectal cancer. *Nature* [Internet]. 2012;487(7407):330–7. Available from: <https://doi.org/10.1038/nature11252>
153. Germano G, Lamba S, Rospo G, Barault L, Magri A, Maione F, et al. Inactivation of DNA repair triggers neoantigen generation and impairs tumour growth. *Nature* [Internet]. 2017;552(7683):116–20. Available from: <https://doi.org/10.1038/nature24673>
154. Luchini C, Bibeau F, Ligtgenberg MJL, Singh N, Nottegar A, Bosse T, et al. ESMO recommendations on microsatellite instability testing for immunotherapy in cancer, and its relationship with PD-1/PD-L1 expression and tumour mutational burden: a systematic review-based approach. *Ann Oncol Off J Eur Soc Med Oncol*. 2019 Aug;30(8):1232–43.
155. Wang C, Jin H, Gao D, Wang L, Evers B, Xue Z, et al. A CRISPR screen identifies CDK7 as a therapeutic target in hepatocellular carcinoma. Vol. 28, *Cell research*. 2018. p. 690–2.
156. Tsui CK, Barfield RM, Fischer CR, Morgens DW, Li A, Smith BAH, et al. CRISPR-Cas9 screens identify regulators of antibody–drug conjugate toxicity. *Nat Chem Biol* [Internet]. 2019;15(10):949–58. Available from: <https://doi.org/10.1038/s41589-019-0342-2>
157. Park RJ, Wang T, Koundakjian D, Hultquist JF, Lamothe-Molina P, Monel B, et al. A genome-wide CRISPR screen identifies a restricted set of HIV host dependency factors. *Nat Genet* [Internet]. 2017;49(2):193–203. Available from: <https://doi.org/10.1038/ng.3741>
158. Flint M, Chatterjee P, Lin DL, McMullan LK, Shrivastava-Ranjan P, Bergeron É, et al. A genome-wide CRISPR screen identifies N-acetylglucosamine-1-phosphate transferase as a potential antiviral target for Ebola virus. *Nat Commun* [Internet]. 2019;10(1):285. Available from: <https://doi.org/10.1038/s41467-018-08135-4>
159. Arnold C. What’s new in clinical CRISPR? *Nat Med* [Internet]. 2021;27(2):184–5. Available from: <https://doi.org/10.1038/s41591-020-01222-4>
160. Yang Y, Xu J, Ge S, Lai L. CRISPR/Cas: Advances, Limitations, and Applications for Precision Cancer Research [Internet]. Vol. 8, *Frontiers in Medicine*. 2021. p. 115. Available from: <https://www.frontiersin.org/article/10.3389/fmed.2021.649896>
161. DeWeirdt PC, Sangree AK, Hanna RE, Sanson KR, Hegde M, Strand C, et al. Genetic screens in isogenic mammalian cell lines without single cell cloning. *Nat Commun*. 2020 Feb;11(1):752.
162. Evers B, Jastrzebski K, Heijmans JPM, Grertrum W, Beijersbergen RL, Bernards R. CRISPR knockout screening outperforms shRNA and CRISPRi in identifying essential genes. *Nat Biotechnol*. 2016 Jun;34(6):631–3.
163. Sanson KR, Hanna RE, Hegde M, Donovan KF, Strand C, Sullender ME, et al. Optimized libraries for CRISPR-Cas9 genetic screens with multiple modalities. *Nat Commun*. 2018 Dec;9(1):5416.
164. Brinkman EK, Chen T, Amendola M, van Steensel B. Easy quantitative assessment of genome editing by sequence trace decomposition. *Nucleic Acids Res*. 2014 Dec;42(22):e168.
165. Ye S, Enghiad B, Zhao H, Takano E. Fine-tuning the regulation of Cas9 expression levels for efficient CRISPR-Cas9 mediated recombination in *Streptomyces*. *J Ind Microbiol Biotechnol*. 2020 May;47(4–5):413–23.
166. Schep R, Brinkman EK, Leemans C, Vergara X, van der Weide RH, Morris B, et al. Impact of chromatin context on Cas9-induced DNA double-strand break repair pathway balance. *Mol Cell*. 2021 Apr;
167. Najm FJ, Strand C, Donovan KF, Hegde M, Sanson KR, Vaimberg EW, et al. Orthologous CRISPR–Cas9 enzymes for combinatorial genetic screens. *Nat Biotechnol* [Internet]. 2018;36(2):179–89. Available from: <https://doi.org/10.1038/nbt.4048>
168. Henkel L, Rauscher B, Schmitt B, Winter J, Boutros M. Genome-scale CRISPR screening at high sensitivity with an empirically designed sgRNA library. *BMC Biol* [Internet]. 2020;18(1):174. Available from: <https://doi.org/10.1186/s12915-020-00905-1>
169. Joung J, Konermann S, Gootenberg JS, Abudayyeh OO, Platt RJ, Brigham MD, et al. Genome-scale CRISPR-Cas9 knockout and transcriptional activation screening. *Nat Protoc* [Internet]. 2017;12(4):828–63. Available from: <https://doi.org/10.1038/nprot.2017.016>
170. Morgens DW, Wainberg M, Boyle EA, Ursu O, Araya CL, Tsui CK, et al. Genome-scale measurement of off-target activity using Cas9 toxicity in high-throughput screens. *Nat Commun* [Internet]. 2017;8(1):15178. Available from: <https://doi.org/10.1038/ncomms15178>
171. Love MI, Huber W, Anders S. Moderated estimation of fold change and dispersion for RNA-seq data with DESeq2. *Genome Biol* [Internet]. 2014;15(12):550. Available from: <https://doi.org/10.1186/s13059-014-0550-8>
172. Li W, Xu H, Xiao T, Cong L, Love MI, Zhang F, et al. MAGeCK enables robust identification of essential genes from genome-scale CRISPR/Cas9 knockout screens. *Genome Biol*. 2014 Dec;15(12):554.
173. Jain RK, Lee JJ, Hong D, Markman M, Gong J, Naing A, et al. Phase I oncology studies: evidence that in the era of targeted therapies patients on lower doses do not fare worse. *Clin Cancer Res*. 2010 Feb;16(4):1289–97.
174. Jeon M, Kim S, Park S, Lee H, Kang J. In silico drug combination discovery for personalized cancer therapy. *BMC Syst Biol* [Internet]. 2018;12(2):16. Available from: <https://doi.org/10.1186/s12918-018-0546-1>
175. Jin H, Shi Y, Lv Y, Yuan S, Ramirez CFA, Lieftink C, et al. EGFR activation limits the response of liver cancer to lenvatinib. *Nature*. 2021 Jul;595(7869):730–4.

Nederlandse samenvatting

Kankertherapie is significant verbeterd in de afgelopen 10-20 jaar, maar er is nog een lange weg te gaan. Chemotherapie was decennia lang de ruggengraat van de kankerbehandelingen, maar de ontdekking dat kanker een gevolg is van genetische fouten en dat de remming van oncogene eiwitten therapeutische reacties teweegbrengt, wakkerde de ontwikkeling van doelgerichte strategieën aan. Het veld van doelgerichte therapie is in afgelopen jaren geëxplodeerd met dank aan technologische ontwikkelingen, zoals next generation sequencing wat onze kennis over kankerbiologie heeft vergroot. Maar de aanvankelijke hype vervaagde snel, toen we ontdekten dat de meeste geavanceerde tumoren intrinsiek resistent zijn of in korte tijd resistentie ontwikkelen. In mijn PhD thesis streefde ik ernaar het probleem van resistentie tegen geneesmiddelen aan te pakken met rationele maar innovatieve benaderingen. In hoofdstuk 1 van deze thesis bespreken we in detail de kansen die we als veelbelovend beschouwen om resistentie tegen geneesmiddelen te overwinnen en geven we commentaar op het huidige model van geneesmiddelontwikkeling.

Het is algemeen bekend dat combinaties van geneesmiddelen effectiever zijn dan op één middel gerichte geneesmiddelen. Het combineren van medicijnen wordt echter vaak geassocieerd met toxiciteit. We redeneerden dat deze toxiciteit, althans in sommige gevallen, te wijten zou kunnen zijn aan het medicijntoedieningsmodel, d.w.z. de levering van een medicijn aan patiënten met de maximaal getolereerde dosis (MTD). Dit model voor medicijntoediening is decennialang vrijwel onveranderd gebleven, ondanks enig bewijs dat MTD niet altijd nodig is om een klinische respons te bereiken. We redeneerden dat als we de concentratie van geneesmiddelen zouden verlagen, we het toxiciteitsprobleem bij het gebruik van combinaties van geneesmiddelen zouden kunnen elimineren met behoud van de werkzaamheid. In hoofdstuk 2 van deze thesis laten we zien dat gedeeltelijke remming van meerdere componenten van door kanker geactiveerde signaalroutes resulteert in volledige remming van de route, wat moeilijker te omzeilen is dan met een enkel medicijn bij MTD, waardoor de kans op resistentie wordt verminderd. Dankzij de veelbelovende preklinische gegevens bij muizen zijn we bezig met het starten van een klinische proef om de MLD-strategie in de kliniek te testen.

Het toenemende aantal kankerverwekkende stoffen, samen met het idee dat combinaties van geneesmiddelen meer voordelen opleveren, hebben voor een nieuwe uitdaging gezorgd. Het aantal mogelijke combinaties van geneesmiddelen wordt enorm, waardoor het onmogelijk is om alle mogelijke combinaties experimenteel te testen. CRISPR-screens bieden een onbevooroordeelde manier om dit probleem aan te pakken. Ze zijn echter meestal beperkt tot het identificeren van combinaties van 2 geneesmiddelen. En, zoals we in hoofdstuk 2 hebben aangetoond,

kan het gebruik van combinaties van meerdere geneesmiddelen in lage doses een betere benadering zijn om resistentie tegen geneesmiddelen te voorkomen. Deze multidimensionale informatie (doelen en dosis) is iets dat CRISPR-screens niet kunnen bieden. Een manier om dit probleem op te lossen, is door computationele pijplijnen te ontwikkelen die signaleringsnetwerken reconstrueren op basis van experimentele verstoringsexperimenten, veranderingen in signaleringsoutput te verbinden met veranderingen in levensvatbaarheid van cellen, en deze modellen te gebruiken om prioriteit te geven aan combinaties van meerdere geneesmiddelen in silico. In hoofdstuk 3 hebben we een dergelijke benadering ontwikkeld en waren we in staat om combinaties van geneesmiddelen te voorspellen en valideren die selectief waren voor een bepaalde cellijn.

Immunotherapie heeft de afgelopen jaren een revolutie teweeggebracht in de kankertherapie. Dankzij immunotherapie blijven patiënten met (voorheen) ongeneeslijke kankers nu een groot aantal jaren in remissie of worden ze zelfs genezen. Deficiënte MMR en MSI was een van de eerste voorspellende biomarkers die werd goedgekeurd voor het selecteren van patiënten voor immunotherapie. Belangrijk is dat er aanwijzingen zijn dat een subgroep van patiënten met MSS-tumoren ook baat zou kunnen hebben bij immunotherapie, maar omdat ze niet voldoen aan de geschiktheidscriteria, worden ze niet behandeld met immunotherapie. Aangezien inductie van MSI de immunogeniciteit van tumoren verhoogt en bijgevolg de respons op immunotherapie, redeneerden we dat als we nieuwe genen konden identificeren die MSI reguleren, we ze mogelijk zouden kunnen gebruiken als aanvullende voorspellende biomarkers voor immunotherapiebehandeling. Daartoe hebben we in hoofdstuk 4 geprobeerd nieuwe regulatoren van microsatelliet-instabiliteit te vinden door CRISPR-screens uit te voeren in een MSS-celijn met een op fluorescentie gebaseerde MSI-sensor. Opmerkelijk is dat we na meer dan 20 jaar onderzoek naar darmkanker de eersten waren die een nieuw kandidaat-MSI-gen identificeerden: MED12.

Technologie heeft een revolutie teweeggebracht in de moderne wereld en het ongelooflijke tempo waarin de kankerbiologie de afgelopen tien jaar is gevorderd, is grotendeels te danken aan enkele technologische ontwikkelingen. Een van hen, die genetische studies transformeerde van tijdrovend, duur en gespecialiseerd in een routinematige laboratoriumtechniek, is CRISPR. Dankzij CRISPR kunnen we nu vrijwel gratis genomen in enkele dagen tijd bewerken. Maar, net als bij elke techniek, zijn er altijd enkele tweaks die de efficiëntie kunnen verbeteren. En na een tijdje CRISPR te hebben gebruikt, merkte ik dat de bewerkingstijd aanzienlijk kon worden verbeterd door de expressie van Cas9 te vergroten. In hoofdstuk 5 hebben we een uitgebreide studie uitgevoerd om dit probleem aan te pakken en bewijs te leveren dat aangeeft dat het optimaliseren van Cas9-expressie de efficiëntie van CRISPR-schermen kan verbeteren.

Met deze thesis heb ik geprobeerd nieuwe strategieën te ontwikkelen om het probleem van resistentie tegen geneesmiddelen aan te pakken. Een van de dingen die ik tijdens dit proces heb geleerd, is dat we niet altijd het wiel opnieuw hoeven uit te vinden om een verschil te maken, zoals in hoofdstuk 5 wordt aangetoond, en dat het gebruik van rationele benaderingen met een sterke mechanistische basis de beste manier is om nieuwe ontdekkingen te doen. behandelingsstrategieën, zoals geïllustreerd door het hoge percentage mislukkingen van de honderden “trial and error” PD1-onderzoeken. Ondanks alle vooruitgang op het gebied van kanker in de afgelopen jaren, zijn er nog oneindig veel uitdagingen die moeten worden aangepakt. Niettemin boeken we als wetenschappelijke gemeenschap gestaag vooruitgang in ons begrip van resistentie tegen geneesmiddelen en dergelijke bevindingen bereiken de kliniek sneller dan ooit tevoren. Jin et al. hebben bijvoorbeeld het resistentiemechanisme tegen lenvatinib blootgelegd met behulp van een CRISPR-screening en waren in minder dan 2 jaar in staat om klinische proof-of-concept aan te tonen van de combinatie van geneesmiddelen die resistentie tegen lenvatinib overwint. Bevindingen als deze suggereren dat het tempo waarin patiënten kunnen profiteren van wetenschappelijke ontdekkingen de komende jaren zal blijven toenemen, reden genoeg om optimistisch te zijn over de toekomst van de kankerbehandeling.

Curriculum vitae

João Manuel Fernandes Neto

Porto (Portugal), 12th January 1993

joaoneto.ua@gmail.com • +31639099281 • +351910413380

Personal Profile

Ambitious and versatile scientist with 7+ years of international experience in preclinical and translational cancer research. Team player who easily integrates in new environments, with a critical and creative mindset and strong analytical abilities. A firm believer that motivation fosters the best results in any organization.

Management and Leadership Skills

- Project management, including supervision of 4 M.Sc. students, based on interpersonal and leadership skills.
- Analytical and problem-solving approach based on solid research background.
- Strong self-management and working habits built on strategic planning and time management.
- Highly skilled in communicating and explaining concepts clearly.

Technical Skills

- In vivo intervention studies using tumor xenografts and genetic mouse models
- In vivo and in vitro functional genetic screens (shRNA, CRISPR/Cas9)
- Small molecule inhibitors screens
- Cell biology techniques, mammalian cell culture, microscopy, flow cytometry
- Molecular biology and biochemistry techniques

Languages

- English (full working proficiency)
- Portuguese (native speaker)
- Spanish (good command)

Education

PhD

Cancer, Stem Cells & Developmental Biology

Sept. 2015 to Aug. 2021

Supervisor:

Rene Bernards

The Netherlands Cancer Institute, NL

MSc

Biotechnology

University of Aveiro, PT

Sept. 2013 to Jun. 2015

BSc

Biochemistry

University of Aveiro, PT

Sept. 2010 to Jun. 2013

Publication list

Wang L, de Oliveira RL, Wang C, **Fernandes Neto JM**, Mainardi S, Evers B, et al. High-throughput functional genetic and compound screens identify targets for senescence induction in cancer. *Cell Rep.* 2017;21(3):773–83.

Fernandes Neto JM, Nadal E, Bosdriesz E, Ooft SN, Farre L, McLean C, et al. Multiple low dose therapy as an effective strategy to treat EGFR inhibitor-resistant NSCLC tumours. *Nat Commun [Internet]*. 2020;11(1):3157. Available from: <https://doi.org/10.1038/s41467-020-16952-9>

Bosdriesz E, **Fernandes Neto JM**, Sieber A, Bernards R, Blüthgen N, Wessels LFA. Identifying selective drug combinations using Comparative Network Reconstruction. *bioRxiv [Internet]*. 2020 Jan 1;2020.12.17.423240. Available from: <http://biorxiv.org/content/early/2020/12/18/2020.12.17.423240.abstract>

Settleman J, **Fernandes Neto JM**, Bernards R. Thinking Differently about Cancer Treatment Regimens. *Cancer Discov [Internet]*. 2021 May 1;11(5):1016 LP – 1023. Available from: <http://cancerdiscovery.aacrjournals.org/content/11/5/1016.abstract>

Fernandes Neto JM, Jastrzebski K, Lieftink C, Krenning L, Dias M, Morris B, et al. Optimized Cas9 expression improves performance of large-scale CRISPR screening. *bioRxiv [Internet]*. 2021 Jan 1;2021.07.13.452178. Available from: <http://biorxiv.org/content/early/2021/07/13/2021.07.13.452178.abstract>

Acknowledgements

It has been 7 years since I started my journey at the NKI, and what an incredible journey it has been... I started as a Master student with no idea about what cancer was and I now leave as an expert in the field... I'm very proud of my professional achievements and very grateful for all the personal experiences I lived throughout these 7 years. This was only possible thanks to the amazing group of people I met along the way!

René, thank you for being the best possible supervisor and mentor I could ask for! I will forever be grateful for all the opportunities, the support and the freedom you gave me, which allowed me to grow as an independent scientist. Your energy, positivity and ability to see the big picture are absolutely inspiring!

Rodrigo, it's hard to put into words how grateful I am to you. You took me in as a Master student with no cancer background and mentored me into a scientist. Without you I wouldn't be here today! Thank you for giving me the wings so that I could fly...

Roderick, it took me a while to "understand" you but I'm very glad that eventually I did. Thanks for the many scientific and philosophical discussions, for taking the time and interest in my technology-oriented projects. Our interactions helped me become a better scientist.

I want to thank my reading committee – **Thijn Brummelkamp**, **Emile Voest**, **Daniel Peeper**, **Madelon Maurice** and **Boudewijn Burgering** – for taking the time to evaluate this thesis.

I want to thank my NKI PhD committee – **Lodewick Wessels**, **Thijn Brummelkamp** and **Fred van Leeuwen** – for all the good advice throughout my PhD.

A special thanks to my paranymphs for helping to organise my PhD's celebrations. **Antonio**, you've been like a brother to me... we lived together, partied together, cried together, travelled together, and the list goes on and on... These 7 years would not have been half as fun without you! I hope to be back next year to celebrate your PhD and I hope to share many more moments with you in the future!

Ben, some of the most unforgettable moments in my PhD were spent drinking with you. You are an amazing person when sober and the life of the party when you're drunk! Thanks for all the help in the lab throughout these years, for helping me renovate my apartment and for all the brewing sessions. I still believe we will open

up our (micro)brewery in the future!

Bruno, és uma das poucas pessoas neste mundo com quem posso falar totalmente abertamente, sem filtros, e isso foi algo que apreciei imenso ao longo dos anos que passamos juntos aqui em Amsterdão. Obrigado pela tua companhia em todas as "macumbadas" ao longo destes anos! Espero que um dia voltemos a ser vizinhos em Portugal!

Matheus, I am very glad you joined B7! You made my last two years in the lab much more enjoyable and thanks to you I learned that working in a team is better than working alone... We will definitely keep in touch and I hope to celebrate our LIXT earnings very soon!

Živa, the last 7 years have been quite an adventure... You helped me become a better person and a better scientist and I'll forever be grateful for that.

Isa, thank you for helping me when I was having a hard time in my personal life. Our talks, your group of friends and the party life really helped me out!

To all **B7 members**, thank you for making my PhD journey so enjoyable!

Katrien, **Marielle** and **Annemieke** it was great to share the office with you and have the most experienced people in the lab so close, thanks for all the help! **Patty**, you are the most amazing office manager, thanks for all the help throughout these years. **Evert**, thanks for all help with the many bioinformatics analysis, hope we can keep collaborating in the future! **Cor**, thank you for all the complicated screen analysis! **Giulia**, thanks for all the good times outside the lab! **Liqin**, you were always super friendly to me from day one and always encouraged me to work hard. Too bad we didn't get to collaborate as much as we wanted but I still learned a lot from you, thanks! **Sara**, **Arnout**, **Cun**, **Hoejie**, **Astrid**, **Michiel**, **Kathy**, **Silvana**, **Lorenzo**, **Johan**, **Elke** I'm very happy I got to share the lab with you!

To all **B7 PhD students**, it was great sharing this journey with you! **Sander** those first years were amazing! Hope you find happiness in your next adventure. **Fleur**, **Jeroen** and **Robin** I wish you the best for finishing up your PhDs!

To all **ex-B7 members**, thank you for welcoming me to B7 when I first arrived! In particular, I would like to thank **Bastiaan**, **Anirudh**, **Guus** and **Kristan**, for making me feel at home when I was just a student. **Loredana**, for the helpful advice when I first started the PhD. **Begoña**, for the nice tissue culture talks and friendship. **Wouter**, for answering all my stupid questions about reagents, etc. **Tonci** for your quirkiness.

To my former students **Hannes, Hester, Anouk** and **Daimy**: you are all amazing people and it was great to work with you! I learned a lot from you guys and I wish you a bright future!

To all **(ex-) B7 students**: it's been great to share the lab with you! Over the years students came and went but somehow we've always ended up with a great bunch of people, some of which, I've become good friends with. **Jordi** and **Max** we've had a blast while you were here and I'm happy we've kept in touch.

To all the past and present members of the **Intervention Unit**, and in particular to **Natalie**, a very big thanks for taking such good care of all my mice experiments!

To my PSOE friends **Anke, Melanie, Jacobien** and **Lisanne** thanks for the many memories from the borrels and parties throughout the years!

To the "Tugas NKI" **Suzana, Estela** and **Catarina** thanks for the Portuguese talks and dinners!

To the "NKI Mafia", who made the first years of the PhD so memorable outside the lab. **Anna**, I'll never forget the many memories we shared over the years, from the crazy house parties to the cosy evenings watching Gran Hotel... I'm so glad we are both graduating and I wish you the best for your next adventures! **Mariana**, it was great to have a Portuguese friend in the group, making it possible to comment about something in our "secret" language and have someone who laughed at my Portuguese jokes. Thanks for all the happy times and the more serious talks too. **Ronak**, you are an amazing person and friend. Thanks for all the good moments and for being there when I needed! **Alberto** and **Clara**, my favourite couple, you have been amazing to me when my personal life was not great and I will forever be grateful for your comprehension and friendship. Looking forward to more Spanish dinners and game nights in the future! **Isabel, Jeremy, Eric, Alessandra, Louise, Maria, Mar, Marjon, Mathias, Xabi, Simon, Soufiane, Stefan** and **Celia** we shared so many awesome moments together over the last years and I'm very happy I got to meet you all! Thanks for being part of my journey!

Thanks to all the members of the NKI's core facilities, in particular the FACS facility, the genomics core facility and the animal pathology facility, which I used so many times during my PhD.

Thanks to all the co-authors for their contribution to the chapters of this thesis, science is a team effort and without your contribution this thesis would not have been possible. In particular, to **Olaf** for your continuous support with the in vivo

experiments.

Thanks to all the manuscript reviewers. Your comments significantly improved our manuscripts.

Millie, I'm very glad I got to meet the real you! Thanks for the nice talks, fun times and for trying to get me to sport more.

Jeroen Lohuis, we started almost at the same time as students back in 2014 and I remember the fun times picking shRNA libraries, trying to beat our own records in refreshing screens and, of course, the many borrels. After the internship you went away to finish your studies but I was very happy when you came back to the nki a few years later. Thanks to you I got to meet other incredible people. **Daniel Postrach, Tim, Laura** and **Colinda** I am very glad I got to meet you and spend so many great times with you guys! Wish you the best and let's keep in touch! PS: The Stotland trip had to be postponed indefinitely but I still hope we can do it at some point in the future!

Henri van Luenen and **René Medema** you are both amazing at leading the NKI research forward and you've never lost touch with the people in the "trenches", which is remarkable! Thanks for the great times, talks and advices over the years!

I've met so many incredible people in the past years in the NKI, at the Friday borrels, in conferences and retreats. **Julia Yemel, Ana Krotenberg, Ana Moises, Joana Silva, Angela, Catrin, Chelsea, Jessica, Lisette, Martjn, Christina, Heta, Lenno, Juliana, Alex, Julia Boshuizen, David, Aurora, Judith Haarhuis, Alba Zuidema, Andreia Margarido, Mark de Gooijer, Ewald, Jonne** and many more... It's impossible to name everyone, so forgive me if I forgot to mention some names... Thanks everyone!

Aos meus amigos **João Pinto** e **Joana Sousa** obrigado por terem sempre mantido o contacto apesar da distancia.

Aos meus pais, **Elisa** e **Pedro Neto** obrigado por tudo o que me proporcionaram ao longo da minha vida. É graças a vocês que estou aqui hoje! Obrigado por terem sempre apoiado as minhas decisões e por acreditarem em mim! Amo-vos muito!

To **Peter, Karin, Kirsten** and **Manon**, thank you for welcoming me into your family and making me feel at home! I'm looking forward to sharing family life with you all. **Ferry**, it's been great to have a guy to hang out with in this "girls-only" family :D

Amber, you are the best thing that ever happened to me... Thank you for your support in these last months of the PhD and for making my work worries go away as soon as I got home. I look forward to the rest of our lives together! I love you!
Lucy, you came to our lives in the perfect moment... Even though you were not yet born when I wrote this thesis, you made me have a clear deadline for finishing it, which really helped me to focus. I love you my baby girl...